Novel Characterization of Decorative Coatings using Field-Flow Fractionation and a multi-detector approach.

by

Ashwell Craig Makan

Dissertation presented for the degree of

Doctor of Philosophy in Polymer Science

at

Stellenbosch University

Supervisor: Prof H. Pasch

March 2017

Stellenbosch

Declaration

By submitting this thesis electronically, I declare that the entirety of the work contained therein is my own, original work, that I am the sole author thereof (save to the extent explicitly otherwise stated), that reproduction and publication thereof by Stellenbosch University will not infringe any third party rights and that I have not previously in its entirety or in part submitted it for obtaining any qualification.

March 2017

Ashwell Craig Makan Stellenbosch

Declaration of publications

The nature and the scope of the candidate's contributions in the published manuscripts forming part of Chapter 3 and Chapter 4 were as follow:

Candidate	**Nature**	**Contributions**
Ashwell Makan	1. Experimental execution of various characterization techniques 2. Data analysis and interpretation 3. Preparation of manuscripts 4. Addressing comments and recommendation of journal reviewers.	88 % overall

The following co-authors contributed to the manuscripts in the dissertation as follow:

Co author	**Nature**	**Contributions**
Harald Pasch	1. Mentoring and supervision throughout studies. 2. Revision and correcting of manuscripts for publications.	8 % overall
Madeleine du Toit and Ryan Williams	1. Synthesis of latex particles used in the study for Chapter 3, 4 and 5.	2 % overall
Markus Spallek and Thorsten Klein	1. Assisted with selected data interpretation and correcting of published manuscript in Chapter 3.	2% overall

Declaration by co-authors:

1. The nature and extent of the declaration above accurately reflects the contributions of the candidate and co-authors to the manuscripts in the dissertation.
2. No contributions have been made by any other authors in the dissertation, except the co-authors specified on page IV.
3. All parties granted their consent for the inclusion of the results of the manuscripts into the dissertation. Potential conflicts of interest have been disclosed to all parties.

Abstract

Decorative coatings are present and fulfil and important role in all industry forms from aesthetics, construction, medicine, textiles, manufacturing, packaging and timber. The raw materials used in coatings have an important role to perform and impart various functions, e.g. finishing and feel (gloss or matt), ultraviolet protection against colour fading, resistance against scratches, stains and cracking. Water-based decorative coatings were critically characterized using classical size exclusion chromatography (SEC) and field-flow fractionation (FFF). Various physico-chemical properties were investigated in order to explore potential links between the observed findings and the physical properties of the resultant coating.

Particle size of latices and inorganic additives used in decorative coatings were studied using various FFF techniques coupled to an array of detectors, refractive index (RI), dynamic light scattering (DLS), multiangle laser light scattering (MALLS), ultraviolet (UV) and mass spectrometry (MS). Average particle size and particle size distribution from flow FFF (AF4) and sedimentation (SdFFF) had correlations with each other in comparison to DLS. Additional particle populations, which may be due to secondary reactions during synthesis of these particles, could be identified. Mixtures of latex and TiO_2 particles were tested with an online AF4 - Inductively Coupled Plasma – Mass Spectrometry (ICP-MS) system to investigate the separation power of AF4. The organic latex particles and the inorganic TiO_2 particles could be separated with high resolution using AF4 coupled to UV, MALLS, and ICP-MS.

Molar mass, branching and gel-content of latices used in decorative coatings were explored by comparing SEC and AF4. The outcome pointed towards AF4 having more information-rich outcomes compared to SEC. Larger molar masses were observed using AF4 in comparison to SEC. Conformational plots provided more information on branching within acrylic and styrene-acrylic latices as a function of time during free radical polymerization.

An interaction study between latices and TiO_2 particles using AF4 were conducted to investigate opportunities to minimize TiO_2 content in a typical decorative coating formulation. An in-house synthesized sample were compared against a supplier sample focusing on various latex – to – TiO_2 ratios, as well as the effect of ultrasonication on the retention time of latex and TiO_2 fractograms. Fractionation into narrow fractions and coupling to detection to ICP-MS indicated that the chemical nature of the latex particles as well as the ratio between latex and TiO_2 particles has an effect on the overall quantity of the detected TiO_2 particles. Furthermore, ultrasonication prior to FFF analyses resulted in latex and TiO_2 peaks shifting to earlier retention times, an indication that sonication assist in breaking up large particle agglomerates into smaller and uniform particle populations.

Opsomming

Dekoratiewe deklae is teenwoordig en vervul 'n belangrike rol in alle industrieë vanaf dekor, konstruksie, medikasie, tekstiele, vervaardiging, verpakking en houtwese. Die rou materiale wat in deklae gebruik word, speel 'n sleutelrol om te presteer en om sekere funksies te verrig, bv. afwerking, gevoel, (glans of mat), ultravioletbeskerming teen kleurvervaging, weerstand teen skrape, vlekke en krake. Water-gebaseerde dekoratiewe deklae is krities gekarakteriseer deur gebruik te maak van klassieke grootte-uitsluitingschromatografie (SEC) sowel as veldvloeifraksionering (FFF). Verskeie fisies-chemiese eienskappe is ondersoek om moontlike skakels tussen die genoteerde bevindinge en fisiese eienskappe van die deklae te bewerkstellig.

Partikelgrootte van latekspartikels en anorganiese toevoegings in dekoratiewe deklae is bestudeer deur verskillende veldvloeifraksioneringstegnieke gekoppel aan multidetektors bv. brekingsindeks (RI), dinamiese ligverstrooiing (DLS), multihoek-laserligverstrooiingsdetektors (MALLS), ultraviolet (UV) en massa spektroskopie. Gemiddelde partikelgrootte en partikelgrootteverspreiding vanaf vloei-veldvloeifraksionering en sedimentvloeifraksionering het korrelasies getoon in vergelyking met dinamiese ligverstrooiing. Addisionele partikelpopulasies, wat moontlik toegeskryf kan word aan sekondêre reaksies gedurende sintese van hierdie partikels, is geïdentifiseer.

Gemengde lateks en titaandioksied (TiO_2) partikels is getoets met 'n aanlyn, onsimmetriese vloei-veldvloeifraksionering (AF4), induksie gekoppelde plasma spektroskopie massa spektrometrie (ICP-MS) sisteem om die skeidingskrag van AF4 te evalueer. Die organiese latekspartikels en die anorganiese TiO_2 partikels kon geskei word met hoë resolusie AF4 gekoppel aan UV, MALLS en ICP-MS.

Molekulêre massa, vertakking en die gelinhoud van latekse wat gebruik word in dekoratiewe deklae is bestudeer deur SEC sowel as AF4 met mekaar te vergelyk. Die uitkoms het daarop gedui dat AF4 beter resultate gelewer het in vergelyking met SEC; hoër molekulêre massas is gelewer met AF4 in vergelyking met SEC.

Grafieke wat die strukturele samestelling aandui, het meer insig verskaf met betrekking tot die vertakking van akrilaat sowel as stireenakrilaat as 'n funksie van retensietyd gedurende die vrye-radikaalpolimerisasie. 'n Studie van die interaksie tussen latekse en TiO_2 partikels met AF4 is uitgevoer om die moontlike vermindering van TiO_2 in 'n tipiese deklaagformulasie te bestudeer. 'n In-huis gesintetiseerde monster is getoets teenoor 'n monster van 'n verskaffer deur verskillende lateks – tot – TiO_2 verhoudings te vergelyk, sowel as die impak van ultrasonikasie op die retensietye van die lateks en TiO_2 fraktogramme. Fraksionering in nou fraksies en die koppeling met ICP-MS toon dat die chemiese natuur van die latekspartikels sowel as die verhouding tussen die lateks en TiO_2 partikels 'n rol speel in die hoeveelheid waargeneemde TiO_2. Ultrasonikasie gevolg deur FFF analiese het verder

getoon dat die lateks en TiO_2 pieke na vroeër retensietye geskuif het; 'n aanduiding dat sonikasie 'n rol speel in die opbreking van groot partikelagglomerasies in kleiner, meer uniforme partikelbevolkings.

.

Table of Contents

List of Figures

List of Tables

List of Abbreviations

AF4	asymmetric flow field-flow fractionation (room temperature)
ANOVA	analysis of variance
CE	capillary electrophoresis
DDI	double distilled deionized
D_h	nominal diameter
DI	dispersity index
DLS	dynamic light scattering
Dn/dc	specific refractive index increment
DRI	differential refractive index
DSC	differential scanning calorimetry
FFF	field-flow fractionation
GC	gas chromatography
HDC	hydrodynamic chromatography
HPLC	high performance liquid chromatography
ICP-MS	inductively Coupled Plasma – Mass Spectrometry
MAA	methacrylic acid
MALLS	multiangle laser light scattering
MMA	methyl methacrylate
MMD	molar mass distribution
MS	mass spectrometry
M_w	weight average molar mass
n-BA	n-butyl acrylate
NIST	National Institute of Standards and Technology
ppq	parts per quadrillion

ppt	parts per trillion
PSD	particle size distribution
PVC	pigment volume concentration
PWHH	peak width at half height
R_g	radius of gyration
R_h	hydrodynamic radius
RI	refractive index
SBR	styrene-butadiene rubbers
SdFFF	sedimentation field-flow fractionation
SEC	size exclusion chromatography
SLS	static light scattering
SP-ICP-MS	single particle ICP-MS
Sty	styrene
TEM	transmission electron microscopy
T_g	glass transition temperature
THF	tetrahydrofuran
ThFFF	thermal field-flow fractionation
TiO_2	titanium dioxide
UV	ultraviolet

List of Symbols

A_2	second virial coefficient
c	concentration of analyte (mg/mL)
d	diameter of molecule/particle (nm)
D	diffusion coefficient (m^2/s)
dn/dc	specific refractive index increment (mL/g)
G	gravitational force
k_b	Boltzmann constant (J/K^{-1})
K*	optical constant
m’	effective mass of the particle
M	molar mass of analyte (g/mol)
N_A	avogadro’s number
n_o	refractive index of the mobile phase
P(θ)	particle scattering function
R_h	hydrodynamic radius (nm)
R	retention ratio
R_θ	Rayleigh ratio
T	temperature (K)
T_{gi}	glass transition of homopolymer *i* in the copolymer (˚C)
w_A	weight fraction of monomer *A* in the total copolymer
w_B	weight fraction of monomer *B* in the total copolymer
w_i	weight fraction of the specific monomer *i* in the total copolymer
t^o	retention time of an unretained component or void time (min)
t_r	retention time of analyte (min)
U	flow induced field

V_c	flow rate of the cross flow (mL/min)
V^o	void volume of the FFF channel (cm^3)
V_p	volume of particle (cm^3)
w	width or thickness of the channel (cm)
$\Delta\rho$	difference in density between particle and mobile phase (kg/cm^3)
η	viscosity of mobile phase (g/cm^3)
λ_0	wavelength of the incident light (nm)
π	pi

Chapter 1: Introduction and objectives

1.1 Introduction

Polymers used in coatings and paint formulations consist of complex mixtures of hydrophilic/hydrophobic copolymers, latex particles and polyelectrolytes to name a few [1,2].

Decorative coatings in specific perform an important function in aesthetics and protection against weathering such as UV, stains, scratches in various households, office spaces, and automotive industries [1,3]. Of specific interest are the film forming species in coatings such as latices and their molecular properties, in particular the molar mass and particle size of these species. The synergistic effects these species have with other organic species and their interactions with inorganic species are important and complex.

Designated characterization techniques are important for 1) separation and identification of additives, 2) determination of molar mass and gel content, 3) determination of particle size and particle size distribution and 4) separation of organic and inorganic constituents for detailed interpretation and correlation of the coating constituents to structure-property relationships.

Field-flow fractionation (FFF) has proven to be a suitable technique as a complementary method to address possible limitations encountered in column chromatography since an empty channel is used instead of a stationary phase [4]. By coupling the FFF system to an array of detectors such as light scattering, refractive index and UV detectors, physico-chemical information may be obtained on molar mass, and the presence or absence of insoluble cross-linked material [5,6]. Furthermore, coupling of FFF with spectroscopic techniques such as inductively coupled plasma mass spectrometry (ICP-MS), yields elemental information on the species present in coatings, e.g. titanium dioxide (TiO_2). The characterization of such complex organic-inorganic mixtures is a major challenge and cannot be conducted by column-based chromatography alone. The advantage of coupling a separation method such as FFF to ICP-MS is that organic and inorganic species can be analysed simultaneously and opens up a myriad of possibilities from inorganic particle count and quantification of materials within a complex matrix.

1.2 Objectives

The objective of the study was to investigate water-based decorative coatings in order to address different species typically found in complex formulations.

The aim of the study was to characterize organic and inorganic components of decorative coatings qualitatively utilizing FFF coupled to a multitude of detectors to access specific properties which can be related back to the final properties of an applied coating. The specific focus areas were particle size analyses by FFF-UV-RI, AF4 and SdFFF in comparison to DLS results. Another focus area was the molar mass determination of latices comparing SEC with FFF. Furthermore FFF will be used as a tool to separate organic and inorganic species from each other. Both FFF techniques (AF4 and SdFFF) can potentially be coupled to a multidetector system.

1.3 Layout of thesis

Chapter 2

The basic components of a typical coating system and their respective roles in decorative coatings are briefly discussed. The importance of characterization in coatings is highlighted. The different samples used in the study will be introduced and the experimental procedure of the synthesis of the samples will be briefly outlined. The theories and mechanisms used for the characterization techniques used in this study will be briefly introduced before discussing specific results. Field-flow fractionation (FFF) and size exclusion chromatography (SEC) were the basic separation techniques used in the study with detectors such as multiangle laser light scattering (MALLS), ultraviolet (UV), refractive index (RI) and inductively coupled plasma mass spectrometry (ICP-MS) detectors revealing different properties of the analysed species.

Chapter 3

In this chapter the particles size and particle size distribution of the produced latices are investigated. The importance of particle size analysis in coating formulations is discussed and two modes of FFF, asymmetric flow field-flow fractionation (AF4) and sedimentation field-flow fractionation (SdFFF) are compared to the classical particle size analysis method dynamic light scattering (DLS).

Chapter 4

In this chapter SEC and FFF are compared with the aim of evaluating the novel FFF technique in comparison to classical analytical techniques to determine molar mass and size of different types of latices used in coatings. The presence or absence of gel species is also investigated.

Chapter 5

The separation and characterization of model complex mixtures of organic and inorganic species by FFF is discussed in this chapter. Particle-particle interactions are investigated by analyzing different latex – to – TiO_2 ratios followed by AF4 analyses, collection of fractions and offline ICP-MS analyses. The effect of ultrasonication upon mixing the latex and TiO_2 particles is briefly investigated.

Chapter 6

An overall summary of the results presented in Chapters 3 to 5 is briefly summarized in this chapter, highlighting the different samples and techniques used for the characterization of organic and inorganic constituents in decorative coatings. A short recommendation for future work will be discussed.

1.4 References

[1] J.V. Koleske, Paint and Coating Testing Manual, ASTM International, 1995.

[2] E. Hagan, A. Murray, Effects of Water Exposure on the Mechanical Properties of Early Artists' Acrylic Paints, MRS Online Proceedings Library, 852 (2004) 41-47.

[3] D. Cameron, Introduction to Films and Coatings: Technology and Recent Development, Comprehensive Materials Processing 4 (2014) 1.

[4] F.A. Messaud, R.D. Sanderson, J.R. Runyon, T. Otte, H. Pasch, S.K.R. Williams, An overview on field-flow fractionation techniques and their applications in the separation and characterization of polymers, Prog. Polym. Sci. 34 (2009) 351-368.

[5] S. Podzimek, P. Lebeda, C. Johann, D. Horak, D. Sponarova, Asymmetric Flow Field-Flow Fractionation: Characterization of Polymers That Are Difficult to Analyze With SEC-GPC, Am. Lab. 28 (2009) 1-5.

[6] S. Podzimek, J. Machotova, J. Snuparek, M. Vecera, L. Prokupek, Characterization of molecular structure of acrylic copolymers prepared via latex polymerization using A4F-MALS technique, J. Appl. Polym. Sci. 131 (2014) 40995.

Chapter 2: Historical and theoretical background

2.1 Water-based decorative coatings

2.1.1 Where it all started

Coatings, decorative coatings or paint have been around since prehistoric times for more than 35 000 years. The first coating was discovered by ancient pre-historic men when chalk and pigments were incorporated with fats obtained from hunting animals. The pigment-fat mixture was applied inside cave walls to illustrate their way of life. The Egyptians later discovered different colour pigments and started using waxes instead of fat resulting in a more spreadable paint mixture. The Greeks improved the recipe even further incorporated hot waxes to obtain a thicker paint paste, and making it possible to make blends of coloured paste possible. These discoveries were all done up to 1000 BC.

It is not until the 18th century when the first mass production of paints occurred in Europe and America, slashing paint prices to more affordable levels. It only became common in the 19th century that households started to be painted due to the paint's increased affordability [1,2].

2.1.2 Typical constituents of decorative coatings

A typical decorative coating formula consists of a film forming species or binder, pigments and additives.

The binder type has a very important role to play and affects many different physical properties of the final coating on the substrate. Solvent-based coatings typically consist of resins such as epoxy resins, urethane resins or alkyd resins, typically prepared by polycondensation of a polyol and functional fatty acids, epoxides or phthalics. These resins are typically dissolved in solvents such as xylene and are less environmentally friendly compared to water-based latices. For years solvent-based coatings have been classified as superior to water-based coatings with respect to physical properties [1,3].

In recent years water-based coatings have been developed and formulated to similar qualities compared to solvent-based coatings. The advantages of such coatings are reduced solvent fumes which has several health and environmental benefits due to the absence or reduction of harmful volatiles. The most common water-based binders are latexes prepared via free radical polymerization [4]. Different monomers have been used e.g. styrene, methyl methacrylate, butyl acrylate, methacrylic acid, 2-ethylhexyl acrylate to name a few. Copolymerization of these monomers is typically used with up to four different monomers being present in latex systems. The monomer ratios are selected in such a manner that the latex particles are able to form films at room temperature, i.e. the glass transition temperature (T_g) should typically be below room temperature and is calculated using the Flory-Fox equation from the T_g's of each individual homopolymer in equation 2.1:

$$\frac{1}{T_{g(copolymer)}} = \frac{w_1}{T_{g1}} + \frac{w_2}{T_{g2}} + ... + \frac{w_i}{T_{gi}} \qquad (2.1)$$

where the individual polymer is denoted by T_{gi} and w_i is the weight fraction of the specific monomer in the total copolymer composition [5].

The basic mechanism of such a free radical latex polymerization reaction is displayed in **Figure 2.1** [6]. The constituents needed for latex polymerization are initiators, surfactants, monomers, buffers and the carrier liquid. The initiators are usually peroxides, persulphates or azo-based components [1,4]. Surfactants are required to form micelles with the monomer droplets and also act as stabilizer keeping the formed polymer particles in a stable dispersion. The surfactants may be ionic, non-ionic or polymeric in nature [7]. The carrier is usually water with the percentage solids of the formed latex particles ranging from as low as 1% solids up to high solids of approximately 50 % [7].

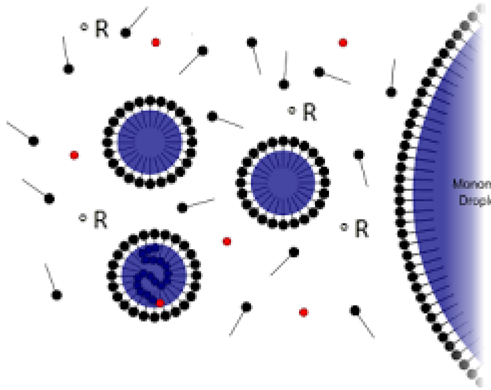

Figure 2.1. Schematic of free radical latex polymerization indicating the monomer droplet, micelles of surfactants and surfactant stabilized polymeric particles, respectively [6].

The choice of monomer used in latex polymerization plays a direct role in the final physical properties when incorporated in a water-based coating. Coatings containing pure acrylic latices typically impart superior physical properties such as stain resistance and yellowing resistance as compared to styrene-acrylic latex containing coatings [8]. The final latex species are typically post-treated with radical scavengers to make sure that any residual initiator molecules do not further polymerize which would result in unwanted side reactions.

The second and third constituents of decorative coatings are pigments and additives, respectively. Pigments such as TiO_2 and colorants (organic and inorganic) impart the final colour of the coating and together with additives such as rheology modifiers, antifouling agents, dispersants and defoamers a complex matrix is formed with the binder or latex particles. Upon application, the binder forms a continuous film on the applied substrate with all the pigments and additives due to the binder particles diffusing or coalescing with each other [1]. The quality of the binder plays a big role in the durability of the coating as well as the pigment volume concentration (PVC) which determines how often the consumers have to re-coat a surface. Low PVC means that the pigment volume-to-binder ratio is low; therefore, there are not enough pigment particles to cover the substrate sufficiently [1]. A high PVC coating has a higher pigment-to-binder ratio, hence sufficient pigment particles are present to cover the substrate sufficiently. On a typical substrate less layers of a high PVC product are required in comparison to the low PVC product, given that the solids content of both coatings are similar. **Figure 2.2** displays the differences between a high and low PVC paint.

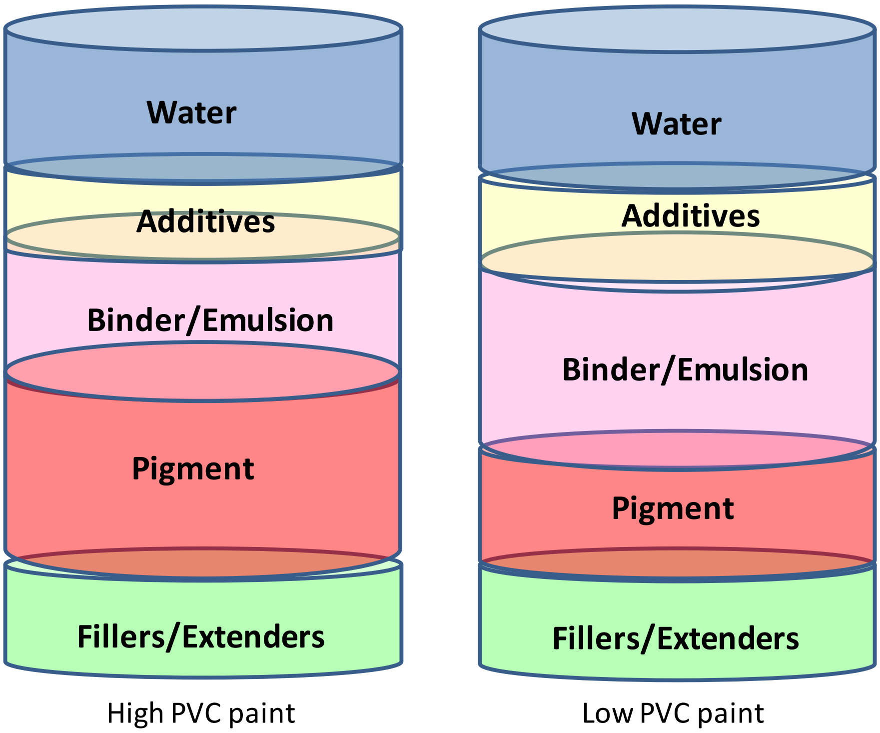

Figure 2.2. Illustration of high and low PVC paints. A high PVC product has more binder and pigment compared to a low PVC paint product.

The particle size of the binder particles together with their interaction with the rest of the coating constituents have a critical function to perform. The particle plays an important role in film formation on the applied substrate. The fusion of particles with each other will affect physical properties such as stain resistance and scratch resistance [9,10]. Together with molar mass which plays a role in toughness as well as resistance to leaching of low molar mass, additives also contribute to the durability of the final coating [11].

Prevention of settlement within a coating system is of importance and affects long term stability and effectiveness of final application. The balance of additive-latex particles with pigment particles within a coating is key and neglecting these interactions during formulation of a coating could affect the final coating properties, specifically the coverage or hiding power and colour strength. Agglomerated particles can affect the appearance of the final coat, i.e. gloss levels, therefore it is important that the primary particle sizes are reached upon mixing the coating constituents [12-14].

The particle size and molar mass analyses using FFF fractionation techniques coupled to a multidetector system are discussed in Chapters 3 and 4, respectively. Particle-particle interaction studies are discussed in Chapter 5, focusing on various latex – to – TiO_2 mixing ratios, followed by fractionation and offline ICP-MS analyses.

2.2 Fractionation techniques used in decorative coatings.

Addressing properties such as molar mass, size as well as the presence of gel are of interest in understanding the eventual performance of the film forming species. The initial determination of molar mass is classically performed by SEC [15-17]. A molar mass sensitive detector or relative calibration with known standards is used to determine molar mass values. Several authors have investigated high molar mass species by SEC and found that anomalies and inaccuracies may arise due to the interaction of the macromolecular chains with the stationary phase of the columns.

An example of these anomalies is the late elution phenomenon where the authors claim that due to topology differences such as branching, higher molar mass species elute together with normal linear analogues of lower molar masses [18-23]. A further study of the observed behaviour was conducted on branched polybutadienes by fractionation of the late eluting fraction after SEC injection. The collected fractions were re-injected into an open channel fractionation technique, field-flow fractionation. The determined molar mass of the late eluting fraction contained species of a higher molar mass [19]. Therefore, SEC does have potential limitations and other fractionation techniques, with field-flow fractionation as a novel replacement or complementary characterization technique of choice, are of interest.

Since its discovery by J. Calvin Giddings in 1966, field-flow fractionation (FFF) has been investigated extensively over the years and several publications have proven that FFF is a novel technique for the characterization of polymers and colloids [24-28].

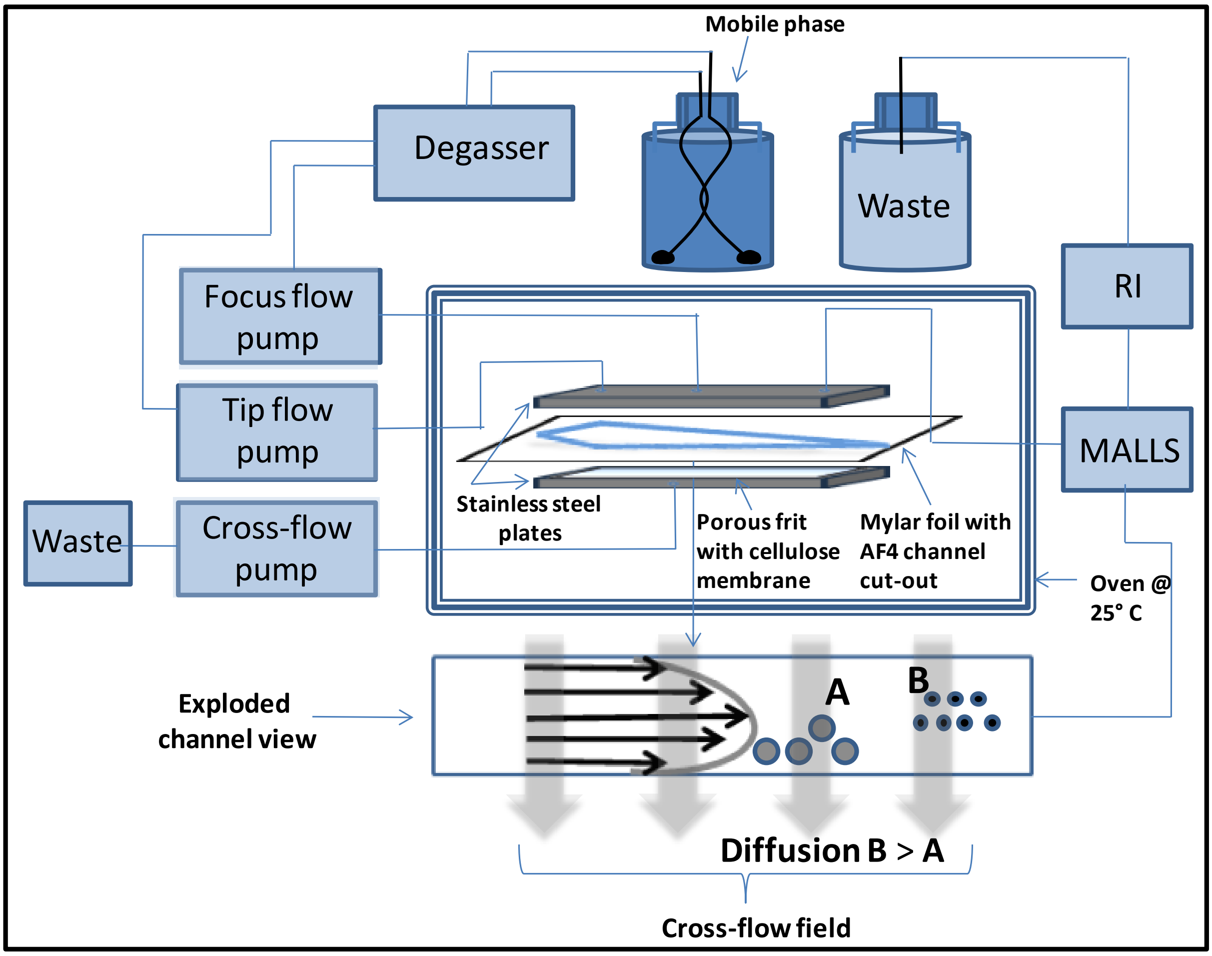

Figure 2.3. AF4 instrumentation setup with a cross-section view of the channel at the bottom [19]. The channel may be a rotational sedimentation FFF channel or thermal FFF channel.

FFF offers the possibility to characterize various samples, ranging from high molar mass macromolecules as well as colloids with particle sizes in the nanometer to micrometer range with high resolution [29-32]. An external force field is applied perpendicular to the FFF channel's longitudinal flow [29,31,32]. In flow FFF (AF4), separation takes place according to differences in diffusion coefficients, whereas in thermal FFF (ThFFF) separation is achieved due to differences in thermal diffusivity and diffusion coefficient [29]. Diffusion coefficient and density differences are the main physico-chemical differences in sedimentation FFF (SdFFF) [29]. AF4, ThFFF and SdFFF are used increasingly and have been commercialized.

The principles of field-flow fractionation have been reported on numerous occasions [17,29] and a basic schematic of the instrument setup is depicted in **Figure 2.3** [33].

2.3 Detectors used in characterization of decorative coatings.

Fractionation techniques are coupled to at least one detector which yields a single property relating to the analyte of interest. The junction of a number of detectors after fractionation is more valuable since a number of physico-chemical properties can be addressed in one single measurement.

2.3.1 Differential refractive index (DRI) and ultraviolet (UV) detectors

Differential refractive index detectors are typically used to track the concentration of the analyte of interest after separation using columns (SEC or HPLC) or channels (AF4, SdFFF or ThFFF). It is a universal detector which is linearly dependent upon an increase in concentration in the analyte species. The specific refractive index increment (dn/dc) values are also of importance in DRI detection with respect to molar mass calculations since different macromolecules have different dn/dc values depending on the solvent used in which the polymeric species are dissolved in [34]. The dn/dc value is used when a RI detector is coupled to a multiangle laser light scattering detector (MALLS) to determine absolute molar mass values [35].

UV detectors are commonly used to monitor chromophore species in solution, e.g. polystyrene is typically monitored at a wavelength of 254 nm since the maximum absorbance takes place at this wavelength.

The molar absorptivity coefficient is determined by plotting concentration as a function of UV response. The slope of the regression line is proportional to the coefficient in question and may be used for molar mass determination in combination with a MALLS detector [36].

2.3.2 Multiangle laser light scattering detection (MALLS)

MALLS detectors are normally used for the determination of absolute molar masses of polymeric species. MALLS and RI or UV coupling are powerful detector combinations to obtain molar mass, size and branching information of macromolecules in solution. The applicability to colloids is also crucial especially for the determination of the particle size of these dispersed particles. The use of an RI detector requires the dn/dc value, the wavelength at which the dn/dc value was determined as well as the temperature of the experiment. The incorporation of a UV detector requires the molar absorptivity coefficient to determine molar mass. The absorbtivity is a function of the solvent in which the experiment is conducted, the wavelength, chemistry of analyte and temperature at which the experiment is conducted.

Light scattering detectors are categorized as either dynamic or static. The particle size determined by batch dynamic light scattering (DLS) gives an average size value based on one detector angle (e.g.

backscattering 173 ° angle) and is a fast and simple way of determining the *z*-average particle size of colloidal species or macromolecules in solution. It does not, however, provide comprehensive information on particle size distribution (PSD) since the dispersity index (DI) in this case only indicates the spread of the particle sizes [37-39].

Nucleation and particle growth mechanisms during free radical latex polymerization are often deduced based on DLS measurements. In DLS, particle size information at the lower size range (e.g. to address secondary particle nucleation in free radical latex polymerization) is suppressed in favour of larger particles due to insufficient size resolution [37]. Small amounts of small particles or molecules may therefore not be detected due to the presence of large particles or molecules which scatters light a lot stronger in comparison to smaller particles. For detailed and reliable information of the actual particle size and PSD, a suitable fractionation according to size is required, the combination of separation and analysis within one method being the key.

Static light scattering has more angles to assist with determination of size and molar mass. Low angle, right angle, dual angle and multiangle laser light scattering detectors are commercially available. The governing equation determining size and molar mass between static light scattering DLS and SLS are displayed in Equations 2.2 to 2.4, respectively. An illustration of DLS and SLS is depicted in **Figure 2.4.**

In principle, DLS characterizes the Brownian motion of particles in solution, and correlates this motion to particle size. According to the Stokes−Einstein equation, the diffusion coefficient is related to the hydrodynamic radius (R_h) of the particle:

$$R_h = \frac{k_b T}{6\Pi \eta D} \qquad (2.2)$$

where η is the solution's viscosity (Pa.s) at temperature T (K) at which the measurement took place and k_b ($J{\cdot}K^{-1}$) is the Boltzmann's constant [17,40].

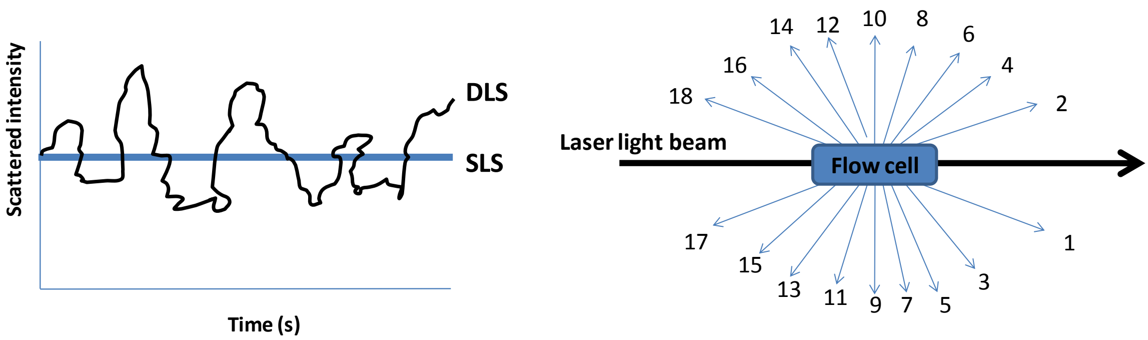

Figure 2.4. An illustration of A) scattering intensity in DLS and SLS, and B) depiction of an 18-angle MALLS detector [33].

The Debye equation is the most commonly used equation for light scattering analysis:

$$\frac{R_\theta}{K^* c} = M_w P(\theta) - 2A_2 c M_w{}^2 P^2(\theta) \qquad (2.3)$$

where R_θ is the Rayleigh ratio, K* is an optical constant, c (mg/mL) is the polymer concentration in solution, M (g/mol) is the molar mass of the analyte, P(θ) is the particle scattering factor (function of angular dependence) and A_2 is the second virial coefficient. The optical constant is:

$$K^* = \frac{4\pi^2 n_0^2}{\lambda_0^4 N_A} \times \left(\frac{dn}{dc}\right)^2 \qquad (2.4)$$

where n_o is the refractive index of the solvent, dn/dc the specific refractive index increment, λ_0 is the vacuum wavelength of the incident radiation and N_A Avogadro's number [17,41,42]. A_2 provides an indication of the thermodynamic quality of the solvent and is equal to positive for good solvents, negative for poor solvents and zero for theta solvents. A_2 is a function of the solvent in which the analyte is dissolved as well as the temperature at which the experiment is conducted.

The particle function P(θ) is a function of size (RMS), the angle between incident and scattered light (θ), as well as the incident wavelength (λ), as displayed in equation 2.5. [17].

$$P(\theta) = 1 - (16\pi^2 / 3\lambda^2)\langle r_{rms}\rangle^2 \sin^2(\theta/2) \qquad (2.5)$$

Upon substituting P(θ) into equation 2.3 the resultant equation is given in 2.6:

$$\frac{R_\theta}{K^* c} = M_w(1 - (16\pi^2 / 3\lambda^2)\langle r_{rms}\rangle^2 \sin^2(\theta/2)) \qquad (2.6)$$

By plotting R_θ/K^*c vs. $\sin^2(\theta/2)$, molar mass and information regarding R_g can be obtained. The intercept of each plot extrapolated to the zero angle (θ=0) is proportional to M_w while the slope of the obtained plot is related to R_g. In addition, information regarding molar mass and radius averages as well as their distributions can be obtained by coupling LS and RI to a separation system such as SEC or FFF.

Conformational information such as the degree of branching can also be deduced using a conformational plot which is a logarithmic plot of R_g vs. molar mass. The slope of the conformation plot has values between 0 and 1. A typical linear random polymer coil in solution has a slope of 0.588 [43]. If branching is present in the polymer chains in a good solvent, the slope decreases to lower values.

2.3.2 Inductively coupled plasma spectrometry ICP-MS

Trace analyses of inorganic elements in complex matrices is of significant importance in many fields, especially in cosmetic, food, environmental, life sciences and forensic investigations [44]. The advantage of identification and quantification using traceable standards at low levels down to parts per trillion (ppt) and even parts per quadrillion (ppq) at high spectral resolution are advantageous in these research fields. ICP-MS has relatively low sensitivities towards salts, therefore coupling the technique with a separation technique such as HPLC or FFF makes it versatile and even more powerful with respect to in-depth characterization and resolution [45]. Offline ICP-MS or single particle ICP-MS (SP-ICP-MS) can be utilized as well as online coupling with a separation technique such as FFF as depicted in **Figure 2.5**.

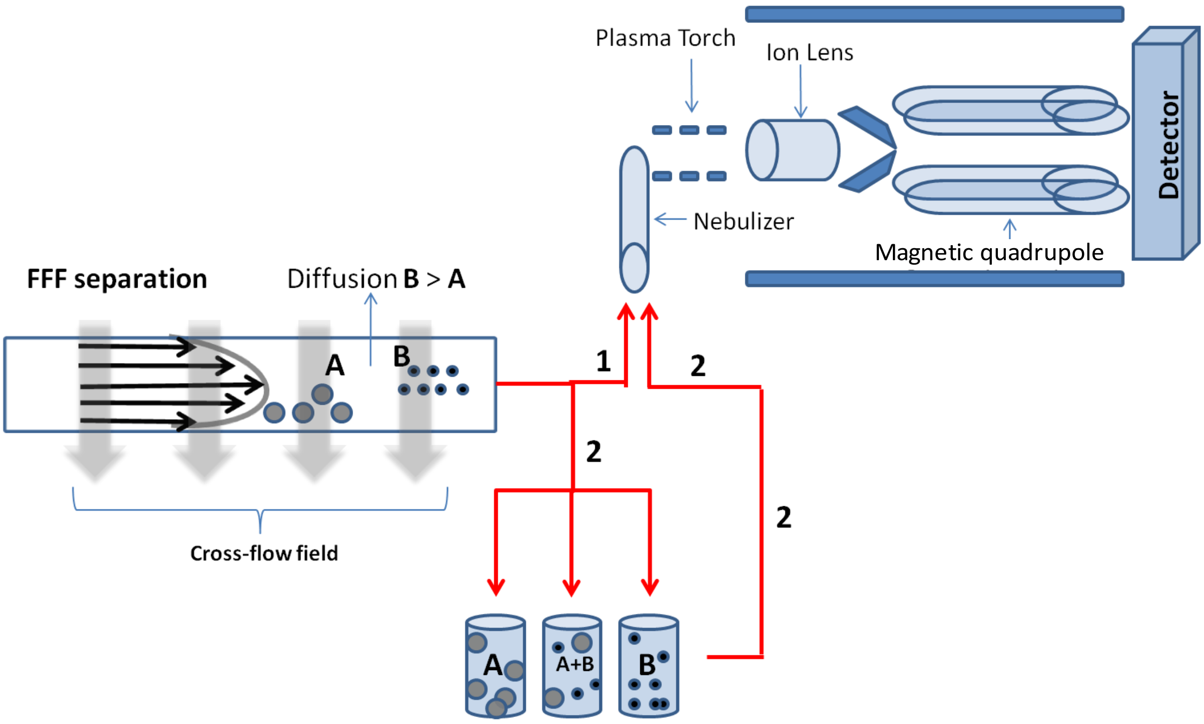

Figure 2.5. FFF-ICP-MS setup in two different modes: 1) Online coupling of AF4 coupled directly to the ICP-MS interface, 2) Manually collected fractions, followed by offline-ICP-MS analyses.

High performance liquid chromatography (HPLC), gas chromatography (GC), capillary electrophoresis (CE) and hydrodynamic chromatography (HDC) coupled to ICP-MS have been studied by various research groups [44,46].

FFF has also attracted much interest, especially from a food, cosmetic and environmental perspective. The study of FFF-ICP-MS of TiO_2 containing species ranges from food and cosmetics where different FFF techniques, mainly AF4 and SdFFF have been applied in recent years [45,47-54].

Nischwitz et al. studied TiO_2 content in sunscreens using AF4-ICP-MS [45], while Kim used SdFFF to study the behaviour of anatase and rutile under a gravitational field [47]. Mitrano and Loeschner conducted AF4-ICP-MS studies on silver nanoparticles, focusing on recoveries and the effects of various FFF parameters on the size information of the nanoparticles [52,55].

The use of ICP-MS complementary to other characterization techniques provide a novel dimension to deciphering known and unknown inorganic species in difficult to analyse sample matrices.

2.4 References

[1] O.C.C. Association, Surface Coatings: Volume 1 Raw Materials and Their Usage, Springer Netherlands, 1993.

[2] D. Cameron, Introduction to Films and Coatings: Technology and Recent Development, Comprehensive Materials Processing 4 (2014) 1.

[3] J.V. Koleske, Paint and Coating Testing Manual, (Gradner-Sward Handbook, 14th Edition), American Society of Testing and Materials, Philadelphia, PA, Color Research & Application 20 (1995) 48-49.

[4] J.M. Asua, Emulsion polymerization: From fundamental mechanisms to process developments, J. Polym. Sci., Part A: Polym. Chem. 42 (2004) 1025-1041.

[5] L. An, D. He, J. Jing, Z. Wang, D. Yu, B. Jiang, Z. Jiang, R. Ma, Effects of molecular weight and interaction parameter on the glass transition temperature of polystyrene mixtures and its blends with polystyrene/poly (2,6-dimethyl-p-phenylene oxide), Eur. Polym. J. 33 (1997) 1523-1528.

[6] H. Berber, in: D.F. Yılmaz (Ed.), Intech, Available from: http://www.intechopen.com/books/polymer-science/emulsion-polymerization-effects-of-polymerization-variables-on-the-properties-of-vinyl-acetate-based, 2013.

[7] M. Okubo, M. Nomura, H. Tobita, K. Suzuki, Polymer Particles, Springer Berlin Heidelberg, 2005, p. 1-128.

[8] J.V. Koleske, Paint and Coating Testing Manual, ASTM International, 1995.

[9] A. Sood, Particle size distribution control in emulsion polymerization, J. Appl. Polym. Sci. 92 (2004) 2884-2902.

[10] M. do Amaral, A. Roos, J.M. Asua, C. Creton, Assessing the effect of latex particle size and distribution on the rheological and adhesive properties of model waterborne acrylic pressure-sensitive adhesives films, J. Colloid Interface Sci. 281 (2005) 325-338.

[11] E. Hagan, A. Murray, Effects of Water Exposure on the Mechanical Properties of Early Artists' Acrylic Paints, MRS Online Proceedings Library, 852 (2004) 41-47.

[12] S. Farrokhpay, A review of polymeric dispersant stabilisation of titania pigment, Adv. Colloid Interface Sci. 151 (2009) 24-32.

[13] F. Karakaş, M.S. Çelik, Effect of quantity and size distribution of calcite filler on the quality of water borne paints, Prog. Org. Coat. 74 (2012) 555-563.

[14] M.P. Diebold, A Monte Carlo determination of the effectiveness of nanoparticles as spacers for optimizing TiO_2 opacity, Journal of Coatings Technology and Research 8 (2011) 541-552.

[15] H.G. Barth, B.E. Boyes, C. Jackson, Size Exclusion Chromatography and Related Separation Techniques, Anal. Chem. 70 (1998) 251-278.

[16] S. Mori, M. Ishikawa, Molecular Weight-Retention Volume Relation for Narrow and Broad Polystyrenes by Size Exclusion Chromatography Equipped With a Light Scattering Detector, Journal of Liquid Chromatography & Related Technologies 21 (1998) 1107-1117.

[17] S. Podzimek, Light Scattering, Size Exclusion Chromatography and Asymmetric Flow Field Flow Fractionation: Powerful Tools for the Characterization of Polymers, Proteins and Nanoparticles, John Wiley & Sons, New York, 2011.

[18] M. Wintermantel, M. Antonietti, M. Schmidt, Structure Determination of Polymers by SEC Equipped with Multiangle Light Scattering, J. Appl. Polym. Sci.: Appl. Polym. Symp. 52 (1993) 91-103.

[19] A.C. Makan, T. Otte, H. Pasch, Analysis of High Molar Mass Branched Polybutadienes by SEC-MALLS and AF4-MALLS, Macromolecules 45 (2012) 5247-5259.

[20] T. Otte, H. Pasch, T. Macko, R. Brüll, F.J. Stadler, J. Kaschta, F. Becker, M. Buback, Characterization of branched ultrahigh molar mass polymers by asymmetrical flow field-flow fractionation and size exclusion chromatography, J. Chromatogr. A 1218 (2011) 4257-4267.

[21] T. Otte, T. Klein, R. Brüll, T. Macko, H. Pasch, Study of the abnormal late co-elution phenomenon of low density polyethylene in size exclusion chromatography using high temperature size exclusion chromatography and high temperature asymmetrical flow field-flow fractionation, J. Chromatogr. A 1218 (2011) 4240-4248.

[22] E.P.C. Mes, H. de Jonge, T. Klein, R.R. Welz, D.T. Gillespie, Characterization of high molecular weight polyethylenes using high temperature asymmetrical flow field-flow fractionation with on-line infrared, light scattering, and viscometry detection, J. Chromatogr. A 1154 (2007) 319-330.

[23] S. Podzimek, The use of GPC coupled with a multiangle laser light scattering photometer for the characterization of polymers. On the determination of molecular weight, size and branching, J. Appl. Polym. Sci. 54 (1994) 91-103.

[24] J.C. Giddings, J.Y. Frang, M.N. Myers, Flow field-flow fractionation: new method for separating, purifying, and characterizing the diffusivity of viruses, J. Virol. 21 (1977) 131-138.

[25] K.G. Wahlund, J.C. Giddings, Properties of an asymmetrical flow field-flow fractionation channel having one permeable wall, Anal. Chem. 59 (1987) 1332-1339.

[26] J.C. Giddings, Field-Flow Fractionation: Analysis of Macromolecular, Colloidal, and Particulate Materials, Science 260 (1993) 1456-1465.

[27] J.C. Giddings, J. Ho, Accurate Measurement of Density of Colloidal Latex Particles by Sedimentation Field-Flow Fractionation, Langmuir 11 (1995) 2399-2404.

[28] S. Lee, S.P. Rao, M.H. Moon, J.C. Giddings, Determination of Mean Diameter and Particle Size Distribution of Acrylate Latex Using Flow Field-Flow Fractionation, Photon Correlation Spectroscopy, and Electron Microscopy, Anal. Chem. 68 (1996) 1545-1549.

[29] M.E. Schimpf, K. Caldwell, J.C. Giddings, Field Flow Fractionation Handbook, John Wiley & Sons, New York, 2000.

[30] F.A. Messaud, R.D. Sanderson, J.R. Runyon, T. Otte, H. Pasch, S.K.R. Williams, An overview on field-flow fractionation techniques and their applications in the separation and characterization of polymers, Prog. Polym. Sci. 34 (2009) 351-368.

[31] H. Cölfen, M. Antonietti, Field-Flow Fractionation Techniques for Polymer and Colloid Analysis, Adv. Polym. Sci. 150 (2000) 67-187.

[32] J. Janca, Field-flow fractionation, J. Chromatogr. Libr. Volume 51, Part A (1992) A449-A479.

[33] Ashwell C. Makan, Chemistry and Polymer Science, Asymmetric Flow Field Flow Fractionation (AF4) of Polymers with Focus on
Polybutadienes and Polyrotaxanes, Stellenbosch, 2012.

[34] http://www.iisrp.com/WebPolymers/00Rubber_Intro.pdf.

[35] S. Maezawa, T. Takagi, Monitoring of the elution from a high-performance gel chromatography column by a spectrophotometer, a low-angle laser light scattering photometer and a precision differential refractometer as a versatile way to determine protein molecular weight, J. Chromatogr. A 280 (1983) 124-130.

[36] D. Cho, S. Park, T. Chang, A. Avgeropoulos, N. Hadjichristidis, Characterization of a 4-miktoarm star copolymer of the (PS-b-PI)3 PS type by temperature gradient interaction chromatography, Eur. Polym. J. 39 (2003) 2155-2160.

[37] H. Hinterwirth, S.K. Wiedmer, M. Moilanen, A. Lehner, G. Allmaier, T. Waitz, W. Lindner, M. Lämmerhofer, Comparative method evaluation for size and size-distribution analysis of gold nanoparticles, J. Sep. Sci. 36 (2013) 2952-2961.

[38] S. Carro, J. Herrera-Ordonez, J. Castillo-Tejas, On the evolution of the rate of polymerization, number and size distribution of particles in styrene latex polymerization above CMC, J. Polym. Sci., Part A: Polym. Chem. 48 (2010) 3152-3160.

[39] S. Carro, J. Herrera-Ordonez, Styrene Emulsion Polymerization above the CMC: New Evidence on Particle Nucleation by means of AFFFF, Macromol. Rapid Commun. 27 (2006) 274-278.

[40] C. Schmitt, B. Grassl, G. Lespes, J. Desbrières, V. Pellerin, S. Reynaud, J. Gigault, V.A. Hackley, Saponins: A renewable and biodegradable surfactant from its microwave-assisted extraction to the synthesis of monodisperse lattices, Biomacromolecules 15 (2014) 856-862.

[41] M. Andersson, B. Wittgren, K.-G. Wahlund, Accuracy in Multiangle Light Scattering Measurements for Molar Mass and Radius Estimations. Model Calculations and Experiments, Anal. Chem. 75 (2003) 4279-4291.

[42] P.J. Wyatt, Mean square radius of molecules and secondary instrumental broadening, J. Chromatogr. A 648 (1993) 27-32.

[43] S. Podzimek, T. Vlcek, C. Johann, Characterization of branched polymers by size exclusion chromatography coupled with multiangle light scattering detector. I. Size exclusion chromatography elution behaviour of branched polymers, J. Appl. Polym. Sci. 81 (2001) 1588-1594.

[44] A.A. Ammann, Inductively coupled plasma mass spectrometry (ICP MS): a versatile tool, J. Mass Spectrom. 42 (2007) 419-427.

[45] V. Nischwitz, H. Goenaga-Infante, Improved sample preparation and quality control for the characterisation of titanium dioxide nanoparticles in sunscreens using flow field-flow fractionation on-line with inductively coupled plasma mass spectrometry, J. Anal. At. Spectrom. 27 (2012) 1084-1092.

[46] E.P. Gray, T.A. Bruton, C.P. Higgins, R.U. Halden, P. Westerhoff, J.F. Ranville, Analysis of gold nanoparticle mixtures: a comparison of hydrodynamic chromatography (HDC) and asymmetrical flow field-flow fractionation (AF4) coupled to ICP-MS, J. Anal. At. Spectrom. 27 (2012) 1532-1539.

[47] S.T. Kim, H.K. Kim, S.H. Han, E.C. Jung, S. Lee, Determination of size distribution of colloidal TiO_2 nanoparticles using sedimentation field-flow fractionation combined with single particle mode of inductively coupled plasma-mass spectrometry, Microchem. J. 110 (2013) 636-642.

[48] I. López-Heras, Y. Madrid, C. Cámara, Prospects and difficulties in TiO_2 nanoparticles analysis in cosmetic and food products using asymmetrical flow field-flow fractionation hyphenated to inductively coupled plasma mass spectrometry, Talanta 124 (2014) 71-78.

[49] C. Claveranne-LamolÃ¨re, G. Lespes, S. Dubascoux, J. Aupiais, F. Pointurier, M. Potin-Gautier, Colloidal transport of uranium in soil: Size fractionation and characterization by field-flow fractionation-multi-detection, J. Chromatogr. A 1216 (2009) 9113-9119.

[50] A.J. Bednar, A.R. Poda, D.M. Mitrano, A.J. Kennedy, E.P. Gray, J.F. Ranville, C.A. Hayes, F.H. Crocker, J.A. Steevens, Comparison of on-line detectors for field flow fractionation analysis of nanomaterials, Talanta 104 (2013) 140-148.

[51] H. Hagendorfer, R. Kaegi, J. Traber, S.F.L. Mertens, R. Scherrers, C. Ludwig, A. Ulrich, Application of an asymmetric flow field flow fractionation multi-detector approach for metallic engineered nanoparticle characterization - Prospects and limitations demonstrated on Au nanoparticles, Anal. Chim. Acta 706 (2011) 367-378.

[52] D.M. Mitrano, A. Barber, A. Bednar, P. Westerhoff, C.P. Higgins, J.F. Ranville, Silver nanoparticle characterization using single particle ICP-MS (SP-ICP-MS) and asymmetrical flow field flow fractionation ICP-MS (AF4-ICP-MS), J. Anal. At. Spectrom. 27 (2012) 1131-1142.

[53] B. Stolpe, L. Guo, A.M. Shiller, G.R. Aiken, Abundance, size distributions and trace-element binding of organic and iron-rich nanocolloids in Alaskan rivers, as revealed by field-flow fractionation and ICP-MS, Geochim. Cosmochim. Acta 105 (2013) 221-239.

[54] I.C. Regelink, L. Weng, G.F. Koopmans, W.H. van Riemsdijk, Asymmetric flow field-flow fractionation as a new approach to analyse iron-(hydr)oxide nanoparticles in soil extracts, Geoderma 202-203 (2013) 134-141.

[55] K. Loeschner, J. Navratilova, S. Legros, S. Wagner, R. Grombe, J. Snell, F. von der Kammer, E.H. Larsen, Optimization and evaluation of asymmetric flow field-flow fractionation of silver nanoparticles, J. Chromatogr. A 1272 (2013) 116-125.

Chapter 3: Advanced Analysis of Polymer Latices: Particle size and Particle Size Distribution by Field-Flow Fractionation and Dynamic Light Scattering

Journal of Chromatography A, 1442 (2016) 94–106

Contents lists available at ScienceDirect

Journal of Chromatography A

journal homepage: www.elsevier.com/locate/chroma

Advanced analysis of polymer emulsions: Particle size and particle size distribution by field-flow fractionation and dynamic light scattering

Ashwell C. Makan[a,b], Markus J. Spallek[c], Madeleine du Toit[a], Thorsten Klein[c], Harald Pasch[b,*]

[a] Kansai Plascon Research Centre, Polymer Science Building, Room 2028, University of Stellenbosch, 7602, Matieland, South Africa
[b] Department of Chemistry and Polymer Science, University of Stellenbosch, Private Bag X1, Matieland, 7602, South Africa
[c] Postnova Analytics GmbH, Max-Planck-Strasse 14, 86899 Landsberg, Germany

ARTICLE INFO

Article history:
Received 6 October 2015
Received in revised form 19 February 2016
Accepted 6 March 2016
Available online 9 March 2016

Keywords:
Asymmetrical flow field-flow fractionation
Sedimentation field-flow fractionation
Emulsions
Inorganic additives
Inductively coupled plasma mass spectrometry

ABSTRACT

Field flow fractionation (FFF) is an advanced fractionation technique for the analyses of very sensitive particles. In this study, different FFF techniques were used for the fractionation and analysis of polymer emulsions/latexes. As model systems, a pure acrylic emulsion and emulsions containing titanium dioxide were prepared and analyzed. An acrylic emulsion polymerization was conducted, continuously sampled from the reactor and subsequently analyzed to determine the particle size, radius of gyration in specific, of the latex particles throughout the polymerization reaction. Asymmetrical flow field-flow fractionation (AF4) and sedimentation field-flow fractionation (SdFFF), coupled to a multidetector system, multi-angle laser light scattering (MALLS), ultraviolet (UV) and refractive index (RI), respectively, were used to investigate the evolution of particle sizes and particle size distributions (PSDs) as the polymerization progressed. The obtained particle sizes were compared against batch-mode dynamic light scattering (DLS). Results indicated differences between AF4 and DLS results due to DLS taking hydration layers into account, whereas both AF4 and SdFFF were coupled to MALLS detection, hence not taking the hydration layer into account for size determination. SdFFF has additional separation capabilities with a much higher resolution compared to AF4. The calculated radii values were 5 nm larger for SdFFF measurements for each analyzed sample against the corresponding AF4 values. Additionally a low particle size shoulder was observed for SdFFF indicating bimodality in the reactor very early during the polymerization reaction. Furthermore, different emulsions were mixed with inorganic species used as additives in cosmetics and coatings such as TiO_2. These complex mixtures of species were analyzed to investigate the retention and particle interaction behavior under different AF4 experimental conditions, such as the mobile phase. The AF4 system was coupled online to inductively coupled plasma mass spectrometry (ICP-MS) for elemental speciation and identification of the inorganic additive. SdFFF had a larger separation power to distinguish different particle size populations whereas AF4 had the capability of separating the organic particles and inorganic TiO_2 particles, with high resolution.

1. Introduction

Polymer emulsions are typically complex formulations that consist of various components including the polymer part, emulsifiers, pigments (e.g. TiO_2) and other additives. The chemical heterogeneity of an emulsion can vary significantly and the final composition, particle size and particle size distribution (PSD) is of high importance for various applications [1]. Emulsions with very small particle sizes can result in very high viscosities, while very large particle sizes could lead to unstable emulsion particles [2,3]. The particle size determined by batch dynamic light scattering (DLS) gives an average size value based on one detector angle (e.g. 173° or 90°) and is a fast and simple way of determining the hydrodynamic radius of colloidal species [4–6]. Nucleation and particle growth mechanisms during free radical emulsion polymerization are often deducted based on DLS measurements [7]. For more in-depth and reliable particle size information, a fractionation method with suitable detectors for the determination of different

* Corresponding author.
E-mail address: hpasch@sun.ac.za (H. Pasch).

http://dx.doi.org/10.1016/j.chroma.2016.03.013

3.1 Abstract

Field-flow fractionation (FFF) is an advanced fractionation technique for the analyses of very sensitive particles. In this study, different FFF techniques were used for the fractionation and analysis of polymer latices. As model systems, a pure acrylic latex and latex-titanium dioxide blends were prepared and analyzed. An acrylic latex polymerization was conducted, continuously sampled from the reactor and subsequently analyzed to determine the particle size, radius of gyration in specific, of the latex particles throughout the polymerization reaction. Asymmetric flow field-flow fractionation (AF4) and sedimentation field-flow fractionation (SdFFF), coupled to a multidetector system, multiangle laser light scattering (MALLS), ultraviolet (UV) and refractive index (RI), respectively, were used to investigate the evolution of particle sizes and particle size distributions (PSDs) as the polymerization progressed. The obtained particle sizes were compared against batch-mode dynamic light scattering (DLS). Results indicated differences between AF4 and DLS results due to DLS taking hydration layers into account, whereas both AF4 and SdFFF were coupled to MALLS detection, hence not taking the hydration layer into account for size determination. SdFFF has additional separation capabilities with a much higher resolution compared to AF4. The calculated radii values were 5 nm larger for SdFFF measurements for each analyzed sample against the corresponding AF4 values. Additionally a low particle size shoulder was observed for SdFFF indicating bimodality in the reactor very early during the polymerization reaction. Furthermore, different latices were mixed with inorganic species used as additives in cosmetics and coatings such as TiO_2. These complex mixtures of species were analyzed to investigate the retention and particle interaction behaviour under different AF4 experimental conditions, such as the mobile phase. The AF4 system was coupled online to inductively coupled plasma mass spectrometry (ICP-MS) for elemental speciation and identification of the inorganic additive. SdFFF had a larger separation power to distinguish different particle size populations whereas AF4 had the capability of separating the organic particles and inorganic TiO_2 particles, with high resolution.

3.2 Introduction

Polymer latices are typically complex formulations that consist of various components including the polymer part, emulsifiers, pigments (e.g. TiO_2) and other additives. The chemical heterogeneity of a latex can vary significantly and the final composition, particle size and particle size distribution (PSD) is of high importance for various applications [1]. Latices with very small particle sizes can result in very high viscosities, while very large particle sizes could lead to unstable latex particles [2,3]. The particle size determined by batch dynamic light scattering (DLS) gives an average size value based on one detector angle (e.g. 173 ˚or 90˚) and is a fast and simple way of determining the hydrodynamic radius of colloidal species [4-6]. Nucleation and particle growth mechanisms during free radical latex polymerization are often deducted based on DLS measurements [7]. For more in-depth and reliable particle size information, a fractionation method with suitable detectors for the determination of different size parameters is key towards a better understanding of complex organic nanoparticle systems.

Field-flow fractionation (FFF) invented by Giddings in 1966 is a separation technique based on chromatographic-like principles which separates particles and molecules by an external force which is applied orthogonally to the sample flow streamline [8]. The most common FFF techniques used for particle size analysis are asymmetric flow field-flow fractionation (AF4) and sedimentation field-flow fractionation (SdFFF). AF4 features a second axial flow (cross-flow), applied perpendicular to the longitudinal sample flow. Separation takes place inside a ribbon-like, trapezoidal channel with particles being separated according to their diffusion coefficients, which is related to hydrodynamic radius (R_h), and subsequently the radius of gyration (R_g) [9,10]. In SdFFF a centrifugal field ensures sample separation according to hydrodynamic radius and density of the particles [11]. The centrifugal force, which is applied perpendicular to the axial flow in SdFFF, can be varied to achieve particle separation.

Recently, applications of FFF in drug delivery [4,12-19], cosmetic [20], environmental [21-25], and food industry [26-31] have increased significantly. FFF of latex particles has been studied by various research groups. Polystyrene latexes have been studied by DLS and asymmetric flow field-flow fractionation coupled to multiangle laser light scattering detection (AF4-MALLS) to evaluate band broadening effects in nanoparticle analysis [7]. Polystyrene particles synthesized by unseeded latex polymerization have been studied by AF4 and compared to DLS to investigate the presence of primary particles during the synthesis procedure [5,6]. Similarly, Bartsch et al. investigated the particle size development in seeded styrene polymerization by AF4-MALLS in comparison to the disc centrifugation method [32]. Schauer investigated pigments, fillers as well as latices used in coatings by symmetric and asymmetric flow FFF based on a single detector (UV) system in comparison with offline DLS [33]. The effect of pH and ionic strength on the swelling behaviour in core-shell latex particles was studied by Frankema et al. to investigate changes in particle size upon changing these variables using AF4-MALLS and ultraviolet (UV) detection, or AF4-MALLS-UV [9]. Thermal FFF has also been used in ABS and polystyrene latex particles. Mes et al. studied the effect of surfactants on the calculated particle size [34].

The coupling of AF4 to element-sensitive detectors such as inductively coupled plasma mass spectrometry (ICP-MS) has been under utilized compared to other hyphenated techniques. Nanoparticles, especially gold nanoparticles have been studied by hydrodynamic chromatography and AF4, with both techniques coupled to online ICP-MS (AF4-ICP-MS) to determine particle size and quantification of nanoparticles in submicron dispersions [35,36]. A recent review article on FFF-ICP-MS by Pornwilard M-M and Atitaya Siripinyanond briefly covered the main FFF-ICP-MS applications [37], attributed to the first offline coupling of FFF and ICP-MS in 1991 by Beckett [38] and Taylor [39] in 1992. More recently Bednar, Gray and Mitrano studied online coupling of FFF with single particle ICP-MS [24,36,40], respectively. TiO_2 separation with multi-detection by SdFFF and AF4 has been studied by a few research groups [20,41,42].

In this study, online AF4-MALLS-UV as well as an online refractive index detector (AF4-MALLS-UV-RI), online sedimentation FFF with MALLS and UV detection (SdFFF-MALLS-UV), and DLS were utilized for detailed characterization of styrene-acrylic and pure acrylic latices used primarily in coatings, which were synthesized by free radical polymerization. During the latex polymerization, samples were taken from the reaction vessel at pre-defined time intervals. The obtained particle sizes and PSDs of both latex systems were subsequently compared using AF4 and SdFFF with multiple detectors, and batch DLS. The DLS measurements were conducted in different laboratories under identical experimental conditions.

Furthermore, model blends of polymer latex and TiO_2 particles were analyzed online using AF4-MALLS-UV-RI detection as well as an ICP-MS detector coupled as AF4-MALLS-UV-RI-ICP-MS in order to separate, specify and identify the organic and inorganic species dispersed in solution. Styrene-acrylic and pure acrylic latices were studied independently and spiked with TiO_2 before analysis.

3.3 Experimental

3.3.1 Theory of separation techniques

AF4 and SdFFF both have a parabolic flow velocity profiles inside its respective channels.

As per first FFF principles for a constant force field the force acting on the particles or macromolecules are given by Equation 1 and 2 for AF4 and SdFFF, respectively [8,41,43-45].

$$F_{AF4} = \mathrm{f}\left|\mathrm{U}\right| = \frac{kT\left|U\right|}{D} = 3\pi\eta\left|U\right|\mathrm{d} \tag{1}$$

Where d (nm) is the diameter of molecule or particle, D (m^2/s) is the diffusion coefficient and U represents the-field induced velocity.

$$F_{SdFFF} = \mathrm{m}'\mathrm{G} = \mathrm{V_p}\left|\Delta\mathrm{p}\right|\mathrm{G} = \frac{\pi}{6d^3}\left|\Delta\mathrm{p}\right|\mathrm{G} \tag{2}$$

where m’ (g) is the effective mass of the particle, V_p (cm^3) is the particle volume, Δp (g/cm^3) the difference in density between particles and mobile phase and G (m/s^2) is the gravitational force. Similarly, the hydrodynamic diameter can be determined, deducted from equations 1 and 2, respectively. In AF4 the diameter is calculated by:

$$d_H = \frac{2kTV^0}{\pi\eta w^2 V_c t^0} t_r \tag{3}$$

where k denotes Boltzmann constant, V^0 (cm^3) is the void volume of the channel, η (g/cm^3) is the mobile phase viscosity at absolute temperature T (K), w (cm) is the thickness of the channel, V_c (mL/min) is the subsequent cross-flow rate while the void time and retention time are denoted by t^0 (min) and t_r (min), respectively. For SdFFF:

$$d_H = \left(\frac{6kT}{\pi G w \Delta\rho t^0} t_r \right)^{\frac{1}{3}} \tag{4}$$

where G (m/s^2) is the acceleration speed of the rotating channel. The added parameter, density during separation has an added benefit, adding a higher resolution power in comparison to AF4. Both FFF techniques can be complementary or superior to DLS depending on the nature of the analyzed material. DLS is known to be a fast tool to screen nanoparticles. DLS lacks separation power since average particle size of particles in dispersion are analyzed, therefore sizes may be erroneously calculated due to overestimation as a result of small amounts of large aggregated particles. This phenomenon is overcome by the fractionation and resolution power of AF4 and SdFFF. In this study, the latex particles are subjected to a larger field force in SdFFF which is proportional to $1/d^3$, which imparts very large resolution depending on the strength of the gravitational force. In AF4 the force acting on the particles are proportional to d and $1/V_c$ as variables for resolution improvement.

3.3.2 Materials and sample preparation

The pure acrylic latex (sample 1) featuring a low glass transition temperature (T_g) was synthesized with n-butyl acrylate (n-BA), methyl methacrylate (MMA) and methacrylic acid (MAA) while the styrene-acrylic (sample 2) latex was produced using styrene (Sty), n-BA, MMA and MAA as monomers, respectively.

The monomers were added in specific ratios into a 5L glass reactor with mechanical overhead stirring in a temperature controlled water bath to produce copolymers with the desired T_g. The ratio of each monomer was approximated using the Flory-Fox equation and consequently adjusted once the actual copolymer was analyzed. Specific monomer ratios are discussed in section 4.3.1. For the pure acrylic sample (1) and styrene-acrylic sample (2) the targeted T_g was between 0–3 °C and 17–20 °C, respectively. The T_g values were confirmed with differential scanning calorimetry (DSC). The surfactant mixture (Disponal A3065, Cognis GmbH, Düsseldorf, Germany and Aerosol EF-800, Cytec, Vlaardingen, Netherlands) was used above the critical micelle concentration and added in the range of 2.0-2.5 wt% active material to total monomer. A pre-latex was prepared with the predetermined ratio that corresponds to the T_g calculations. The reactor was pre-charged with water, surfactant and buffer and 5 vol% of the pre-latex was fed into the reactor to form an in-situ seed. Seed formation was allowed to proceed until a drop in the reaction exotherm was noticed. This was measured by a reactor thermocouple. An optimum time for seed formation was found to be between 7 and 10 minutes. The rest of the latex was fed into the reactor over three hours. The feed of the initiator solution (ammonium persulphate) was started two minutes prior to the latex feed and continued parallel to the latex feed. The temperature of the reaction was kept constant at 85°C. At the end of the latex and initiator feed the reactor contents were allowed to post-polymerize for an additional 35 minutes.

The temperature of the reactor contents was then lowered to 40°C after which t-butyl hydroperoxide and sodium metabisulphite were added to eliminate free monomer and ensure that conversion is maximized. After the reactor contents reached room temperature, the pH was adjusted with a sodium hydroxide solution to increase the pH range to 7.5–8.5. The final non-volatile contents of the latexes were between 49.5–50.0 wt% and reached a viscosity between 200–700 cPs. Samples were drawn from the reactor vessel throughout the reaction starting 7 minutes after the seed was formed. A total of 11 samples (US001 to US011) of approximately three grams each were collected from the reactor at 30 minute intervals. After the reaction was completed the last sample (US 011) was taken which represents the final processed latex. The sampling procedure of the pure acrylic latex (sample 1) and the time dependent samples removed from the vessel (US 001 – US 011) are summarized in **Table 3.1**.

Table 3.1 Sampling procedure during the polymerization reaction for sample 1.

Sample code	Sampling details	Sampling time (hrs)
US 001	After in-situ seed formation for 7 minutes	0.0
US 002	30 minutes after feed started	0.5
US 003	1 hour after feed started	1.0
US 004	1.5 hours after feed started	1.5
US 005	2 hours after feed started	2.0
US 006	2.5 hours after feed started	2.5
US 007	3 hours after feed started	3.0
US 008	Monomer feed ends	3.5
US 009	20 minutes after delayed initiator	4.0
US 010	4.5 hours after feed started	4.5
US 011	Final particle size	6.0

The commercial TiO_2 samples used in the study had average particle diameters of 230 nm (supplier X) and 250 nm (supplier Y), respectively, obtained from Huntsman, Kwazulu Natal, South Africa. The carrier liquid used for all analyses was a 0.2 % v/v solution of Novachem in doubly distilled deionized water. The Novachem surfactant is a mixture of anionic and non-ionic surfactants Novachem®, C-SUR-100, Postnova Analytics, Landsberg, Germany.

Spherical polystyrene latex particle standards with nominal sizes (60 nm, 125 nm and 350 nm) were obtained from Postnova (Landsberg, Germany) and were used in both AF4- and SdFFF-MALLS for normalization of the MALLS detector. Normalization of the MALLS detector are conducted by using the 60 nm polystyrene latex particles in order to scale each of the detector angles relative to the 90˚ scattering angle.

All monodisperse nano polystyrene spheres are certified by the National Institute of Standards and Technology (NIST), using microscopy (350 nm particles) or transmission electron microscope (125 and 60 nm particles). The average particle size and uncertainties using the two microscopy techniques were 57 nm ± 4 nm, 125 nm ± 1 nm and 350 nm ± 6nm, respectively.

In two laboratories, Lab A – Kansai Plascon, Stellenbosch, South Africa, Lab B – Postnova, Landsberg, Germany, DLS measurements were conducted using the in-house test method of Lab A for hydrodynamic radii determinations of latices which entail the dilution of a droplet of latex with 10 mL deionized water.

In order to ensure that dilute solution conditions were met, the solution of sample US 015 was further diluted another 10 times (total of 100x dilution) followed by another DLS measurement to determine if the initially used concentration (10x dilution) were diluted sufficiently. The calculated R_g was similar to the sample that was diluted with 10 mL DDI water (**Table 3.2**). Therefore each of the analyzed samples was only diluted ten times before DLS analyses were performed.

A polystyrene latex particle standard with R_g of 23 nm (22 nm ± 1.5 nm) as per reference certificate was used to verify that accurate measurements were obtained for analyses on the DLS instrument. The polystyrene latex particles were measured in triplicate in DDI water and the obtained R_g was 24.1 nm ± 0.2 nm

3.3.3 Instrumentation setup and analysis conditions

DLS measurements were performed on a Zetasizer Nano-S ZEN1600 (Malvern instruments, Malvern, United Kingdom) in the two different laboratories.

AF4 experiments were performed on a medium temperature AF4-Instrument (MT2000, Postnova Analytics, Landsberg/Germany) which was coupled to MALLS (PN3621), RI (PN3150) and DAD-UV (PN3241) detectors from Postnova Analytics, Landsberg, Germany, defined as AF4-MALLS-UV-RI. The channel was connected to three different pumps (tip, focus and cross-flow) while the injection port was equipped with a 100µL sample loop of which 20µL was injected for each measurement. A 350 µm Mylar spacer defining the channel height and a regenerated cellulose membrane was installed for the AF4 (average molar mass cut-off of 5 kDa, Z-AF4-MEM-612-5kD, Postnova, Landsberg, Germany). Elution was realized using two pumps (tip- and focus-flow rates, PN1122). Two in-line solvent filters (0.1µm pore size, 13mm diameter, PTFE) were positioned between channel and pumps to reduce the detector background. The sample bypassed the filters thus entering the channel unaffected.

SdFFF analyses were performed on a CF2000 instrument (Postnova Analytics, Landsberg, Germany), with an inner channel thickness of 250 µm and rotor radius of 90 mm. The injection volume was 20 µL for each measurement. The CF2000 was coupled to MALLS (PN3621) and UV (PN3241) detectors from Postnova Analytics, SdFFF-MALLS-UV. An ICP-MS (7700 series, Agilent Technologies) and ICP-MS Interface (PN 9050), AF4-MALLS-UV-RI-ICP-MS, were used for the detection of the elemental traces of TiO_2 after mixing the inorganic TiO_2 with the organic latex particles. A flow rate of 0.5 mL/min was used, and the elements chosen for trace analysis were set at Ti^{48}, Pb^{208} and Fe^{56}.

An autosampler (PN5300) was used for both AF4 and SdFFF for sample injection. For AF4, the tip flow-rate during injection and focusing of the sample was 0.2 mL/min for a period of four minutes. After the sample was introduced into the channel, during the relaxation period, the cross-flow flow-rate was maintained at 1.0 mL/min and the focus flow was set to 1.3 mL/min in order to maintain a constant detector flow of 0.5 mL/min. Four minutes after injection and focusing, the focus flow rapidly decreased to zero within one minute, while the tip flow increased to 1.5 mL/min. After another 0.2 min, the cross-flow decreased exponentially to 0 mL/min. The tip flow also decreased until a flow rate of 0.5 mL/min was reached. The tip-flow rate was kept constant for a further ten minutes ensuring that all particles have eluted from the channel before the next injection.

In SdFFF, the samples were introduced into the channel over a period of 201 seconds followed by relaxation for 15 minutes. The flow rate was kept constant at 0.5 mL/min while the starting rotation speed of the channel was setup at 4900 rpm (maximum field). After relaxation the rotation speed was kept constant for 12 minutes at 4900 rpm, after which the speed decreased to 500 rpm with an exponential field-decay function with an exponent of 0.4.

3.4 Results and discussion

3.4.1. Particle radii investigation of sample 1: pure acrylic latex

3.4.1.1 DLS analysis

The eleven polymerized latex samples (**Table 3.1**), removed periodically from the reaction vessel for sample 1 (pure acrylic), were each analyzed using DLS after dilution. The hydrodynamic radii obtained by DLS were converted to radius of gyration (R_g), assuming spherical latex particles for both pure-and styrene-acrylic latex systems. The calculated R_g was obtained from the relationship R_g = 0.775 multiplied by R_h for homogeneous hard sphere latex particles [9,10,46]. The results obtained from DLS analysis are summarized in **Table 3.2**.

The R_g values increase rapidly during polymerization (US 001 to US 004). The rapid rate of particle size growth is indicative of very fast particle nucleation in a very short time. From US 005 to US008, with a decreasing trend is noticeable, forming a plateau after US 008 [47,48]. US 008 correspond to the time where the monomer feed was stopped in the reactor. The non-uniform rapid increase in R_g is explained in more detail in the following section in comparison with the FFF results. The calculated R_g of samples US 009 to US 011 remained constant, even after the delayed addition of initiator. This observation points towards a steady state in the polymerization progress. These findings support that R_g was not affected by post treatment additions, where tertiary butyl hydroperoxide and sodium metabisulphite were added to eliminate free monomer.

The obtained results allow tracking the correlation of the particle size to the synthesis procedure. In particular, the point of time at which the maximum particle radius is reached can be easily determined for the specific synthesis procedure. In the early stages of the polymerization, a steep slope is observed due to a rapid propagation of particles, followed by a slower rate to a constant value forming a plateau. In addition, the average particle radius of three different batches of the same pure acrylic latex which were synthesized over a six month period (A: US 013, B: US 014 and C: US 015 in **Figure3.1. A),** were determined and compared to US 011. The obtained average particle radii corresponded very well to the final particle radius obtained from US 011 (**Table 3.2**).

In a separate latex system the final sample (US 012) of a styrene-acrylic polymerization was analyzed in comparison to the pure acrylic based system. **Table 3.2** shows that R_g was similar in distilled and double distilled deionized (DDI) water, while the solution with surfactant (Novachem) decreased R_g by an average size of 1.5 nm.

In order to investigate the effect of the surfactant in deionized water on R_g, all the samples were analyzed in comparison with normal DDI H_2O and distilled H_2O. The same organic surfactant was used to characterize the samples with AF4 and SdFFF coupled to UV, RI and MALLS detection. Therefore, the effect of the surfactant solution on R_g was investigated. The hydrodynamic radii converted to R_g assuming spherical particles (from **Table 3.2**) for US 001 to US011 were compared as a function of the sampling sequence (US 001 to US 011). It is apparent that the latex particles obtained from 0.2 vol% surfactant solution as mobile phase followed an identical increasing particle size trend as measured in pure DDI H_2O (Supplementary data, **Figure S1**). The average calculated R_g of the samples in the surfactant solution was marginally smaller compared to DDI H_2O and distilled H_2O, which had near identical R_g averages. The maximum R_g difference between DDI and 0.2 % Novachem was 1.6 nm. The slight reduction in R_g could be caused by the effect of a higher salt concentration on the compression of the electric double layer [49,50]. In particular, a small amount of surfactant is known to add a lubrication effect that allows particles to have a larger diffusion coefficient, hence more rapid movement (Brownian motion) through the medium [51]. This effect results in the calculated R_h being slightly lower as compared to the particles in distilled and DDI H_2O [50]. To support the data, a single factor analysis of variance (ANOVA) test was performed on samples US 001, US 005 and US 011, respectively, at a 95% confidence interval and a p-value of 0.05. Statistically, there was no difference between the distilled and DDI H_2O data sets, with a calculated p value > 0.5 and $F < F_{crit}$, while a statistical difference was observed between the 0.2% Novachem solution and distilled- or DDI H_2O, due to $p < 0.05$ and $F > F_{crit}$. The finding of the three sets of measurements performed under the same experimental conditions using three different media (Dist. H_2O, DDI, H_2O and 0.2% Novachem solution) on the same DLS model underlined the within sample reproducibility of the DLS results.

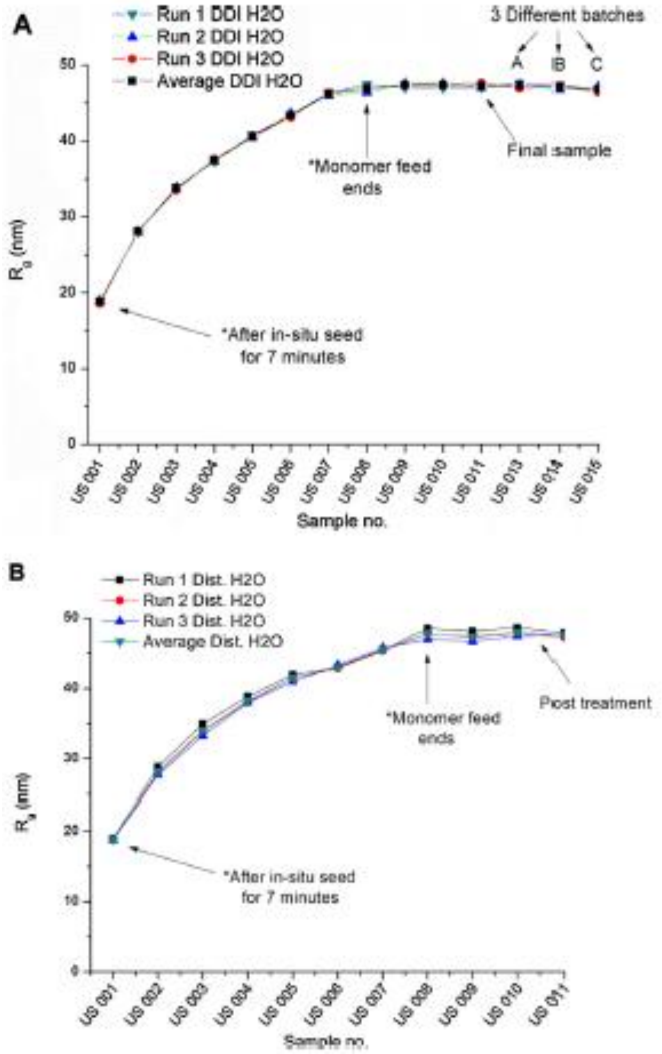

Figure 3.1. Particle radii (R_g) obtained from DLS analysis of US 001 to US 015 (sample 1-pure acrylic). **A:** Lab A. **B:** Lab B.

Table 3.2 Particle radii (R_g) of samples 1 (pure acrylic) and 2 (styrene acrylic) determined by DLS. The hydrodynamic radius (R_h) was converted to radius of gyration (R_g) assuming the latex particles resemble hard spheres. Results were obtained from two independent laboratories (A and B). Measurements were done in triplicate.

Sample code	Lab A (Distilled H_2O) R_g (nm) ± STDEV	Lab B (Deionized H_2O) R_g (nm) ± STDEV	Lab B (Deionized H2O + 0.2 % surfactant) R_g (nm) ± STDEV
US 001	18.8 ± 0.1	18.8 ± 0.2	20.1 ± 0.1
US 002	28.2 ± 0.6	28.1 ± 0.1	27.9 ± 0.2
US 003	34.1 ± 0.9	33.8 ± 0.2	33.5 ± 0.1
US 004	38.3 ± 0.5	37.5 ± 0.1	36.9 ± 0.2
US 005	41.5 ± 0.5	40.6 ± 0.2	40.1 ± 0.1
US 006	43.1 ± 0.2	43.4 ± 0.2	42.6 ± 0.1
US 007	45.5 ± 0.2	46.3 ± 0.2	45.2 ± 0.1
US 008	47.8 ± 0.8	46.9 ± 0.5	46.2 ± 0.2
US 009	47.4 ± 0.7	47.4 ± 0.3	46.6 ± 0.1
US 010	48.0 ± 0.6	47.4 ± 0.3	46.4 ± 0.1
US 011	47.6 ± 0.4	47.3 ± 0.3	46.2 ± 0.2
US 013	n.d*	47.3 ± 0.3	46.3 ± 0.5
US 014	n.d	47.2 ± 0.3	46.6 ± 0.1
US 015	n.d	46.8 ± 0.4	45.9 ± 0.1
US 015 (10x diluted)	n.d	n.d	46.1 ± 0.1
US 012 (styrene acrylic)	27.1	27.8 ± 0.1	26.3 ± 0.1

*nd – not determined

3.4.1.2 AF4-MALLS-RI-UV for particle radius and PSD determination.

The pure acrylic latex (sample 1) was analyzed using AF4 to compare the evolution of R_g in detail and throughout the reaction in comparison to batch DLS results. **Figure 3.2 (A – C)** shows the RI, UV and MALLS detector signals of US 001 to US 011 analyzed by AF4. The RI signal shows a large void peak at approximately 7 minutes followed by a small RI response for the particles of interest, due to the particles being present in a very low concentration resulting in a refractive index similar to that of the mobile phase. Elution of samples US 001 – US 011 occurs between 12 and 25 minutes, respectively.

The UV signal (**Figure 3.2 B**) gave high detector response with a good signal-to-noise ratio for all chosen UV wavelengths (220 nm, 254 nm, 280 nm and 320 nm), and was therefore chosen as the concentration detector for AF4 and SdFFF analyses. UV 254 nm and MALLS signals were used to obtain particle radius (R_g) and concentration information for the analysed samples. The experimentally determined radii of gyration (R_g) obtained from DLS and AF4-MALLS-UV is reported in **Figures. 2 D, E and F**.

The differential PSDs of US 001 – US 011 are displayed in **Figure 3.2 D**, showing a narrow distribution in the early stages during monomer feed after seed formation from zero to two hours (US 001 – 004). As the monomer feed continues after two hours (US 004 – 007), the PSD starts to broaden with fronting towards smaller R_g values. Broadening takes place until the monomer feed has stopped (US 008) and remains constant throughout post polymerization additions.

The cumulative R_g are displayed in **Figure 3.2 E** which support the findings of PSD in **Figure 3.2 D**. In particular, the PSD proved to be narrow in the beginning, starting to broaden towards the latter stages of the polymerization progress where the particle radii span in a range from 25 nm to 50 nm. The average radius of gyration from DLS (after conversion from hydrodynamic radius) and R_g obtained from AF4 are compared in **Figure 3.2 F**. The trend observed for the evolution of R_g as obtained from AF4 is identical to the DLS results as a function of polymerization time. Furthermore, by comparison of the steep increase in the two slopes, the observed deviation of R_g (AF4) and R_g (DLS) with 5 nm remains constant. Since DLS delivers hydrodynamic radii, the difference in radius of 5 nm expresses the formation of the hydration shell around the latex particles. The measure is in good agreement with observed hydration shells [7,52]. Since the hydration shell is affected by surface charge and carrier conditions, which remain constant during FFF separation and polymerization process (same monomers incorporated) a constant deviation of 5 nm in radius during the polymerization process starting from 15 nm up to 46 nm nanoparticles underlines the observation of a hydration shell. Furthermore, MALLS determines the size of analyte particles, equivalent to a statistical sphere (R_g) whereas DLS provides hydrodynamic radius (R_H) which is equivalent to a homogenous hard sphere. The explanations considered all particles to be hard sphere equivalents, and converted all data to the same size parameter, R_g. [53,54]

By looking at both radii measurements obtained from DLS and AF4, a steep increase in the particle size curvature in the beginning of the monomer feed step (**Figure 3.2 F**) is obtained which levels out from US 008 onwards, since it is the end of the monomer feed.

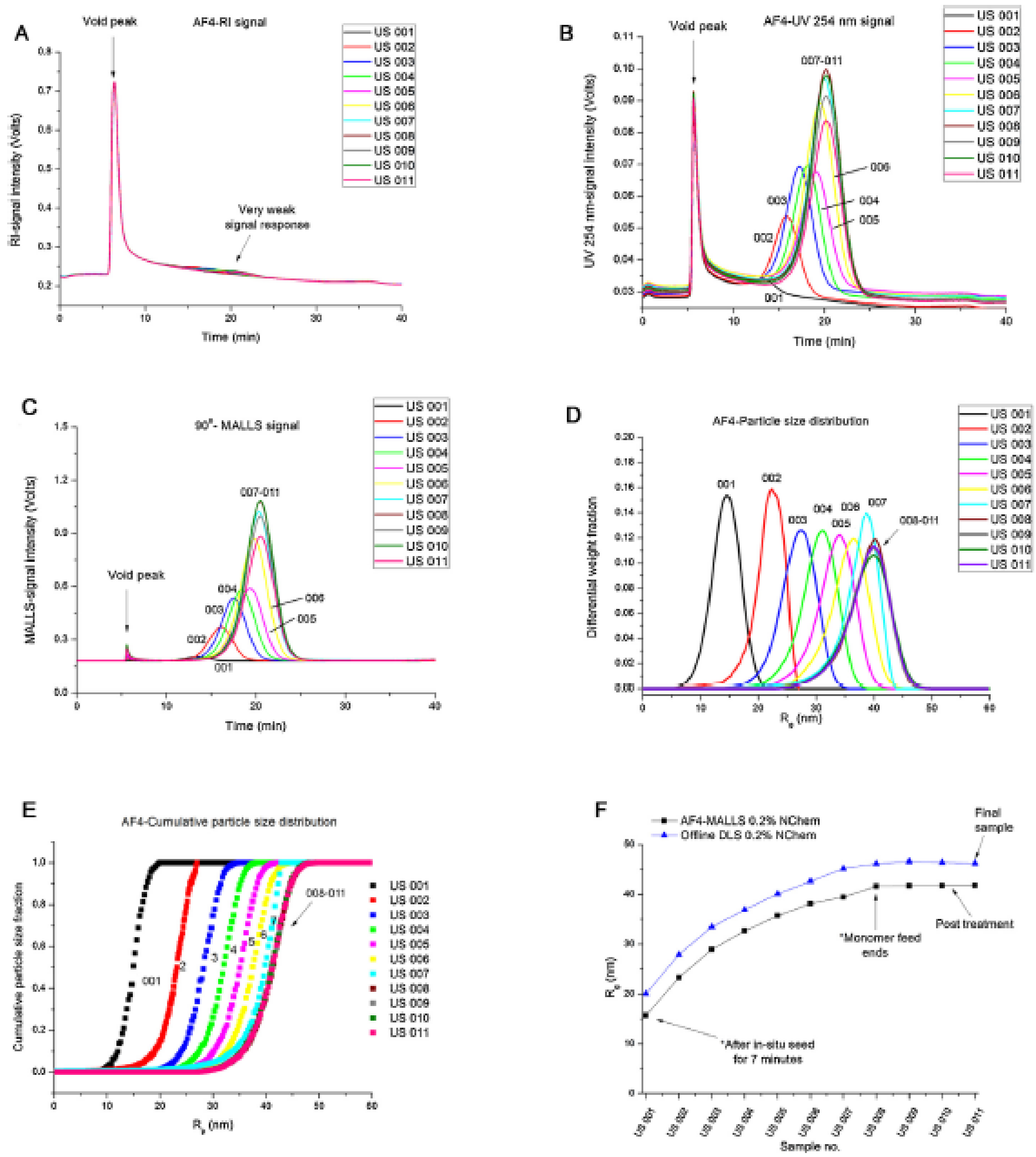

Figure 3.2. AF4 analysis of the pure acrylic latex (sample 1). **A, B** and **C:** RI, UV and MALLS signals as a function of retention time, respectively. **D:** Differential PSD from AF4. **E:** Cumulative radius distribution and **F:** Evolution of particle radii (R_g) as a function of sampling sequence (US 001 – US 011) obtained from DLS and AF4-UV-MALLS, using a solution of 0.2% Novachem in deionized water.

Similar to DLS, the AF4-MALLS radii did not decrease upon post polymerization. This phenomenon is observed throughout **Figure 3.2** for detector signals (A-C) as well as the particle radius graphs (D-F), which supports that the polymerized nanoparticles can be regarded as stable with respect to aggregation, since the particle radii do not change over time.

The observed broadening of PSD may be due to monomer-starved conditions during the polymerization process. Saddaji reported that a typical broadening during the semi-continuous polymerization under starved conditions for styrene is due to different regimes present during monomer feed [49]. He proposed that monomer-starved conditions are preceded by monomer flooded conditions, especially early in the feed process where small formed particles have lower probability of absorbing monomer for particle growth than larger particles. In monomer flooded conditions, the rate of particle growth is high and surfactant molecules are consumed to stabilize the newly formed polymer particles, rather than nucleation of new particles. After the rapid growth period when monomer starved conditions are finally reached, the growth rate is significantly reduced, as new particles are nucleated. Due to the non-linear polymerization rates present in one reaction, the effect leads to broadening of the PSD.

Additionally, growth rates for smaller and larger particles differ under monomer-starved conditions, resulting in a broad PSD towards the end of monomer feed. The third postulation is stochastic broadening, which occurs as a result of larger particles outgrowing the smaller particles over time. This phenomenon is attributed to the fact that the smaller non-growing particles remain in the reactor together with the newly formed larger particles, which results in a broad PSD [55]. It was proven that during monomer feed, just after the seed formation of semi-continuous latex polymerization for styrene, particle radii which are even smaller than those obtained from the seed formation are obtained. Broad and even bimodal PSDs were observed and confirmed by transmission electron microscopy (TEM) as well as capillary hydrodynamic fractionation. In the current study, the steep increase in particle radii is observed in both DLS and AF4-MALLS-UV. It was shown that monomer-starved conditions are reached after 2 hours of polymerization (US 005 in **Figure 3.2 F**), since the rate of growth is decreasing (plateau) much faster as the monomer feed approaches the end after 3.5 hours (US 008). As a result of the difference in growth rates, a range of particle radii is present in the system at the end of the polymerization process, resulting in a broader PSD compared to the beginning of the monomer feed, where the growth rate dominates particle formation. As monomer-starved conditions are met, particle formation dominates over particle growth. The particle radii remain constant after the addition of the remaining initiator during post treatment. The observed phenomenon is an indication that any new particles forming did not alter the average particle radii or PSD. New particle formation towards the end of the polymerization is unlikely since any free monomer present in the reactor would be deactivated. The polymer content at each interval was not determined for corresponding gravimetric analyses for particle number calculations.

The cross-flow strength, together with the focus-flow plays an important role in the resolution of multiple species in the AF4 channel [56]. Varying the cross-flow profile from constant to linear to exponential has been pivotal in obtaining efficient separation without compromising time, mobile phase consumption and physico-chemical information [57].

The effect of increasing focus times and various cross-flow strengths were evaluated and compared against the particle radii information obtained from the DLS measurements in the preceding section. The fractograms of the pure acrylic (US 011, top) and styrene-acrylic (US 012, bottom) latices are displayed in the Supplementary Data (see **Figure S2**). The different focus times were subtracted from the fractograms in order to compare the different times displayed as an overlay. The intensity of the void peak decreased as the focus time was increased, while the sample peak intensity increased for the 90˚-MALLS signal. The reason for the decrease in the void peak intensity could be due to small unretained species lost through the membrane and the increase in sample peak intensity which may arise from incomplete sample focusing. For the 2 and 4 minute focus times, a second peak appeared early in the fractograms between 5 and 10 minutes, highly likely due to unrelaxed species eluting in this time frame. From 6 minutes onwards a single peak was observed.

The PSD at peak width at half height (PWHH) for the various focus times for the bulk styrene-acrylic and pure acrylic samples are displayed in the Supplementary Data (see **Figure S3**). The observed PSD did not shift to higher values as the focus time was increased. The PSD of the styrene-acrylic latex was constant between approximately 2-27 nm, while the pure acrylic latices PSD ranged between 37-47 nm. The influence of cross-flow on the PSD for the styrene-acrylic sample (US 012) is displayed in the Supplementary Data (see **Figure S4**). An increase in cross-flow strength from 0.75 to 1.5 mL/min shows an increase in resolution without compromising peak width at the expense of an increase in retention time of 4 minutes. The PSD for the styrene-acrylic latex gave a comparable PSD width in comparison to the focus-flow study (**Figure S4**, supplementary information), with an increase in cross-flow having no significant effect on the lower (± 23 nm) and upper (± 28 nm) particle radii range. A cross-flow of 1.0 mL/min and focus flow of 4 minutes was chosen for all analyzed samples. After 2 minute focusing the void peak baseline did not reach zero. A prolonged focusing time of approximately 6 minutes to reach a zero baseline was avoided to minimize secondary effects due to over focusing, such as sample loss through the membrane, stress on the particle shape and unwanted interactions with the cellulosic membrane. In summary, it can be concluded that no aggregation occurred upon an increase in focus time or cross-flow strength, which is an indication that the chosen AF4 experimental conditions were suitable for both latex systems.

3.4.1.3 SdFFF - MALLS-UV for the determination of average particle radii and Particle Size Distribution.

SdFFF is a unique FFF technique used for the particle radius analysis of colloidal species taking advantage of separation, not only by hydrodynamic radius but also according to density [11,29,44,58-62].

SdFFF-MALLS-UV was used as a comparative technique in addition to AF4-MALLS-UV to investigate the size differences between DLS, AF4 and SdFFF. The UV- and MALLS detector signals, PSD and average R_g values are displayed in **Figure 3.3**. Similar to AF4, the UV 254 nm signal was used as the concentration-sensitive signal. Samples US 001 to US 003 could not be completely separated from the void peak which eluted between 20 and 30 minutes. The fractograms of these samples (US 001 to US 003) were integrated nonetheless and the resultant PSD were plotted together with the other samples (**Figure 3.3C**).

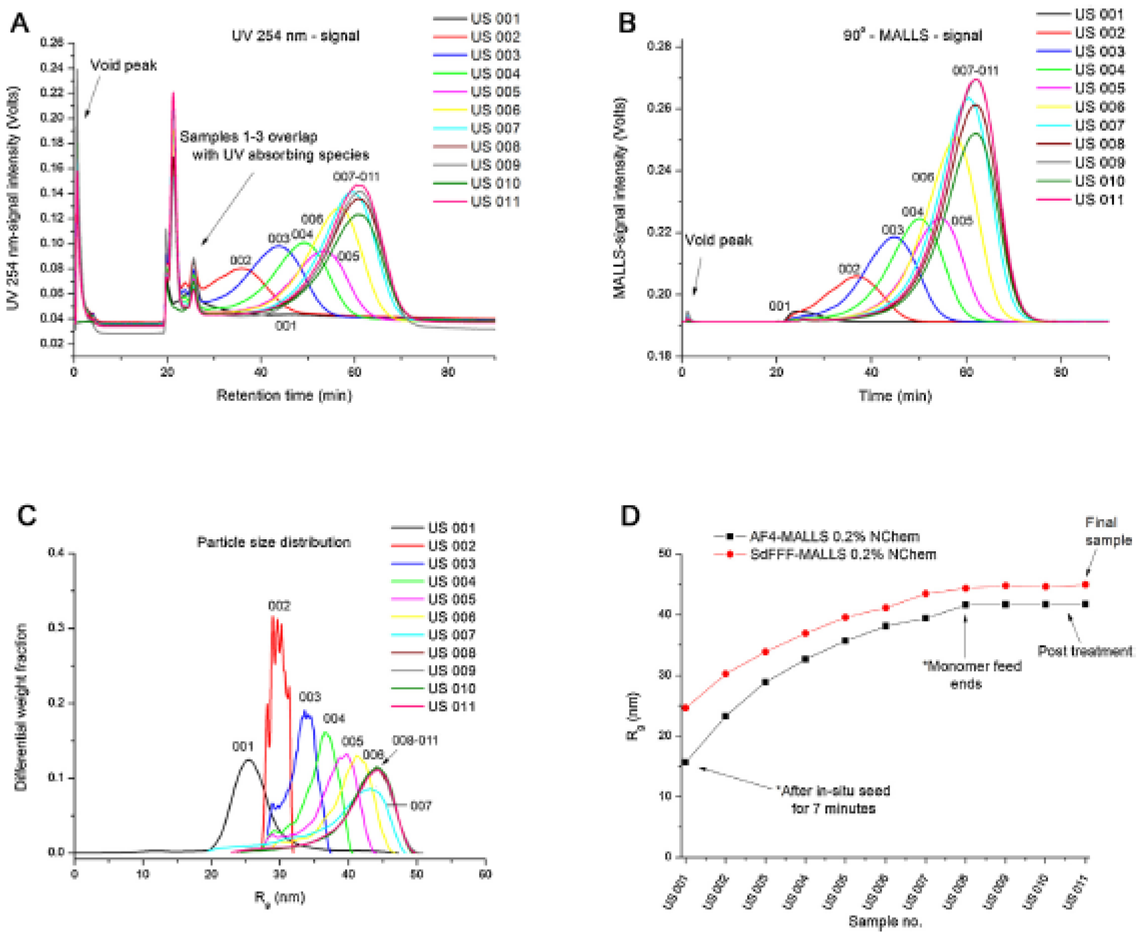

Figure 3.3. Particle radii (R_g) analysis of the pure acrylic latex (sample 1). A and B: UV 254 nm and MALLS signals from SdFFF separation. C: Differential PSD, D: Evolution of particle radii (R_g) obtained from SdFFF- and AF4-UV-MALLS using 0.2 vol% surfactant in deionized water as mobile phase.

These peaks were also present when a blank sample was injected and were only detected in the UV-signal and not in the MALLS-signal. The particles from samples US 001 to US 003 remain unrelaxed due to the small size of the particles under the centrifugal field, although the maximum field (4900 rpm, 2700 G) and a 15 min relaxation time were applied. The relaxation time was determined by varying the relaxation time in 5 minute increments in order to obtain acceptable separation between the void peak and sample peak. 15 minute relaxation was applied to all analyzed samples. The PSD for US 001 – US 003 (**Figure 3.3 C**) indicate a trend towards higher polymer particle radii values as the polymerization progresses. Samples US 004 to US 011 were successfully separated by SdFFF and display a similar trend in the PSD (**Figure 3.3 C**, samples 1 – 11). Furthermore the overall resolution is higher with SdFFF compared to the AF4 results. The analysis time was, however, three times longer for SdFFF (75 minutes) compared to AF4 (25 minutes).

The PSD shows a comparable increase in R_g featuring a shoulder in the low particle radii region (30 nm to 35 nm), as reported in **Figure 3.3 C**, indicating a second PSD, which phases out after the end of monomer feed was reached, characteristic of monomer-starved conditions [55]. Samples labeled US 003 – US 005 indicate that the shoulder remains constant at around 30 nm, which corresponds to the postulation that stochastic broadening takes place as larger particles are present together with the smaller non-growing particles, leading to a broader PSD. This was ascribed to monomer-starved conditions early in the polymerization [55].

These new findings of a second population or shoulder formation were not seen using AF4 technology (**Figure 3.2 E**), which can be attributed to shorter elution times along with better overall resolution capabilities of SdFFF. Similar to the AF4 results, the PSD remained constant after monomer feed has ended, which supports that the two separation principles correlate well with each other using the same detector setup (MALLS-UV). A comparison of the two FFF techniques (AF4, SdFFF) to investigate the evolution of particle radii is displayed in **Figure 3.3 D**.

Separation using SdFFF features additional separation power. In addition to hydrodynamic radii, separation in SdFFF also occurs through density differences between analyte and mobile phase [43]. The centrifugal force exerted on the particles and an axial flow of 0.5 mL/min during separation in SdFFF, result in dissimilar values compared to AF4. A comparison of the PSD obtained from AF4-UV-MALLS is displayed in **Figure 3.4**, which indicates the increase in R_g upon polymerization time up until the end of monomer feed (sample 8), after which the radii distribution width remain constant (sample 9). The increase in R_g followed by a stable reading is apparent for both separation techniques, with the PSD of SdFFF indicating a broader particle radii range.

Comparable results along with high reproducibility render both systems suitable for particle radii analyses of polymerized nano-sized particles. Furthermore, SdFFF represents a complementary technique with additional separation power by density, if differences in particle densities are present. For the current analyses, it is assumed that the particle mass-to-volume ratio remain constant throughout the polymerization reaction, which renders a constant density from sample 001 to 011.

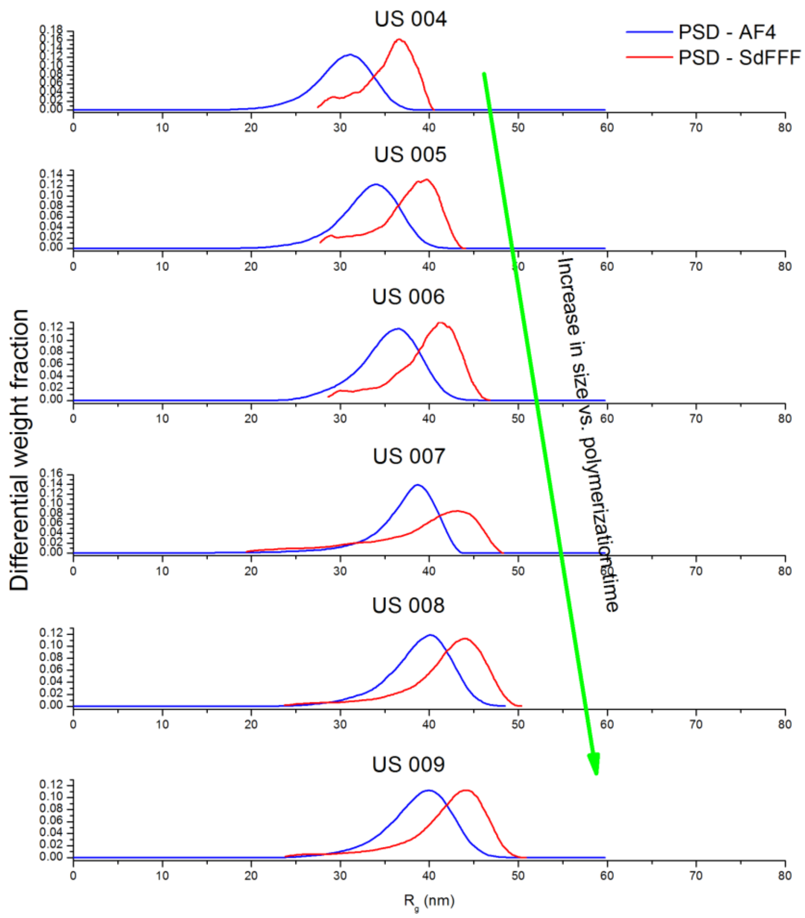

Figure 3.4. AF4 and SdFFF overlay of PSD for US 004 - US 009 .The displayed size information corresponds to radius of gyration (R_g) for both separation techniques.

Giddings and Ho analyzed polystyrene lattices with different particle sizes with similar densities using SdFFF [44]. In SdFFF, the resolution showed to be limited and unresolved for small-sized particles. In this comparative study, both AF4 and SdFFF could reveal information on particle radii for all the samples collected from the reactor during the latex polymerization reaction, thus allowing a deep insight into complex particle systems and their evolution.

3.4.1.4 AF4-MALLS-UV-ICP-MS for the separation and speciation of TiO_2-spiked latices

Latices are typically used as film forming species, while TiO_2 is used in cosmetics (e.g. sunscreen), medical applications and coatings. TiO_2 is used as opacifier in coatings by reflecting light and in addition increasing the degree of whiteness. The analyzed acrylic and the styrene-acrylic latices were separately mixed with TiO_2 nanoparticles (Huntsman) to investigate the retention behaviour under FFF conditions. By utilizing the mixing and shaking technology option of the autosampler (PN 5300) a defined injection of a representative amount of sample was ensured. The AF4-MALLS-UV setup was coupled online via the FFF-interface directly to the ICP-MS analyzer for continuous detection of Ti^{48} eluting from the channel to investigate particle-particle interactions between latex and TiO_2 particles. For the polymer-TiO_2 interaction studies, the final (bulk) samples of the pure acrylic latex (US 011) and the styrene-acrylic (US 012) latex were investigated.

Figure 3.5 displays the results obtained by AF4-MALLS-UV-ICP-MS. Initially, the pure latex and pure TiO_2 samples which were diluted in 0.2 vol% surfactant solution were analyzed separately (**Figures. 6 A and B**) before analyzing the titanium dioxide spiked mixture (**Figure 3.5 C**). Identical AF4 separation conditions were used as in the initial PSD study discussed in the preceding section. The ICP-MS analysis of the pure samples showed sufficient separation capabilities with respect to retention time and gave acceptable results for the mixed organic-inorganic sample mixture (**Figure 3.5 C**). After evaluation of the pure and mixed samples by AF4, separation showed adequate resolution to obtain particle radii and the data were processed to perform a distribution analysis and to speciate the separated analytes in the complex mixture.

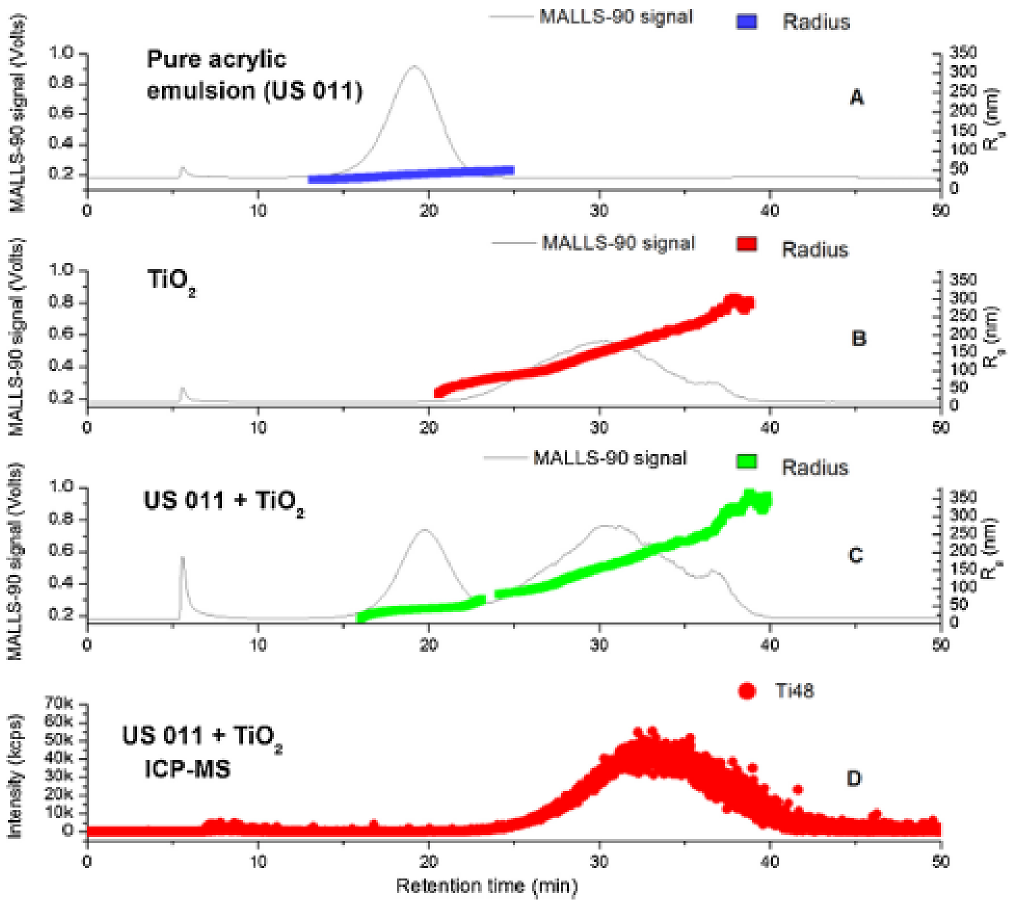

Figure 3.5. A: Particle radii of pure acrylic latex (US 011) obtained by MALLS. B: Particle radii of TiO_2 assessed by MALLS. C: Particle radii of the TiO_2-spiked latex mixture. D: ICP-MS traces of Ti^{48} after separation of the polymerized latex and TiO_2.

The results of the coupling of AF4 to ICP-MS are displayed in **Figure 3.5 D**. The obtained Ti^{48} trace corresponds well with the TiO_2 peak observed in the organic-inorganic mixture as well as the individual TiO_2 fractogram. Based on the ICP-MS results obtained and the resolution achieved it was proven that the different species, in particular titanium dioxide nanoparticles and acrylic nanoparticles present in the latex did not interfere during the mixing process. Since no Ti^{48} trace was observed during elution of the acrylic latex peak, both ingredients can be expected to be stable and independently present within the formulation.

A similar study was conducted with the styrene-acrylic latex (US 012). The hydrodynamic radii of this latex (**Table 3.2**) were smaller than the pure acrylic latex and, upon spiking the latex with TiO_2, a better separation was obtained with the two peaks being completely baseline separated (**Figures.3. 6 A and B**). Similar to the pure acrylic latex sample, no Ti^{48} trace was observed for the styrene-acrylic latex-TiO_2 mixture in the ICP-MS traces (**Figure 3.6 C**), proving that no latex-TiO_2 interaction took place for the respective organic-inorganic mixture.

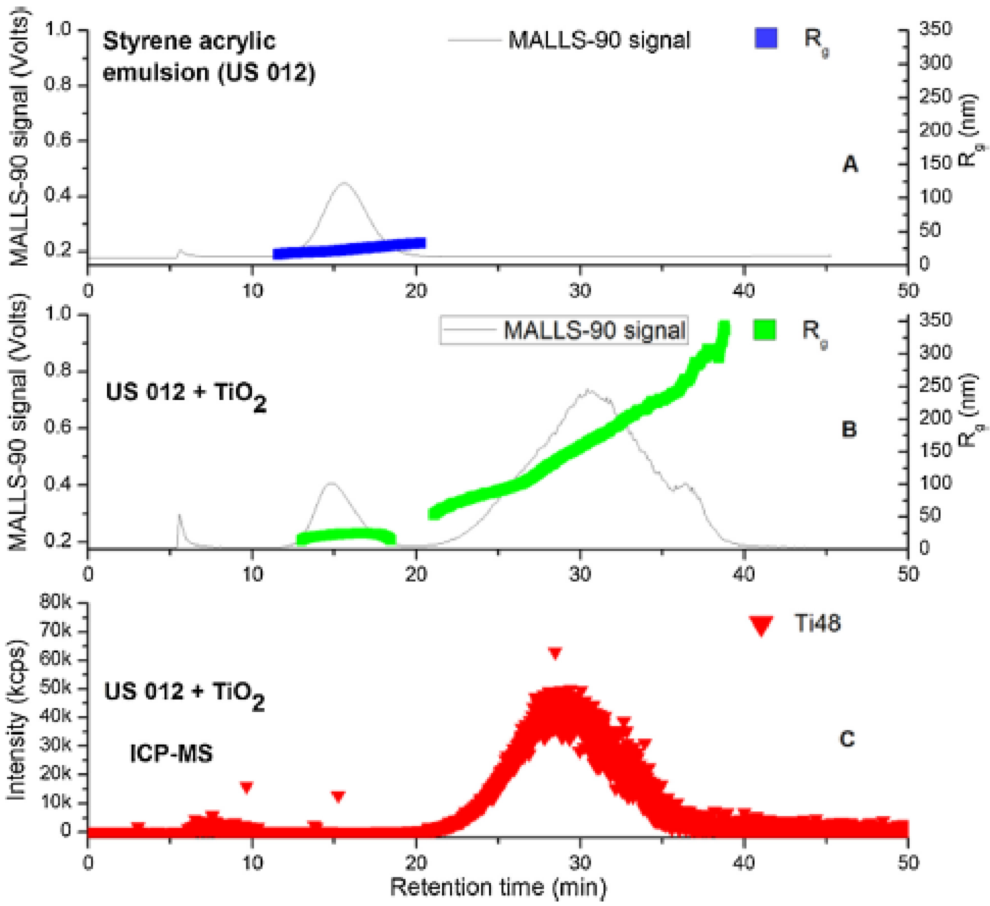

Figure 3.6. A: Particle radii of styrene-acrylic latex (US 012) obtained by MALLS. B: Particle radii of the TiO_2-spiked latex mixture. C: ICP-MS traces of Ti^{48} after separation of the polymerized styrene acrylic latex and TiO_2.

The effect of increasing concentration on the detector AF4-MALLS-UV response was evaluated for the acrylic latex sample (US 011) at a wavelength of 254 nm. The latex sample showed an increase in peak area for the UV 254 nm signal (**Figure 3.7**) and peak broadening towards earlier retention times as the concentration increased. From the peak areas, quantification of latex particles in solution would be possible if additional concentrations would be injected, followed by the generation of a calibration curve (Supplementary information).

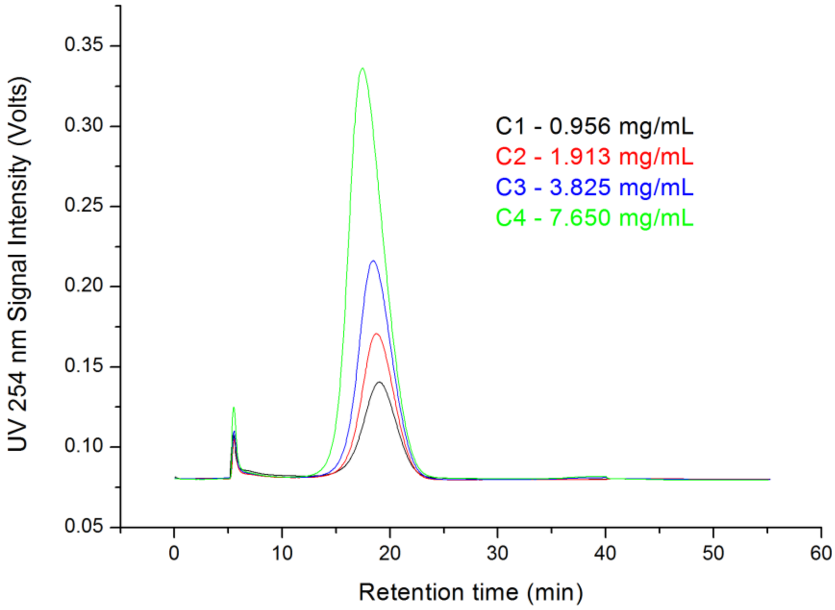

Figure 3.7. Increase in sample concentration on the UV 254 nm signal for the pure acrylic (US 011) latex upon AF4-UV-MALLS analyses.

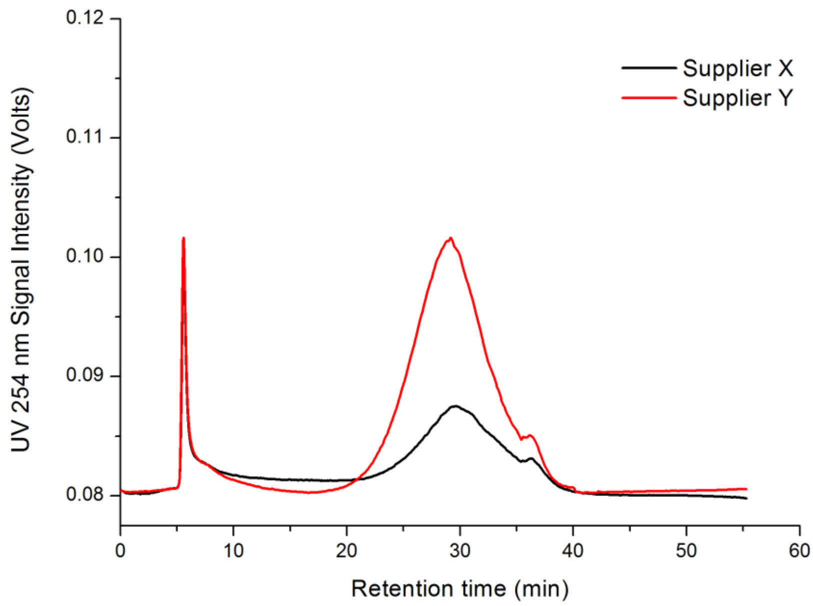

Figure 3.8. AF4-UV fractograms of two commercial TiO_2 samples. The concentrations for both samples were 0.1 mg/mL, monitoring the UV-254 nm signal.

Two commercial grades of TiO_2 (supplier X and US supplier Y) with average particle diameters of 230 nm and 250 nm, respectively were injected using the AF4-MALLS-UV-RI configuration at a concentration of 0.1 mg/mL in order to monitor the elution profile of the inorganic species (**Figure 3.8**). The TiO_2 grade from Supplier X indicate a lower signal in comparison to the TiO_2 sample of supplier Y. Due to a higher average particle, the scattering of supplier Y TiO_2 were a lot more intense in comparison to supplier X. Both samples had a small shoulder eluting at retention times. The small shoulder may be due to agglomeration of small amounts of TiO_2 particles size, or an indication of bimodality within the sample [26]. An increase in concentration revealed that the shoulder for both samples increased in intensity, but not in retention time.

3.4. Conclusions

A combination of AF4 and SdFFF technology with a multi-detection system (MALLS, UV, RI) has been implemented to investigate R_g and its distribution of acrylic and styrene-acrylic latices synthesized by free radical polymerization. Recognizable R_g trends were evident when comparing all FFF results with the classical batch DLS results. Similar R_g trends were observed in AF4, SdFFF and DLS. A lack of separation power was observed for the small nano-sized polymer particles (US 001 – US 003) by SdFFF in the initial stages of polymerization. The PSDs obtained by SdFFF gave rise to a second size population present up to the end of the monomer feed; remarkably this population was only resolvable by the centrifugal force acting on the particles. These secondary particle populations were more pronounced due to the separation resolution capabilities of SdFFF. However, FFF proved to be the technique of choice for monitoring of the polymerization progress in detail regarding particle radii and PSD. Both techniques of AF4 and SdFFF complement each other and deliver insightful results. Furthermore, to our knowledge we showed for the first time the performance of both FFF techniques on similar samples to address how particle radii and PSDs are affected by the different separation forces.

For an even deeper insight into complex particle-latex mixtures, in particular to evaluate the interaction of inorganic nanoparticles with organic nanoparticles, the latex samples (acrylic or styrene-acrylic) were spiked with TiO_2 and analyzed by online AF4-MALLS-UV-ICP-MS coupling. The organic latex samples were successfully separated from the TiO_2 nanoparticles in the mixture and the inorganic material was identified by ICP-MS detection of the Ti^{48} trace. The styrene-acrylic latex was separated from the TiO_2 species with a higher resolution, in comparison to the pure acrylic latex. FFF coupled to a multi-detector system is a valuable tool for the determination of particle radii information and distribution analysis of polymer latices. By coupling the FFF device to an elemental speciation detector, such as ICP-MS, trace levels of different inorganic species, especially in the coatings industries can be identified in a straightforward manner.

3.5. Acknowledgements

We would like to thank the synthesis team of Kansai Plascon Research Centre in Stellenbosch, South Africa, for the preparation of the latex samples. The Postnova Analytics team in Landsberg, Germany, is thanked for making their lab instrumentation available to conduct experiments and for the valuable discussions.

3.6 References

[1] J.V. Koleske, Paint and Coating Testing Manual, ASTM International, 1995.

[2] M. do Amaral, A. Roos, J.M. Asua, C. Creton, Assessing the effect of latex particle size and distribution on the rheological and adhesive properties of model waterborne acrylic pressure-sensitive adhesives films, J. Colloid Interface Sci. 281 (2005) 325-338.

[3] A. Sood, Particle size distribution control in emulsion polymerization, J. Appl. Polym. Sci. 92 (2004) 2884-2902.

[4] H. Hinterwirth, S.K. Wiedmer, M. Moilanen, A. Lehner, G. Allmaier, T. Waitz, W. Lindner, M. Lämmerhofer, Comparative method evaluation for size and size-distribution analysis of gold nanoparticles, J. Sep. Sci. 36 (2013) 2952-2961.

[5] S. Carro, J. Herrera-Ordonez, J. Castillo-Tejas, On the evolution of the rate of polymerization, number and size distribution of particles in styrene emulsion polymerization above CMC, J. Polym. Sci., Part A: Polym. Chem. 48 (2010) 3152-3160.

[6] S. Carro, J. Herrera-Ordonez, Styrene Emulsion Polymerization above the CMC: New Evidence on Particle Nucleation by means of AFFFF, Macromol. Rapid Commun. 27 (2006) 274-278.

[7] H. Kato, A. Nakamura, K. Takahashi, S. Kinugasa, Accurate Size and Size-Distribution Determination of Polystyrene Latex Nanoparticles in Aqueous Medium Using Dynamic Light Scattering and Asymmetrical Flow Field Flow Fractionation with Multiangle Light Scattering, Nanomaterials 2 (2012) 15-30.

[8] F.A. Messaud, R.D. Sanderson, J.R. Runyon, T. Otte, H. Pasch, S.K.R. Williams, An overview on field-flow fractionation techniques and their applications in the separation and characterization of polymers, Prog. Polym. Sci. 34 (2009) 351-368.

[9] W. Frankema, M. van Bruijnsvoort, R. Tijssen, W.T. Kok, Characterisation of core-shell latexes by flow field-flow fractionation with multiangle light scattering detection, J. Chromatogr. A 943 (2002) 251-261.

[10] H. Thielking, W.-M. Kulicke, On-Line Coupling of Flow Field-Flow Fractionation and Multiangle Laser Light Scattering for the Characterization of Macromolecules in Aqueous Solution As Illustrated by Sulfonated Polystyrene Samples, Anal. Chem. 68 (1996) 1169-1173.

[11] M.E. Schimpf, K. Caldwell, J.C. Giddings, Field Flow Fractionation Handbook, John Wiley & Sons, New York, 2000.

[12] L. Böhmert, M. Girod, U. Hansen, R. Maul, P. Knappe, B. Niemann, S.M. Weidner, A.F. Thünemann, A. Lampen, Analytically monitored digestion of silver nanoparticles and their toxicity on human intestinal cells, Nanotoxicology 8 (2014) 631-642.

[13] S. Schachermeyer, J. Ashby, W. Zhong, Aptame-protein binding detected by asymmetric flow field flow fractionation, J. Chromatogr. A 1295 (2013) 107-113.

[14] D. Lattuada, B. Roda, C. Pignatari, R. Magni, F. Colombo, A. Cattaneo, A. Zattoni, I. Cetin, P. Reschiglian, G. Bolis, A tag-less method for direct isolation of human umbilical vein endothelial cells by gravitational field-flow fractionation, Anal. Bioanal. Chem. 405 (2013) 977-984.

[15] V. Sarrazy, N. Vedrenne, N. Bordeau, F. Billet, P. Cardot, A. Desmoulière, S. Battu, Fast astrocyte isolation by sedimentation field flow fractionation, J. Chromatogr. A 1289 (2013) 88-93.

[16] Tsutomu Arakawa, John S. Philo, Daisuke Ejima, Kouhei Tsumoto, F. Arisaka, Aggregation Analysis of Therapeutic Proteins, Part 1, BioProcess International 4 (2006) 42-43.

[17] J. Kuntsche, C. Decker, A. Fahr, Analysis of liposomes using asymmetrical flow field-flow fractionation: Separation conditions and drug/lipid recovery, J. Sep. Sci. 35 (2012) 1993-2001.

[18] K.H. Kim, J.Y. Kim, M.O. Kim, M.H. Moon, Two dimensional (pI & d_s) separation of phosphorylated proteins by isoelectric focusing/asymmetrical flow field-flow fractionation: Application to prostatic cancer cell line, Journal of Proteomics 75 (2012) 2297-2305.

[19] J.Y. Kim, S.-K. Kim, D. Kang, M.H. Moon, Dual Lectin-Based Size Sorting Strategy to Enrich Targeted N-Glycopeptides by Asymmetrical Flow Field-Flow Fractionation: Profiling Lung Cancer Biomarkers, Anal. Chem. 84 (2012) 5343-5350.

[20] V. Nischwitz, H. Goenaga-Infante, Improved sample preparation and quality control for the characterisation of titanium dioxide nanoparticles in sunscreens using flow field flow fractionation on-line with inductively coupled plasma mass spectrometry, J. Anal. At. Spectrom. 27 (2012) 1084-1092.

[21] I.C. Regelink, L. Weng, G.F. Koopmans, W.H. van Riemsdijk, Asymmetric flow field-flow fractionation as a new approach to analyse iron-(hydr)oxide nanoparticles in soil extracts, Geoderma 202-203 (2013) 134-141.

[22] B. Stolpe, L. Guo, A.M. Shiller, G.R. Aiken, Abundance, size distributions and trace-element binding of organic and iron-rich nanocolloids in Alaskan rivers, as revealed by field-flow fractionation and ICP-MS, Geochim. Cosmochim. Acta 105 (2013) 221-239.

[23] A.D. Pifer, J.L. Fairey, Improving on SUVA254 using fluorescence-PARAFAC analysis and asymmetric flow-field flow fractionation for assessing disinfection byproduct formation and control, Water Res. 46 (2012) 2927-2936.

[24] D.M. Mitrano, A. Barber, A. Bednar, P. Westerhoff, C.P. Higgins, J.F. Ranville, Silver nanoparticle characterization using single particle ICP-MS (SP-ICP-MS) and asymmetrical flow field flow fractionation ICP-MS (AF4-ICP-MS), J. Anal. At. Spectrom. 27 (2012) 1131-1142.

[25] M. Baalousha, J.R. Lead, Rationalizing Nanomaterial Sizes Measured by Atomic Force Microscopy, Flow Field-Flow Fractionation, and Dynamic Light Scattering: Sample Preparation, Polydispersity, and Particle Structure, Environmental Science & Technology 46 (2012) 6134-6142.

[26] S. Kenta, V. Raikos, A. Vagena, D. Sevastos, J. Kapolos, A. Koliadima, G. Karaiskakis, Kinetic study of aggregation of milk protein and/or surfactant-stabilized oil-in-water emulsions by Sedimentation Field-Flow Fractionation, J. Chromatogr. A 1305 (2013) 221-229.

[27] M. Ulmius, G. Önning, L. Nilsson, Solution behaviour of barley Î²-glucan as studied with asymmetrical flow field-flow fractionation, Food Hydrocolloids 26 (2012) 175-180.

[28] H. Rübsam, M. Krottenthaler, M. Gastl, T. Becker, An overview of separation methods in starch analysis: The importance of size exclusion chromatography and field flow fractionation, Starch 64 (2012) 683-695.

[29] S. Kenta, V. Raikos, J. Kapolos, A. Koliadima, G. Karaiskakis, Sedimentation field-flow fractionation as a tool for the study of milk protein-stabilized model oil-in-water emulsions: effect of protein concentration and homogenization pressure, Journal of Liquid Chromatography & Related Technologies 36 (2013) 288-303.

[30] S. Juna, A. Huber, Molecular characteristics of native sago starch and isolated fractions determined using asymmetrical flow field-flow fractionation, Starch 64 (2012) 171-180.

[31] S. Juna, A. Huber, Effect of varying flow regimes upon elution behaviour, apparent molecular characteristics and hydrodynamic properties of amylopectin isolated from normal corn starch using asymmetrical flow field-flow fractionation, J. Chromatogr. A 1219 (2012) 161-172.

[32] S. Bartsch, W.M. Kulicke, I. Fresen, H.U. Moritz, Seeded emulsion polymerization of styrene: Determination of particle size by flow field-flow fractionation coupled with multiangle laser light scattering, Acta Polym. 50 (1999) 373-380.

[33] L. Dulog, T. Schauer, Field flow fractionation for particle size determination, Prog. Org. Coat. 28 (1996) 25-31.

[34] E.P.C. Mes, R. Tijssen, W.T. Kok, Influence of the carrier composition on thermal field-flow fractionation for the characterisation of sub-micron polystyrene latex particles, J. Chromatogr. A 907 (2001) 201-209.

[35] H. Hagendorfer, R. Kaegi, J. Traber, S.F.L. Mertens, R. Scherrers, C. Ludwig, A. Ulrich, Application of an asymmetric flow field flow fractionation multi-detector approach for metallic engineered nanoparticle characterization - Prospects and limitations demonstrated on Au nanoparticles, Anal. Chim. Acta 706 (2011) 367-378.

[36] E.P. Gray, T.A. Bruton, C.P. Higgins, R.U. Halden, P. Westerhoff, J.F. Ranville, Analysis of gold nanoparticle mixtures: a comparison of hydrodynamic chromatography (HDC) and asymmetrical flow field-flow fractionation (AF4) coupled to ICP-MS, J. Anal. At. Spectrom. 27 (2012) 1532-1539.

[37] M.M. Pornwilard, A. Siripinyanond, Field-flow fractionation with inductively coupled plasma mass spectrometry: Past, present, and future, J. Anal. At. Spectrom. 29 (2014) 1739-1752.

[38] R. Beckett, Field flow fractionation icp ms a powerful new analytical tool for characterizing macromolecules and particles, At. Spectrosc. 12 (1991) 228-232.

[39] H.E. Taylor, J.R. Garbarino, D.M. Murphy, R. Beckett, Inductively coupled plasma-mass spectrometry as an element-specific detector for field-flow fractionation particle separation, Anal. Chem. 64 (1992) 2036-2041.

[40] A.J. Bednar, A.R. Poda, D.M. Mitrano, A.J. Kennedy, E.P. Gray, J.F. Ranville, C.A. Hayes, F.H. Crocker, J.A. Steevens, Comparison of on-line detectors for field flow fractionation analysis of nanomaterials, Talanta 104 (2013) 140-148.

[41] S.T. Kim, H.K. Kim, S.H. Han, E.C. Jung, S. Lee, Determination of size distribution of colloidal TiO_2 nanoparticles using sedimentation field-flow fractionation combined with single particle mode of inductively coupled plasma-mass spectrometry, Microchem. J. 110 (2013) 636-642.

[42] I. López-Heras, Y. Madrid, C. Cámara, Prospects and difficulties in TiO_2 nanoparticles analysis in cosmetic and food products using asymmetrical flow field-flow fractionation hyphenated to inductively coupled plasma mass spectrometry, Talanta 124 (2014) 71-78.

[43] J.C. Giddings, Measuring colloidal and macromolecular properties by FFF, Anal. Chem. 67 (1995) 592A-598A.

[44] J.C. Giddings, J. Ho, Accurate measurement of density of colloidal latex particles by sedimentation field-flow fractionation, Langmuir 11 (1995) 2399-2404.

[45] J. Choi, H.D. Kwen, Y.S. Kim, S.H. Choi, S. Lee, Y-ray synthesis and size characterization of CdS quantum dot (QD) particles using flow and sedimentation field-flow fractionation (FFF), Microchem. J. 117 (2014) 34-39.

[46] J.R. Runyon, M. Ulmius, L. Nilsson, A perspective on the characterization of colloids and macromolecules using asymmetrical flow field-flow fractionation, Colloids and Surfaces A: Physicochemical and Engineering Aspects 442 (2014) 25-33.

[47] K. Tauer, R. Deckwer, I. Kühn, C. Schellenberg, A comprehensive experimental study of surfactant-free emulsion polymerization of styrene, Colloid. Polym. Sci. 277 (1999) 607-626.

[48] K. Tauer, H. Hernandez, S. Kozempel, O. Lazareva, P. Nazaran, Towards a consistent mechanism of emulsion polymerization—new experimental details, Colloid. Polym. Sci. 286 (2007) 499-515.

[49] S. Sajjadi, Particle formation under monomer-starved conditions in the semibatch emulsion polymerization of styrene. I. Experimental, J. Polym. Sci., Part A: Polym. Chem. 39 (2001) 3940-3952.

[50] E.A. Mun, C. Hannell, S.E. Rogers, P. Hole, A.C. Williams, V.V. Khutoryanskiy, On the Role of Specific Interactions in the Diffusion of Nanoparticles in Aqueous Polymer Solutions, Langmuir 30 (2014) 308-317.

[51] Y. Hwang, C. Lee, Y. Choi, S. Cheong, D. Kim, K. Lee, J. Lee, S.H. Kim, Effect of the size and morphology of particles dispersed in nano-oil on friction performance between rotating discs, Journal of Mechanical Science and Technology 25 (2011) 2853-2857.

[52] J.G. McGrath, Synthesis and characterization of core/shell hydrogel nanoparticles and their application to colloidal crystal optical materials, School of Chemistry and Biochemistry & Petit Institute for Bioengineering and Bioscience, Georgia Institute of Technology, Georgia, 2007, p. 1-236.

[53] A.M. Striegel, Hydrodynamic chromatography: packed columns, multiple detectors, and microcapillaries, Anal. Bioanal. Chem. (2011) 1-5

[54] L. Pitkänen, A.M. Striegel, AF4/MALS/QELS/DRI characterization of regular star polymers and their "span analogs", Analyst 139 (2014) 5843-5851.

[55] J. Zeaiter, J. A. Romagnoli, G. W. Barton, V. G. Gomes, B. S. Hawkett, R. G. Gilbert, Operation of semi-batch emulsion polymerisation reactors: Modelling, validation and effect of operating conditions, Chem. Eng. Sci. 57 (2002) 2955-2969.

[56] T. Otte, H. Pasch, T. Macko, R. Brüll, F.J. Stadler, J. Kaschta, F. Becker, M. Buback, Characterization of branched ultrahigh molar mass polymers by asymmetrical flow field-flow fractionation and size exclusion chromatography, J. Chromatogr. A 1218 (2011) 4257-4267.

[57] T. Otte, R. Brüll, T. Macko, H. Pasch, T. Klein, Optimisation of ambient and high temperature asymmetric flow field-flow fractionation with dual/multiangle light scattering and infrared/refractive index detection, J. Chromatogr. A 1217 (2010) 722-730.

[58] R. Beckett, J. Ho, Y. Jiang, J.C. Giddings, Measurement of mass and thickness of adsorbed films on colloidal particles by sedimentation field-flow fractionation, Langmuir 7 (1991) 2040-2047.

[59] P. Blau, R.L. Zollars, Sedimentation field-flow fractionation of nonspherical particles, J. Colloid Interface Sci. 183 (1996) 476-483.

[60] T. Hoshino, M. Suzuki, K. Ysukawa, M. Takeuchi, Effects of detergent on the elution profiles of latex beads in sedimentation field-flow fractionation, J. Chromatogr. A 400 (1987) 361-369.

[61] J.T. Li, K.D. Caldwell, Sedimentation field flow fractionation in the determination of surface concentration of adsorbed materials, Langmuir 7 (1991) 2034-2039.

[62] P.S. Williams, M.H. Moon, Y. Xu, J.C. Giddings, Effect of viscosity on retention time and hydrodynamic lift forces in sedimentation/steric field-flow fractionation, Chem. Eng. Sci. 51 (1996) 4477-4488.

3.7 Supplementary Data

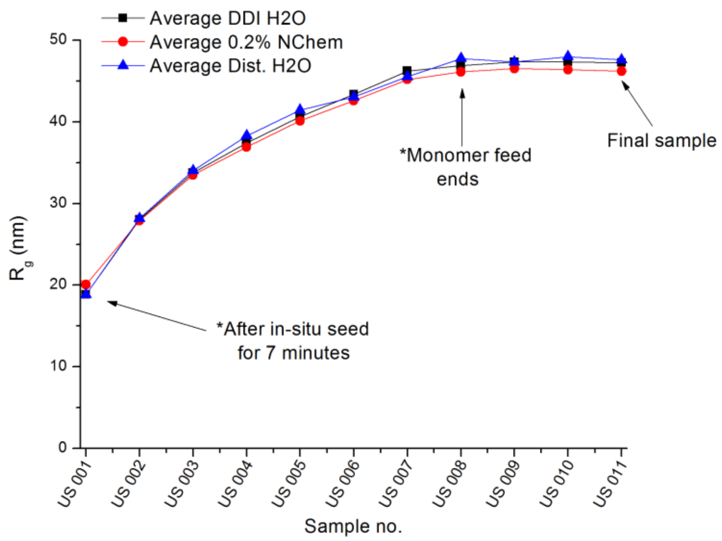

Figure S1. Particle radii (R_g) of US 001 – US 011 in distilled, DDI and 0.2% surfactant-containing (Novachem) DDI water, respectively..

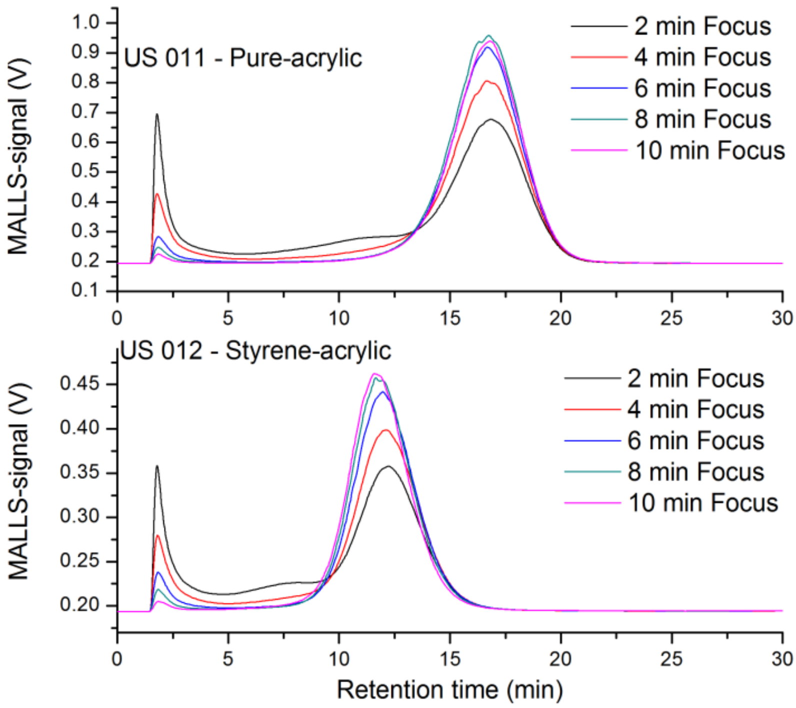

Figure S2. AF4-MALLS fractograms of pure-acrylic (sample 1, US 011, **top**) and styrene-acrylic (sample 2, US 012, **bottom**) latices after post treatment varying the focus times. The focus times were subtracted from the fractograms.

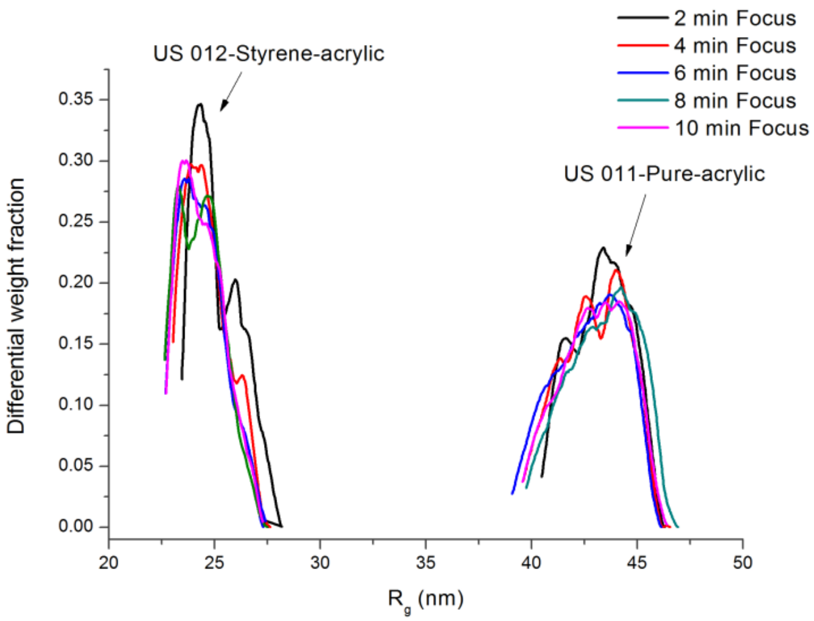

Figure S3. Effect of different focus times on differential PSD of the pure (sample 1) - and styrene-acrylic (sample 2) latices.

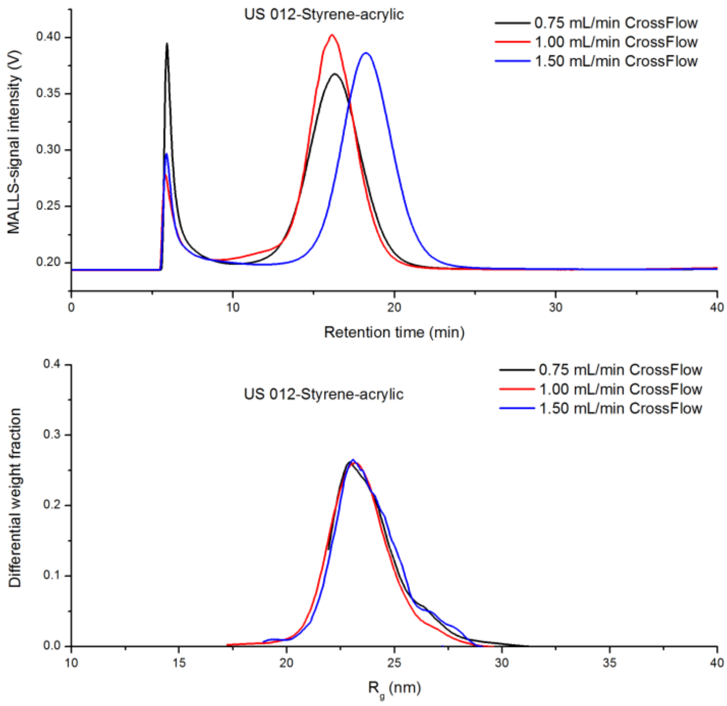

Figure S4. Effect of an increase in AF4 cross-flow strength on the retention time (MALLS, **top**) and corresponding differential PSD (**bottom**) integrated at Peak width at half height (PWHH), for the styrene-acrylic (sample 2) latex.

Chapter 4: Field-Flow Fractionation for the Size, Molar Mass and Gel Content Analysis of Latex Polymers for Water-Based Coatings

Full Paper

Macromolecular Journals

Macromolecular Chemistry and Physics

Field Flow Fractionation for the Size, Molar Mass, and Gel Content Analysis of Emulsion Polymers for Water-Based Coatings

Ashwell C. Makan, Ryan P. Williams, Harald Pasch*

In the present investigation, styrene-acrylic and pure acrylic emulsions used in water-based decorative coatings are characterized by size exclusion chromatography (SEC) and asymmetric flow field-flow fractionation (AF4). Both the separation techniques are coupled online to multiangle laser light scattering (MALLS) and refractive index detection to investigate the molar mass properties during the course of the free radical polymerization reaction. For the acrylic emulsion, kinetic samples are taken from the reactor at fixed time intervals and analyzed. In SEC-MALLS, unusual elution behavior is observed which is found previously for highly branched polymer species. In contrast, the AF4 fractograms indicate normal mode elution without any unusual behavior as compared to the SEC analyses. The molar masses obtained by AF4 are significantly higher compared to the SEC results. Further, AF4 is used to determine the gel contents of the kinetic samples of the acrylic emulsion and for both the acrylic and styrene-acrylic emulsions, AF4 proves to be a robust and feasible tool allowing for improved correlations of the molecular and materials properties of water-based polymer emulsions.

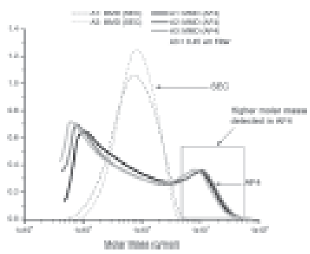

1. Introduction

Film forming components in coating formulations are typically complex polymer formulations based on styrene and a number of acrylates/methacrylates. Most frequently, these polymers are synthesized by free radical emulsion polymerization.[1] Emulsion polymers are well established in various fields including styrene-butadiene rubbers (SBR) in the automotive industry, amphiphilic polymers in food technology and core shell particles in drug delivery systems.[2–4] Typical emulsion systems for water-based coatings contain styrene, acrylic monomers, and crosslinking agents. The chemical heterogeneity of an emulsion can be significant and molecular properties like the final chemical composition and the molar mass distribution are of high importance for the final coating properties.[5] An emulsion polymer with too low molar mass can cause low molar mass additives to leach out of the coating toward the surface causing defects on the coating surface.[6]

Molar masses of emulsion polymers are typically determined by size exclusion chromatography (SEC) using classical calibration techniques[7–9] based on a set of calibration standards, e.g., polystyrene or polymethyl methacrylate. The resolution and the upper molar mass limit in SEC are determined by the type of the stationary phase, its particle and pore size distributions. For SEC analysis, the polymer samples are dissolved in a thermodynamically

A. C. Makan, R. P. Williams
Kansai Plascon Research Centre
Polymer Science Building, Room 2028
University of Stellenbosch
7602, Matieland, South Africa
A. C. Makan, Prof. H. Pasch
Department of Chemistry and Polymer Science
University of Stellenbosch
Private Bag X1, Matieland 7602, South Africa
E-mail: hpasch@sun.ac.za

Macromol. Chem. Phys. 2016, 217, 2027–2040

wileyonlinelibrary.com
DOI: 10.1002/macp.201600208

4.1 Abstract

In the present investigation, styrene-acrylic and pure acrylic latices used in water-based decorative coatings are characterized by size exclusion chromatography (SEC) and asymmetric flow field-flow fractionation (AF4). Both separation techniques are coupled online to multiangle laser light scattering (MALLS) and refractive index (RI) detection to investigate the molar mass properties during the course of the free radical polymerization reaction. For the acrylic latex, kinetic samples are taken from the reactor at fixed time intervals and analyzed. In SEC-MALLS, unusual elution behaviour was observed which was found previously for highly branched polymer species. In contrast, the AF4 fractograms indicated normal mode elution without any unusual behaviour as compared to the SEC analyses. The molar masses obtained by AF4 are significantly higher compared to the SEC results. Further, AF4 is used to determine the gel contents of the kinetic samples of the acrylic latex and for both the acrylic and styrene-acrylic latices AF4 proves to be a robust and feasible tool allowing for improved correlations of the molecular and materials properties of water-based polymer latices.

4.2 Introduction

Film forming components in coating formulations are typically complex polymer formulations based on styrene and a number of acrylates/methacrylates. Most frequently, these polymers are synthesized by free radical latex polymerization.[1] Latex polymers are well established in various fields including styrene-butadiene rubbers (SBR) in the automotive industry, amphiphilic polymers in food technology and core shell particles in drug delivery systems.[2-4] Typical latex systems for water-based coatings contain styrene, acrylic monomers and crosslinking agents. The chemical heterogeneity of latex particles have a significant impact on molecular properties, i.e. the final chemical composition and the molar mass distribution are of high importance for the final physical properties of coatings.[5] A latex polymer with too low molar mass can cause low molar mass additives to leach out of the coating towards the surface causing defects on the coating surface.[6]

Molar masses of latex polymers are typically determined by size exclusion chromatography (SEC) using classical calibration techniques [7-9] based on a set of calibration standards, e.g. polystyrene or polymethyl methacrylate. The resolution and the upper molar mass limit in SEC are determined by the type of the stationary phase and its particle and pore size distributions. For SEC analysis, the polymer samples are dissolved in a thermodynamically good solvent such as tetrahydrofuran (THF). Before the sample solution is injected onto the column, it is typically filtered through a 0.45 μm filter. If the polymer solution contains gel particles (which is frequently the case for latex polymers), these particles together with very high molar mass polymer fractions are filtered off and only the soluble part of the sample will be fractionated and analyzed. The resulting molar mass information will be inaccurate and not representative for the complete sample. Typically, the calculated molar masses will be lower than the true molar masses. Latex polymers may also contain ultrahigh molar mass fractions which might be shear-degraded in the SEC column by the pores of the stationary phase or the column frits.[10] This will also result in inaccurate molar mass analyses.

Field-flow fractionation (FFF) is a separation technique that can overcome some of the drawbacks observed in SEC.[11] Since no stationary phase is used, shear degradation is largely reduced. For FFF the upper molar mass limit is much higher than for SEC and, therefore, much higher molar mass polymers can be properly analyzed.[12] As no stationary phase is present, filtering of the samples is not required and the soluble and gel containing fractions of the complex samples can be analyzed without problems. Thermal FFF (ThFFF) has been used for analysis of SBR latices,[2] while sedimentation FFF (SdFFF) has extensively been used to characterize particle size distributions of colloidal species.[13] Striegel and co-workers have measured the particle size and shape distribution of colloidal species using hydrodynamic chromatography (HDC).[14, 15] Up to date, there are not many applications of using asymmetric flow field-flow fractionation (AF4) in the field of polymer latices used in coatings. Podzimek et al. showed that acrylic latices can be characterized in both aqueous and organic media using AF4-coupled to multiangle laser light scattering (MALLS).[16, 17] Makan et al. studied the behaviour of latex particles, synthesized by free radical polymerization, using AF4-UV-MALLS and SdFFF-UV-MALLS in aqueous media. Latices were blended with inorganic particles including TiO_2 and monitored using AF4 coupled to online inductively coupled mass spectrometry (AF4-UV-MALLS-ICP-MS). AF4 analyses revealed that the latices and the TiO_2 particles could be separated from each other with high resolution while SdFFF had a larger separation power to distinguish different particle size populations.[18]

In the present study SEC- and AF4-MALLS-RI were utilized for the molar mass characterization of styrene-acrylic and acrylic latices synthesized by free radical polymerization. During the acrylic latex polymerization, samples were removed periodically from the reactor at fixed time intervals. These were fractionated subsequently by SEC and AF4 and the molar mass information was compared. The gel contents of the acrylic latices were successfully determined by AF4.

4.3 Experimental

4.3.1 Materials and sample preparation

The pure acrylic latex (sample 1) featuring a low glass transition temperature (T_g) was synthesized with n-butyl acrylate (n-BA), methyl methacrylate (MMA) and methacrylic acid (MAA) while the styrene-acrylic latex (sample 2) was produced using styrene (Sty), n-BA, MMA and MAA as monomers, respectively. The monomers were added in specific ratios to produce copolymers with the desired T_g. The ratio of each monomer was approximated using the Flory-Fox equation and consequently adjusted once the actual copolymer was analyzed. For the pure acrylic sample (1) and styrene-acrylic sample (2) the targeted T_g was between 0–3 °C and 17–20 °C, respectively. The T_g values were confirmed with differential scanning calorimetry (DSC). The surfactant mixture (Disponal

A3065, Cognis GmbH, Düsseldorf, Germany and Aerosol EF-800, Cytec, Vlaardingen, Netherlands) was used above the critical micelle concentration and added in the range of 2.0-2.5 wt% active material to total monomer. A pre-latex was prepared with the predetermined ratio that corresponds to the T_g calculations. A 5L reactor was charged with water, surfactant and buffer and 5 vol% of the pre-latex was fed into the reactor to form an in-situ seed. The rest of the latex was fed into the reactor over three hours. The feed of the initiator solution (ammonium persulphate) was started two minutes prior to the latex feed and continued parallel to the latex feed. The reaction was run at 85°C. At the end of the latex and initiator feed the reactor contents were allowed to post-polymerize for an additional 35 minutes.

Table 4.1. Sampling procedure during the polymerization reaction for sample 1.

Sample code	Sampling details	Sampling time (hrs)
US 001	After in-situ seed formation for 7 minutes	0.0
US 002	30 minutes after feed started	0.5
US 003	1 hour after feed started	1.0
US 004	1.5 hours after feed started	1.5
US 005	2 hours after feed started	2.0
US 006	2.5 hours after feed started	2.5
US 007	3 hours after feed started	3.0
US 008	Monomer feed ends	3.5
US 009	20 minutes after delayed initiator	4.0
US 010	6.0 hours after feed started – final sample	6.0

The temperature of the reactor contents was then lowered to 40°C after which t-butyl hydroperoxide and sodium metabisulphite were added maximising the conversion. After the reactor contents reached room temperature, the pH was adjusted with a sodium hydroxide solution to increase the pH range to 7.5–8.5. The final non-volatile contents of the latexes were between 49.5–50.0 wt% and reached a viscosity between 200–700 cPs. Samples were drawn from the reactor vessel throughout the reaction starting 7 minutes after the seed was formed. A total of 11 samples (US001 to US010) of approximately three grams each were collected from the reactor at 30 minute intervals. After the reaction was completed, the last sample (US 010) was taken which represents the final processed latex. The sampling procedure of the pure acrylic latex (sample 1) and the time dependant samples removed from the vessel (US 001 – US 010) are summarized in **Table 4.1**. The latex samples were prepared for further analysis by drying small droplets placed onto Teflon sheets and air drying them overnight. The dried polymer spots were then dissolved in HPLC grade THF with an end concentration of approximately 3 mg/mL for SEC and 7 mg/mL for AF4. The samples were dissolved for two days at room temperature, followed by 3 hours of heating at 50 °C. After heating, the solutions were cooled to room temperature and stirred overnight at a very low rotation speed before being analyzed by SEC. The samples were filtered through a 0.45 µm filter prior to each SEC measurement. The dn/dc values for each sample were calculated by taking the sum of the weight fraction of each monomer multiplied by the respective dn/dc values of each homopolymer in THF (equation 1).

$$(dn/dc)_{emulsion} = w_A\,(dn/dc)_A + w_B\,(dn/dc)_B + \ldots \qquad (1)$$

where w_A and w_B denote the weight fractions of each monomer added to the latex feed.[9] The dn/dc values of the various latices used in the study are reported in **Table 4.2**. The monomer ratios were constant throughout the monomer feed of the polymerization reaction and the conversion reached was more than 99%.

Table 4.2. Monomer, monomer ratio, gel and dn/dc information of samples A, B and C.

Sample	Monomer system[a] (monomer ratio in mol L^{-1})	Gel	Calculated dn/dc (mL/g)
A. Styrene acrylic	Sty, BA , MMA, MAA (3.7/39/39.25/1)	None	0.072
B. Pure acrylic	BA, MMA, MAA (251/283/1)	Yes	0.078
C. Pure acrylic	BA, MMA (0.88/1)	Yes	0.078

[a] Sty: styrene, MMA: methyl methacrylate, BA: n-butyl acrylate, MAA: methacrylic acid

The Kansai Plascon test method to determine gel content entails drying the latex sample, followed by immersion in THF over a 1 week period. The supernatant is sampled from the stirred volumetric flask and dried until constant weight. The ratio of dried sample to the amount of sample dissolved in THF gives an indication of how much sample was dissolved. This method was compared against an FFF method, described later in the manuscript.

4.3.2 Instrumentation setup and analysis conditions

AF4 experiments were performed on an ambient temperature AF4 instrument (AF2000, Postnova Analytics, Landsberg/Germany) which was coupled to a MALLS (Dawn DSP, Wyatt Technology, Santa Barbara, USA) and a RI detector (PN 3140, Postnova Analytics, Landsberg/Germany). The channel was connected to three different pumps (tip, focus and cross-flow) while the injection port was equipped with a manual injection valve (Rheodyne, Rohnert Park, USA) with a 200 µL sample loop. A regenerated cellulose membrane was installed for the AF4 channel with an average molar mass cut-off of 5 000 g/mol. The Mylar spacer used for definition of the channel height had a thickness of 350 µm. The samples were introduced into the channel by manual injection. The tip flow rate before the injection of the sample was 0.2 mL/min for a period of 4 min. While the samples were injected, the cross flow was constant at 1.0 mL/min and the focus flow was automatically adjusted to 1.3 mL/min in order to maintain a constant detector flow of 0.5 mL/min. After the sample was injected, the focus flow rapidly decreased to zero within a minute, while the tip flow increased to 1.5 mL/min. After 2.5 min, the cross flow and the tip flow decreased exponentially to a value of 0.01 and 0.51 mL/min, respectively. The SEC setup consisted of a set of two PL Gel columns (mixed B and mixed C) (Church Stretton, UK) in series. The columns had dimensions of 300x7.5 mm i.d. The inlet of the mixed B column was connected to the tip pump while the outlet of the mixed C column was connected to the detectors (MALLS and RI). The flow rate used in SEC was 0.5 mL/min. Both SEC and AF4 used THF as mobile phase.

4.4 Results and discussion

4.4.1. SEC and AF4 analysis of sample A: styrene-acrylic latex

As an initial study the styrene-acrylic latex was analyzed by SEC and AF4 since it contained no gel content. The Kansai Plascon test method (PTM 0192) was used to determine the gel content gravimetrically which confirmed that no gel was present. It is well known that a small amount of styrene monomer incorporated into an acrylic latex system leads to negligible or no gel content due to the bulky pendant styrene groups.[1]

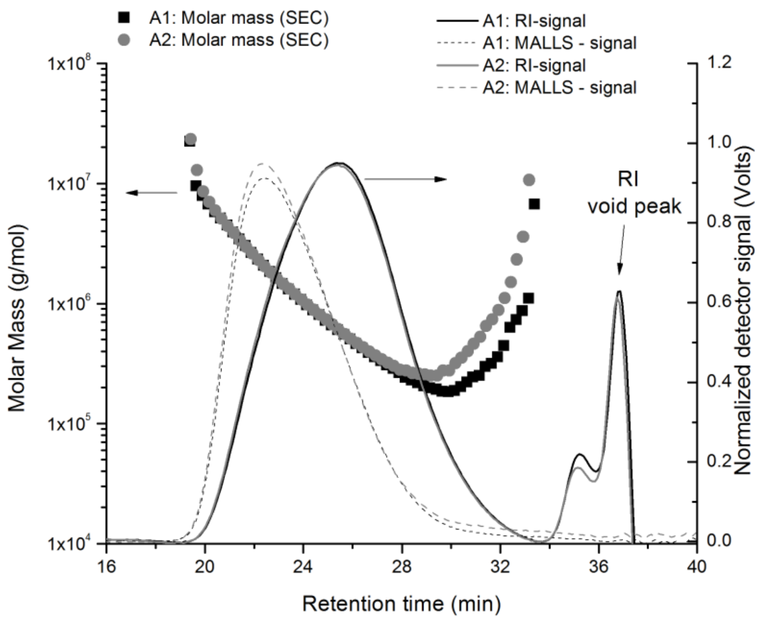

Figure 4.1. Molar mass vs. retention time plots of the styrene-acrylic latex (sample A) via SEC (duplicate measurements). The RI and MALLS (90 °) signals are overlaid. The molar mass readings are obtained from the MALLS detector (90 °) signal.

The SEC-MALLS results for the styrene-acrylic latex are presented in **Figure 4.1**. As expected from the mechanism of SEC, which separates molecules according to hydrodynamic volume, the molar mass readings obtained from the MALLS detector decrease as the retention time increases. After a retention time of 29 minutes an unexpected increase in molar mass reading is observed. This phenomenon is usually observed when a (linear) sample contains branched species.[10, 12, 19-26] Branched polymers have lower hydrodynamic sizes at high molar masses compared to their linear analogues and may co-elute with regular lower molar mass linear species similar in hydrodynamic size as a result of anchoring of the branches in the pores of the stationary phase of the column.[9] Based on the SEC behaviour it can be assumed that the later eluting fractions (29 min onwards) contain a mixture of low (linear) and high (branched) molar mass species that are co-eluting. An alternative explanation for the late elution could be due to high molar mass species being retarded or stretched in a coil formation inside the pores of the stationary phase, known as slalom chromatography.[27] An accurate molar mass analysis of the late-eluting SEC fractions is, therefore, not possible. Instead of the expected decrease an increase in molar mass is observed. It has to be noted that the MALLS signal intensity is low in the region after 29 min which could also result in inaccurate molar mass readings. In previous work, multiple fractionations of the late eluting SEC fractions of branched polyolefins and polybutadienes have been performed and were characterized by AF4.[10, 28] The authors proved that high molar mass species are present after fractionation by SEC followed by re-injection into AF4. Furthermore, the polybutadiene samples showed that two different shapes of branched species were present in the late eluting fractions by observing two different slopes in the conformation plot R_g vs. molar mass.

The conformation plot of sample A (**Figure 4.2**) indicates that the slopes of SEC and AF4 are different. Results from SEC indicate highly branched macromolecules, due to the R_g-M slope being smaller than 0.588[19, 20] . AF4 has a larger slope in comparison to the SEC measurement at 0.42, indicating that the material has less branching than what is portrayed by the SEC results. Based on the conformation plot from AF4, branching is apparent for sample A.

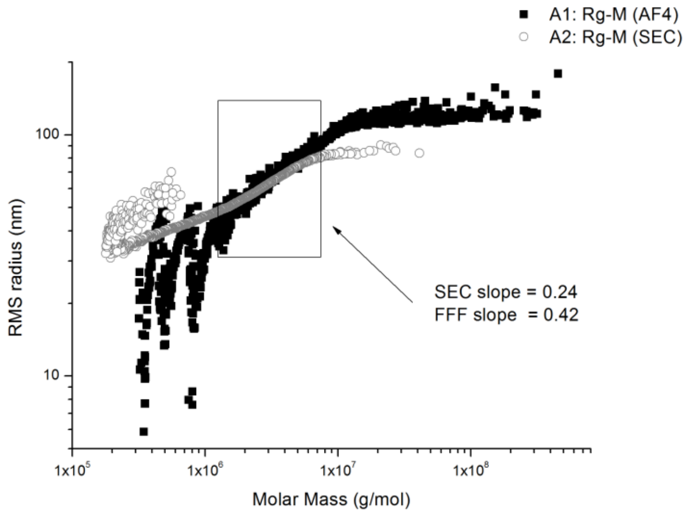

Figure 4.2. Conformation plot (R_g-M) of sample A indicating the different slopes obtained from SEC and AF4.

In agreement with the principles of the AF4 method, where separation is based on diffusion coefficient differences, the AF4 fractograms show an increase in the molar mass values as the retention time increases, see **Figure 4.3**, which corresponds to normal mode AF4. Much higher molar masses are detected in AF4 compared to SEC due to the increased accessible molar mass range. In addition, lower molar mass fractions compared to SEC are observed. This might be due to the fact that co-elution of larger and smaller macromolecules does not take place in AF4 and proper separation of macromolecules according to size from small to large is obtained.

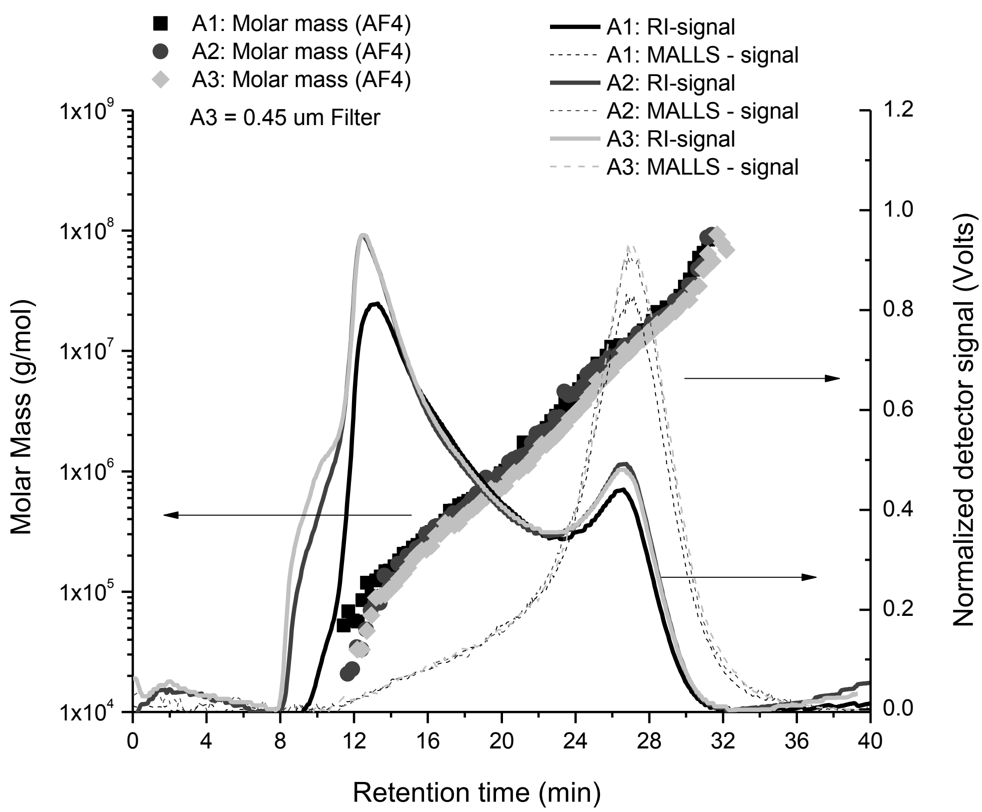

Figure 4.3. Molar mass vs. retention time plots of the styrene-acrylic latex (AF4) (duplicate measurements). A third measurement was done after filtering the sample through a 0.45 µm filter. The RI and MALLS (90 °) signals are overlaid. Molar masses are obtained from the MALLS-90 ° signal.

While the elution profile in SEC is monomodal as shown by the RI and MALLS signals (**Figure 4.1**), bimodality is observed in the RI signal of the AF4 measurements (**Figure 4.3**) while a tailing peak is visible in the MALLS signal at low retention times (**Figure 4.3**). This indicates that species of significantly different molar masses are present in the styrene-acrylic latex. The later eluting species (23 min onwards) have molar masses in excess of 10 x 10^6 g/mol indicating that ultrahigh molar mass species are present in the polymer system. Using a 0.45 µm filter followed by AF4 analysis (A3 in **Figure 4.3**) confirmed that the molar mass reading was comparable to the unfiltered measurements in AF4. This is a good indication that the sample was well dissolved. With both SEC and AF4 good recoveries were obtained, being 98 % and approximately 88 %, respectively.

Information on the molar mass distribution (MMD) was obtained by applying a first order fit to the molar mass readings of the SEC and AF4 measurements in **Figure 4.1** and **Figure 4.3**. The differential weight fraction (obtained from the RI-signal) is given as a function of molar mass as displayed in **Figure 4.4** to yield information about the MMDs. The MMD obtained from SEC appears to be much narrower compared to the MMD of AF4.

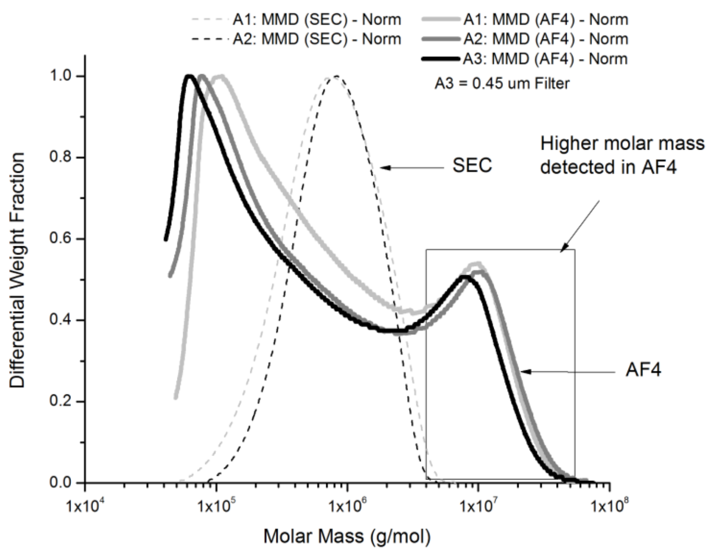

Figure 4.4. Normalized Molar mass distribution (MMD) obtained from SEC (dotted lines) and AF4 (solid lines) for the styrene-acrylic latex (sample A). A first order fit to the obtained molar mass readings in **Figure 4.1** and **Figure 4.3** was applied. Sample A3 represents a filtered sample injected in AF4.

The observed minimum and maximum molar mass values are lower (± 40 x 10^3 g/mol) and higher (± 80 x 10^6 g/mol) in AF4 compared to SEC, which possibly indicates that the very large polymer chains were gradually shear-degraded in the SEC columns. As a result, the MMD appears much narrower than what the actual distribution is. The absent lower molar masses in the SEC distribution curves are a result of the fact that the later eluting fractions cannot be correctly analyzed due to the co-elution effects.

In AF4 the true upper molar mass is presented in a more accurate way compared to SEC where the resolution of the upper molar masses is determined by the pore size of the selected column set.[10, 12] The MMD of the filtered sample was marginally lower at the high molar mass end compared to the unfiltered measurements.

When comparing the calculated molar mass values from the three different techniques in **Table 4.3**, it is evident that the results are significantly different. AF4-MALLS clearly illustrates that much higher molar masses are detected compared to the SEC technique, even after filtration. Moreover, the filtered sample measurement confirms that some ultrahigh molar mass material was removed by filtering, since the reported weighted average molar mass (M_w) value is lower than the result for the unfiltered sample.

Table 4.3. Average molar mass values (M_w) of sample A, from SEC- and AF4-MALLS, in duplicate. A third measurement was conducted in AF4 after filtering with a 0.45 μm filter.

Sample name	SEC-MALLS M_w ($x10^3$ g/mol)	AF4-MALLS M_w ($x10^3$ g/mol)
A1	934	3269
A2	1040	3542
A3 filtered	-	2354

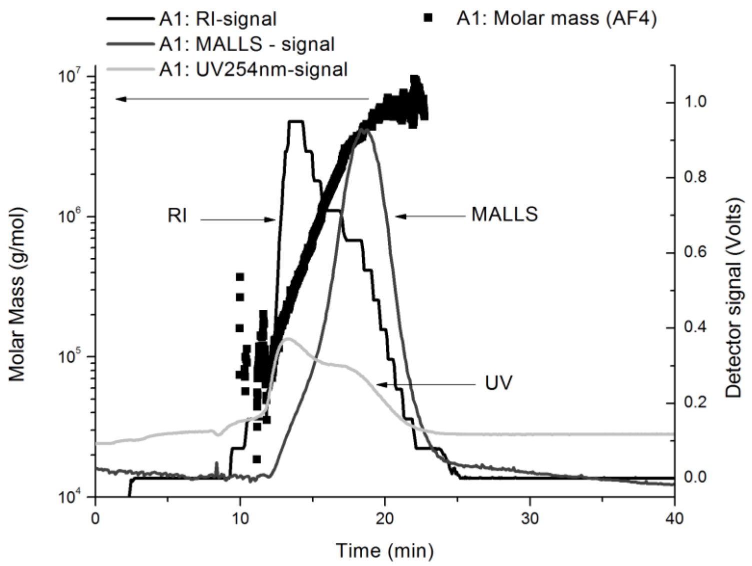

Figure 4.5. RI (black), MALLS (dark grey) and UV (light grey) detector signals of sample A as obtained after AF4 fractionation, with the molar mass reading (black squares) overlaid. The UV trace indicates bimodality in the styrene containing species, also observed in the RI signal.

The molar mass bimodality as shown by the fractograms was further investigated by coupling the AF4 setup with a UV detector. A wavelength of 254 nm was chosen to monitor styrene-containing species. The resulting fractograms (**Figure 4.5**) indicate a bimodal UV signal. This is indicative of the polymer having two styrene-containing distributions of different hydrodynamic size and molar mass. Additional chemical information can be obtained by fractionation of each eluting species followed by NMR spectroscopy. A similar study has been conducted using AF4-MALLS-UV-RI coupled off-line to NMR. Polyisoprene homopolymer was separated from the polystyrene-polyisoprene block copolymer, respectively.[28]

4.4.2 SEC and AF4 analysis of samples B and C: acrylic latex

4.4.2.1 SEC-MALLS-RI

When butyl acrylate is used in a copolymerisation, intramolecular back-biting takes place leading to the formation of heavily branched macromolecules as well as gel containing species.[1] The presence of gel species makes it very difficult to filter these samples through a 0.45 μm filter. Large portions of gel species are removed from the sample and are consequently excluded from the SEC measurements.

Table 4.4. Percentage recovery, average molar mass and radius of gyration of the kinetic samples of the acrylic latex (sample B, with MAA) obtained from SEC-MALLS-RI.

Sample	% Recovery	M_w (x 10^5 g/mol)	R_z (nm)
S1	67.6 ± 0.6	10.3 ± 0.6	63.0 ± 2.3
S2	68.5 ± 1.3	10.9 ± 0.1	72.3 ± 4.3
S3	67.2 ± 1.1	13.8 ± 0.1	82.2 ± 6.6
S4	51.7 ± 1.2	9.7 ± 0.1	69.7 ± 2.1
S5	42.9 ± 0.9	8.4 ± 0.1	62.0 ± 9.5
S6	34.9 ± 0.5	7.8 ± 0.1	58.2 ± 0.4
S7	35.5 ± 0.7	7.4 ± 0.1	52.6 ± 5.1
S8	32.4 ± 0.8	6.4 ± 0.1	49.5 ± 9.8
S9	22.9 ± 0.2	5.5 ± 0.1	47.4 ± 0.8
S10	24.9 ± 0.1	5.2 ± 0.1	46.2 ± 2.5

The samples were injected with a 200 μL sample loop to ensure that a good signal-to-noise ratio was obtained for reproducible determination of molar mass and recovery determinations.

During the acrylic latex polymerisation, 10 kinetic samples were collected from the reactor during the course of the polymerization and subsequently analyzed by SEC-MALLS-RI. The dn/dc value for the kinetic samples was constant at 0.078 mL/g since the wt% composition of the monomers used in the latex reaction was kept constant throughout the feed. For sample C that was synthesized without MAA only six selected samples were analyzed, i.e. S1, S2, S3, S4, S7 and S10. The RI and MALLS signals together with the molar mass readings of the kinetic samples S1 to S10 are reported in **Figure 4.6. A** and **B**. The recovery, molar mass and size information for sample B (with MAA) are tabulated in **Table 4.4** and graphically displayed in **Figure 4.7**. The corresponding values obtained for sample C (without MAA) are tabulated in **Table 4.5** and displayed as an overlay with sample B in **Figure 4.7** A-C, respectively. Each sample was analyzed in triplicate. The percentage recovery was calculated by taking the ratio of the calculated mass derived from the RI signal and the injected mass:

$$\%\,\text{Recovery} = {}^{\text{mass calculated}}\!\big/\!{}_{\text{mass injected}} \times 100 \qquad (2)$$

Table 4.5. Percentage recovery, average molar mass and radius of gyration of the kinetic samples of the acrylic latex (sample C, without MAA) obtained from SEC-MALLS-RI.

Sample	% Recovery	M_w (x 10^5 g/mol)	R_z (nm)
S1	82.0 ± 1.8	12.9 ± 0.1	57.3 ± 2.8
S2	84.21± 2.9	15.6 ± 0.2	67.8 ± 0.4
S3	66.5 ± 7.0	17.4 ± 3.5	63.2 ± 1.6
S4	48.5 ± 6.9	19.2 ± 1.7	70.3 ± 4.4
S7	40.1 ± 5.5	15.8 ± 3.8	63.2 ± 7.9
S10	24.6 ± 4.0	62.6 ± 2.1	46.4 ± 6.2

Based on the data represented in **Figures 4.6** and **4.7** an apparent trend can be observed towards lower values for the percentage recovery, average molar mass as well as the radius of gyration.

The observed trends are a clear indication for the formation of gels during the latex polymerization reaction. The void peak (total permeation) of the present SEC system appears at approximately 35 min and it is evident that the intensity of this peak increases from S1 to S10. Low molar mass species that are not retained on the column elute together with the void peak at later elution times. In a typical latex these low molar mass species can be residual surfactant, initiator, redox species or buffer salts.

It can be seen in **Figure 4.7 B** for sample B that the average M_w values pass through a maximum at S3. During the latex polymerization it is expected that the average M_w remains relatively constant as a function of conversion. However, the M_w remained constant for S1 and S2 only. S3 shows an increase in the molar mass after which a decrease in the average M_w is observed.

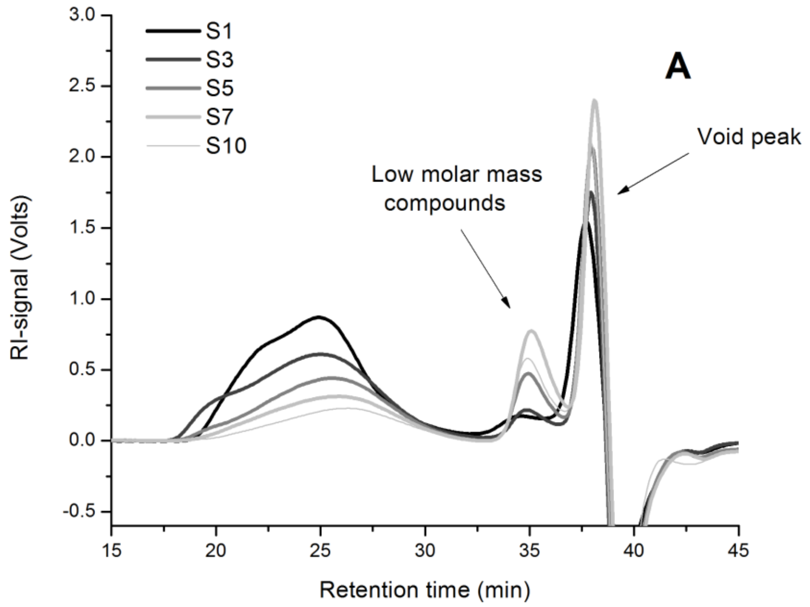

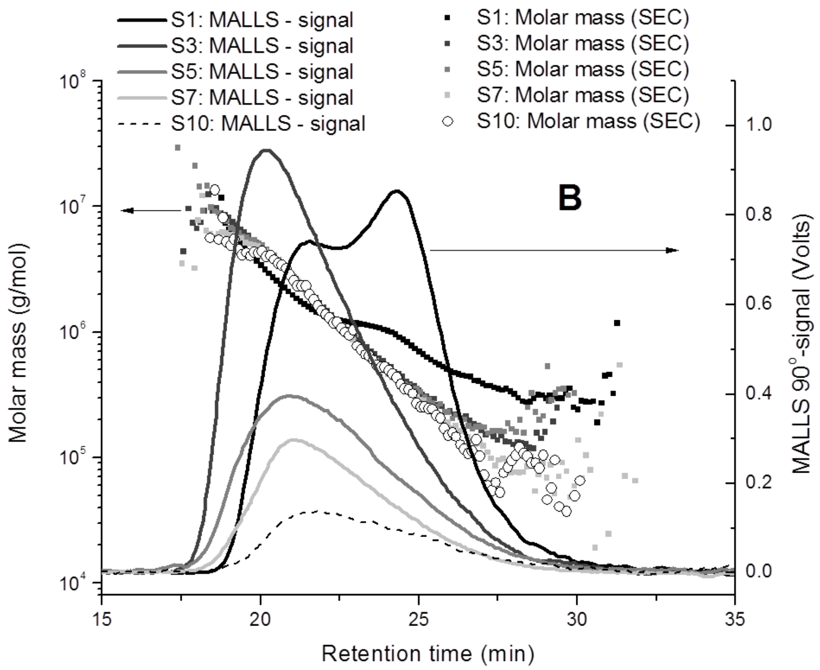

Figure 4.6. A) RI signal of the SEC separation of S1 to S10 of the acrylic latex (sample B) illustrates a decrease in intensity as samples were taken throughout the duration of the reaction. B) MALLS 90° signals and molar mass readings from S1 to S10.

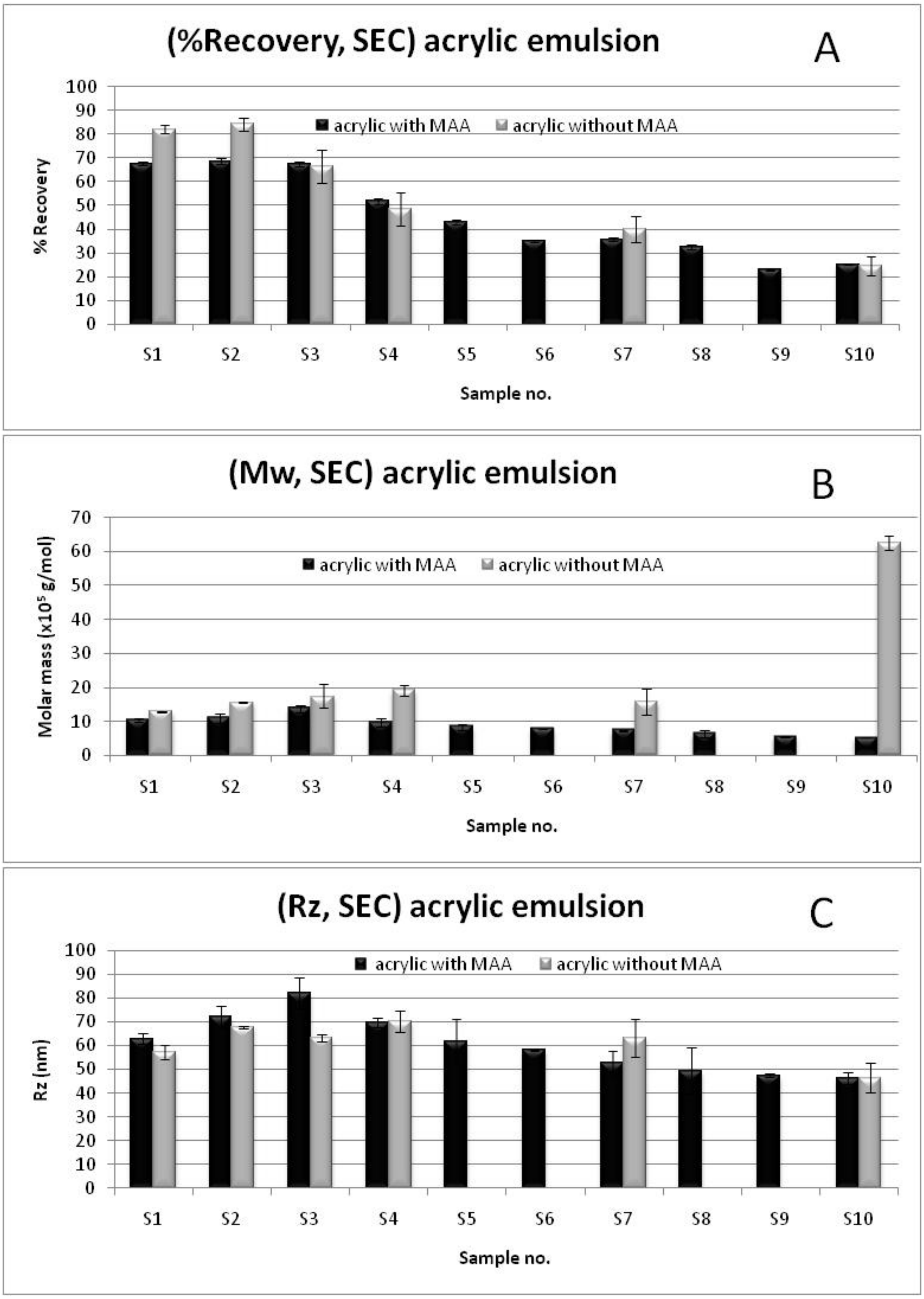

Figure 4.7. Percentage recovery (A), average molar mass M_w (B) and radius of gyration (C) for the kinetic samples S1 to S10 of sample B. Selected kinetic samples for sample C (without MAA) are compared to sample B (with MAA).

The decrease in the average molar masses coincides with the decrease in the percentage recoveries (**Figure 4.7 A**) as well as a corresponding decrease in the average radius of gyration (**Figure 4.7 C**). This decrease in molar mass observed in SEC is in good agreement with the theory of high molar mass macromolecular chains that are entrapped in a gel network in solution.[29] When the THF solution is filtered, these soluble high molar mass species are filtered out and as a consequence only lower molar mass soluble species can pass the filter prior to SEC measurements. Another explanation could be due to the larger macromolecules forming gels more readily and therefore the smaller macromolecules increase their relative concentration**.** An increase in molar mass is observed for the sample without MAA for S10. A subsequent increase in size for S10 is not observed, however, being an indication that the degree of polymerization increases towards the end of the reaction without affecting its size in solution. This may be due to extensive branching which eventually leads to very compact, smaller in size macromolecular structures, which are higher in molar mass, most likely as a result of an autoaccelaration effect also known as the Tromsdorff effect where the rate of chain termination is reduced towards the end of the polymerization reaction and the gel effect starts to come into effect with a spike in molar mass towards the end of the latex polymerization reaction.[30]

The decreasing trend in average M_w is observed from S3 up to S10. S3 exhibits a quite high molar mass compared to the other samples, which could indicate that there are flexible high molar species that were able to pass the filter despite the gel species present.[31] These very high molar mass species are most probably in the form of highly branched macromolecular architectures which are still soluble in THF.

To investigate whether branching was present, the slope of the conformation plot (R_g-M) for sample B and C during was monitored, **Figure 4.8**. Sample B (with MAA) show a near linear decrease in the slope from S1 through to S10, an indication that as the polymerization reaction progresses, the degree of branching increases.

Sample C (no MAA) had a constant slope for S1 and S2, but increased for S3, followed by a decrease towards S10. The increase in slope at S3 could be due to highly soluble linear polymeric chains since the slope was approximately 0.57, which is very close to 0.588, the value for linear polystyrene.[19] As polymerization increases, the slope decreases as in sample B, an indication that the ratio of molecular size relative to molar mass decreases.

An interesting trend can be observed in SEC analyses, **Figure 4.7B** and **Figure 4.7C**, indicating that sample B have larger R_z and smaller M_w values compared to sample A. The slope from S1 to S10 is also larger than sample C, indicating that sample B with MAA is less branched in comparison to sample C with no MAA.

It is known from literature that BA forms long chain branches in acrylic latex polymerization through intermolecular transfer to polymer if the concentration of polymer is high enough in the polymer particles.[1] The same author also stipulates that long chain branches are the precursor molecules for gel formation. Gelation results from termination through combination in the polymeric chains inside the latex particles.[32-34] An increase in M_w at S3 is most likely followed by rapid gel formation in the polymer particles which is proven by the observation that the percentage recovery and the average M_w decrease from S3 to S10.

A similar trend can be observed for sample C that was polymerized without MAA. The percentage recoveries were slightly higher as compared to sample B. The explanation for this observation could be that the absence of MAA decreases the gel and possible branch formation in the early stages resulting in polymer species which are readily soluble in THF. The sizes were slightly lower as compared to sample B, most likely due to the absence of MAA. All the trends in recovery, molar mass and size, however, were similar for both samples. The molar mass of sample C showed an abrupt increase for S10 (**Figure 4.7 B**). This is unusual but could most likely be due to radical termination taking place by means of combination,[35] resulting in a mixture of high molar mass species and gel. In the next set of experiments, samples B and C were analyzed by AF4-MALLS-RI to investigate the molecular properties of the prepared latices.

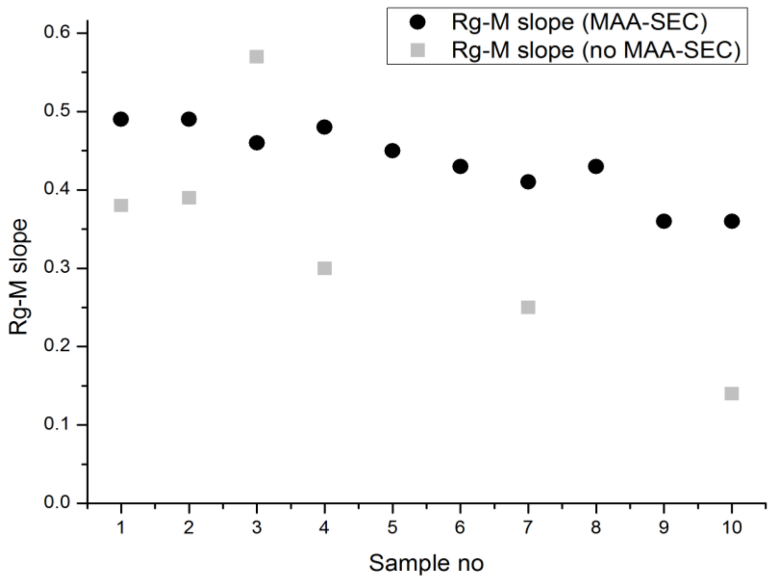

Figure 4.8. Plot of R_g-M (SEC) as a function of polymerization time (sample no.) for sample B and C, respectively.

4.4.2.2 AF4-MALLS-RI

Complementary to SEC, the kinetic samples (S1 to S10) were analyzed by AF4 without any filtration using a 200 µL sample loop. FFF has a higher molar mass cut-off compared to SEC and, therefore, higher average M_w values can be calculated more accurately. Additionally, the gel fraction can be separated and analyzed. The gel amount is calculated by converting the gel mass as detected by the RI detector to a percentage gel fraction.[36]

In the present investigations, the peak area related to the elution time where molar mass determination is not possible anymore or where a plateau in the molar mass reading is observed towards higher elution times is defined as the gel eluting region. The apparent molar mass of the microgel species eluting in this region is constant over this region. The AF4 fractograms of the kinetic samples (S1 to S10) for sample B (with MAA) have bimodal elution peaks present for both the RI and MALLS signals as displayed in **Figure 4.9**. A similar bimodal peak was observed for the sample without MAA.

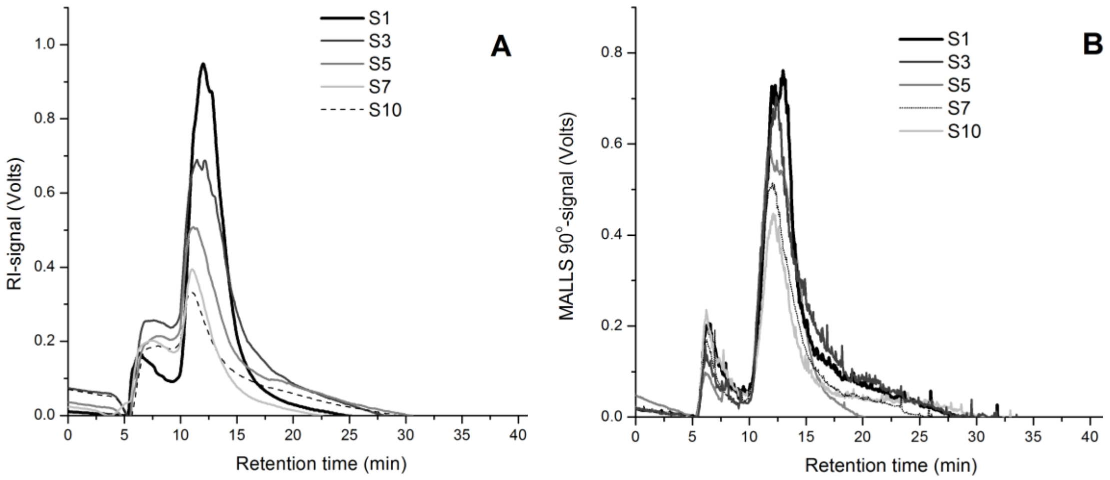

Figure 4.9. RI (A) and MALLS (B) signals from AF4 fractionation with 200 µL sample injected, for samples S1, S3, S5, S7 and S10.

The transition and injection times were varied between 1 to 8 minutes, respectively, in order to better separate the bimodal peaks (**Figure 4.10**). A longer injection time may improve the resolution of the detected species since more time is allowed for the molecules to equilibrate into their respective flow velocity layers. Increasing the transition time may assist when the focus flow decreases to zero, to prevent large sensitive molecules to end up in the flow velocity layers of smaller sizes. A shift towards higher retention times and peak broadening was observed. The 4 min injection with 1 min transition was chosen for all analyzed samples since the corresponding runtime was the shortest with acceptable peak resolution.

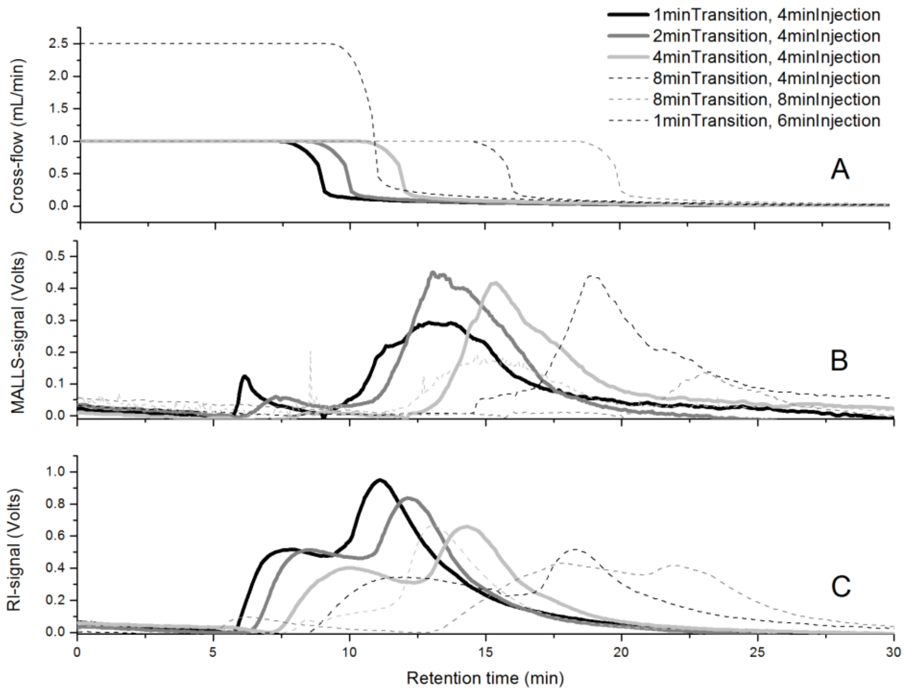

Figure 4.10. Cross-flow profile for varying injection and transition times (A). MALLS (B) and RI (C) signals of the corresponding cross-flow profiles for S10 in A.

The elution range of the first eluting peak appears to be constant at retention times of 6-10 min for all analyzed samples S1, S3, S7 and S10, **Figure 4.11**. The signal intensities of these species do not differ much either. Considering that the second (and major) peak starts eluting at approximately 10 minutes for S1 through to S10, it can be observed that the peak maxima shift towards lower elution times with S8, S9 and S10 eluting much earlier compared to S1.

This observed behaviour is rather peculiar taking into consideration that the sample was not filtered prior to injection and the fact that the initial concentrations of S1 to S10 were quite similar. The normal mode of AF4 separates according to hydrodynamic size typically in the direction of increasing molar mass. The small decrease in molar mass for the eluting species between 5-10 min could be an indication that these species elute in hyperlayer mode.

In hyper-layer mode a very high cross-flow field forces the larger molecules to bounce off the accumulation wall resulting in particles ending up a short distance away from the wall. The elution order is the reverse of normal mode separation (Figure 2.3) where larger molecules or species spend a shorter amount of time inside the channel (elutes earlier) in comparison to the smaller molecules.[9]

In hyperlayer mode the larger particles are eluted first. As soon as normal mode operation is reached, the elution order is reversed again where small species are eluted first and larger species later. The elution mode returns to normal mode from a retention time of 10 min onwards where an increase in molar mass with retention time is seen. The molar mass readings are scattered due to the sample being injected without filtering.

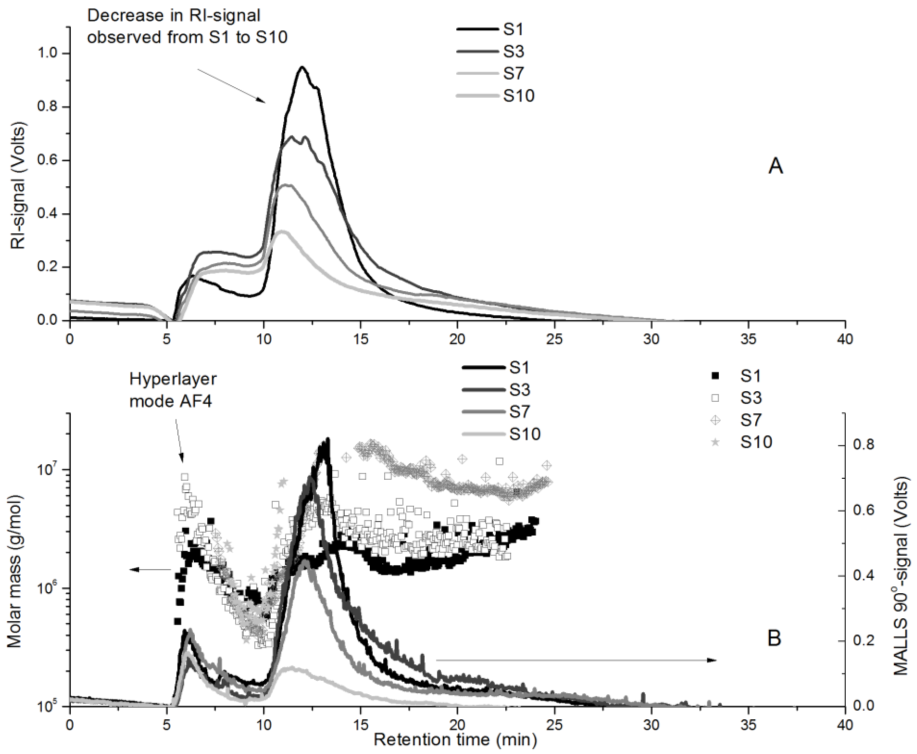

Figure 4.11. RI (A) and 90°-MALLS (B) signals from AF4 measurements of S1 to S10 corresponding to the acrylic latex.

Table 4.6 and **Table 4.7** summarize the percentage recovery, average molar masses and size information for samples S1- S4, S7 and S10 for the acrylic latex samples (with and without MAA), respectively. The results are overlaid and displayed graphically in **Figure 4.12**.

Table 4.6. Percentage recovery and average molar masses of the kinetic samples of the acrylic latex with MAA obtained from AF4-MALLS-RI.

Sample	% Recovery	M_w (x 10^6 g/mol)	R_z (nm)
S1	42.5 ± 3.7	1.6 ± 0.1	80.8 ± 5.0
S2	44.8 ± 8.1	3.9 ± 0.9	108.4 ± 10.9
S4	28.0 ± 5.5	3.3 ± 0.3	102.4 ± 5.4
S7	20.8 ± 1.6	3.9 ± 0.4	134.3 ± 5.4
S10	16.9 ± 0.8	7.7 ± 0.9	161.6 ± 0.9

Table 4.7. Percentage recovery and average molar masses of the kinetic samples of the acrylic latex without MAA obtained from AF-MALLS-RI.

Sample	% Recovery	M_w (x 10^6 g/mol)	R_z (nm)
S1	95.8 ± 1.4	5.9 ± 0.5	78.4 ± 3.0
S2	94.7 ± 1.3	5.8 ± 1.8	92.5 ± 8.3
S3	93.3 ± 3.9	6.2 ± 0.7	108.7 ± 1.4
S4	93.7 ± 1.2	6.9 ± 0.2	109.3 ± 7.2
S7	27.9 ± 3.5	7.6 ± 1.8	147.4 ± 20.8
S10	44.3 ± 12.6	7.8 ± 0.4	113.7 ± 10.9

An increase in the % recovery is expected from S1 - S10 since both the gel and soluble portions should elute from the channel and the subsequent peak mass should be increasing. The exact opposite is observed for sample B, however, where a decrease in recovery (**Figure 4.12 A**) from S1 - S10 is observed which is similar to the SEC recovery trend (**Figure 4.6 A**).

Whether a portion of the gel has a larger affinity for the membrane material (cellulose) due to the presence of MAA or the gel species just being embedded in the pores of the membranes is unclear at present. The low recoveries in sample B (with MAA) could be a strong indication that gel species most likely interact with the membrane inside the channel. The carboxylic groups of the MAA and the hydroxyl groups of the cellulosic membrane might interact with each other leading to lower amounts of sample being detected. The high recoveries of sample C (without MAA) are an indication that the formed polymer species are able to elute through the channel with very little interaction.[37, 38]

In a previous study, gel containing polybutadienes were analyzed by AF4 and it was reported that the diffusion coefficients of gel containing species do not differ comprehensively from the ultrahigh molar mass species.[28] For the current kinetic samples this phenomenon will imply that the coil density of the gel species will increase as the reaction proceeds without a significant change in the diffusion coefficient. No significant change in the later eluting gel species will be observed between S1 to S10 (**Figure 4.11 B**). Since the soluble fraction of the sample decreases as well, the more dense gel coils are expected to elute at later retention times. The decrease in RI signal from S1 - S10 can also be attributed to refractive index differences that are similar for the eluting gel and the mobile phase (THF), especially since the dn/dc values for acrylates are very low in THF.

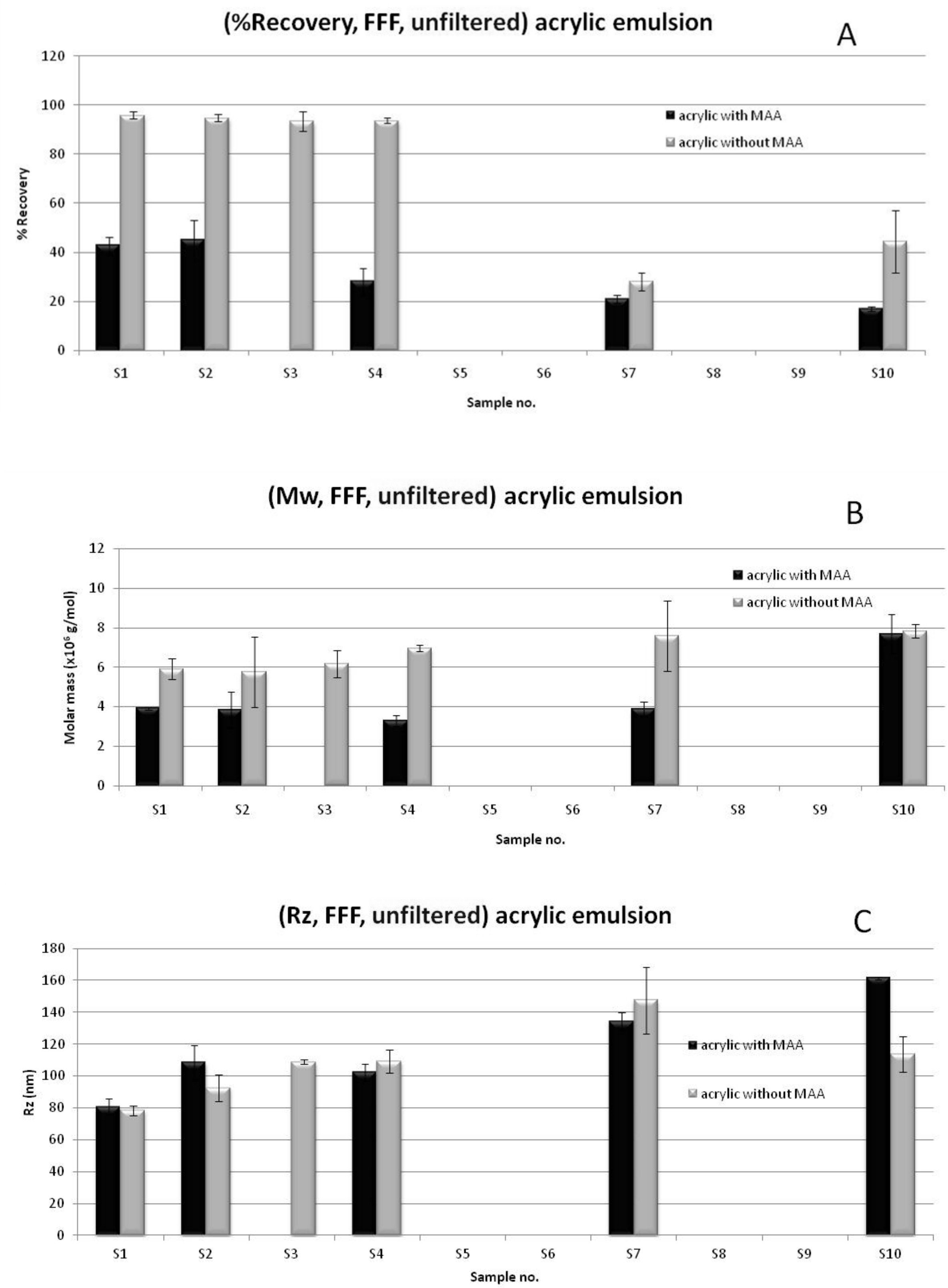

Figure 4.12. Graphical representation of percentage recovery (A), average molar mass (M_w) (B) and radius of gyration (C) for samples B (with MAA) and sample C (without MAA).

If the refractive indices of mobile phase and the eluting sample are identical, the RI detector will give a very weak signal response. Other authors have used MALLS and RI before to quantify gel content. Dubascoux et al. studied the mesostructure of natural and synthetic rubber quantifying microgel content present in the samples.[36] Lee determined the gel content using thermal FFF,[39] while Lohmann studied acrylic adhesives using ThFFF.[40] The recovery percentage of sample C (no MAA) indicated that the samples were readily soluble in THF since the recovery was approximately 98 % for S1 - S4. The recovery % decreased to lower values for S7 and S10, most likely due to small amounts of gel starting to form at later stages in the latex polymerization reaction.

The average molar mass values illustrate a different trend compared to SEC. The average M_w values are more or less constant from S1 to S9 as observed in **Figure 4.12 B** for sample B (with MAA), after which a sudden increase is observed for S10. The average molar mass of sample C (without MAA) had a similar trend, with slightly higher average molar mass values.

The observed experimental M_w trend is in good agreement with batch free radical polymerization where the molar mass of particles only increases once the monomer reservoir is depleted (Interval III)[35] in which an increase is observed from S1 to S10 (**Figure 4.12 B**). The entire solution is being injected into the AF4 system, therefore no gel or any high molar mass species are excluded from each measurement. Although the soluble fraction decreased (**Figure 4.12 A**), molar mass calculations were possible. The calculated radii of gyration for sample B and sample C (**Figure 4.12 C**) showed an increasing trend towards larger values from S1-S10 indicating that the molecular size in solution increased with conversion as well as an indication of normal mode elution in AF4. The size of S10 for sample C was slightly lower as compared to the size of S10 for sample B, similar to the trend observed in SEC measurements.

Figure 4.13 displays the slopes of the R_g-M plots for sample B and C, respectively. Similarly to the SEC results, sample B indicate a decrease in the slope and a corresponding increase in branching degree. Identical to SEC, sample C also display an increase in the slope to 0.45 for S3. From AF4 measurements, this is an indication that you have more linear than branched species in this sample. In SEC, the slope was very high and could have been due to overlapping of separation regimes or mechanisms. Sample C also indicate that as polymerization progresses, the coils become very compact. The drop in R_z for S10 in **Figure 4.12 C** (sample C), could be due to the excessive branching in the sample, supported by the low observed R_g-M slope value.[20]

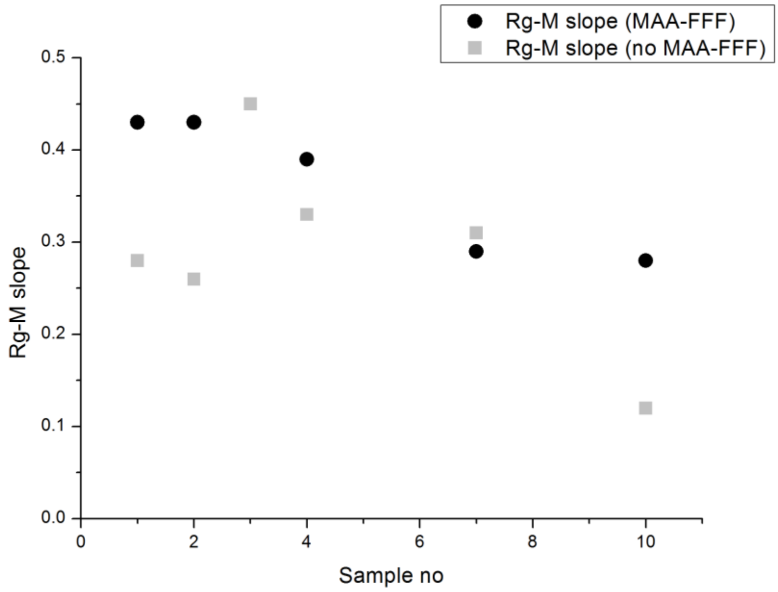

Figure 4.13. Plot of R_g-M (AF4) as a function of polymerization time (sample no.) for sample B (MAA) and C (no MAA), respectively.

The elution time at which the gel eluting species (insoluble fraction) was taken from was the point where no molar mass deviation took place in the molar mass vs. time plot (**Figure 4.11**). This represents the small grey rectangle as a percentage (**Figure 4.14**).

The gel content was calculated by:

$$\%\,\text{Gel fraction} = \frac{\text{Constant molar mass plateau onset}}{\text{total calculated mass}} \times 100 \qquad (3)$$

Table 4.8 indicates the percentage gel content of S1 to S10 as calculated by AF4-RI. S1, S2, S4, S7 and S10 were measured in triplicate.

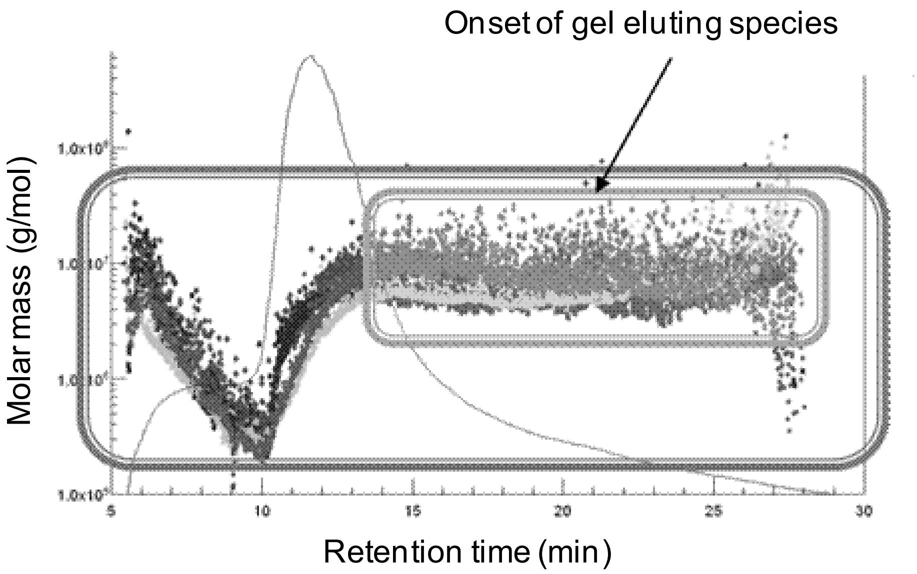

Figure 4.14. AF4: Molar mass vs. time plot of S4 indicating the point where the percentage gel fraction is calculated from in the RI signal. The time where gel starts eluting for S4 is approximately 14 minutes. S4 was injected four times. Small grey rectangle: calculated gel mass, large black rectangle: total mass calculated.

The obtained samples for Sample B (with MAA) indicate that the gel content increases throughout the duration of the latex reaction (**Figure 4.15**). The decrease in recovery obtained from SEC together with the increase in gel content as calculated from AF4 supports the assumption that gel does form as the reaction proceeds. The obtained samples for sample C (without MAA) indicate that no gel was formed for the first part of the polymerization, but eventually forms later in the reaction since the recoveries of sample S7 and S10 started to decrease.

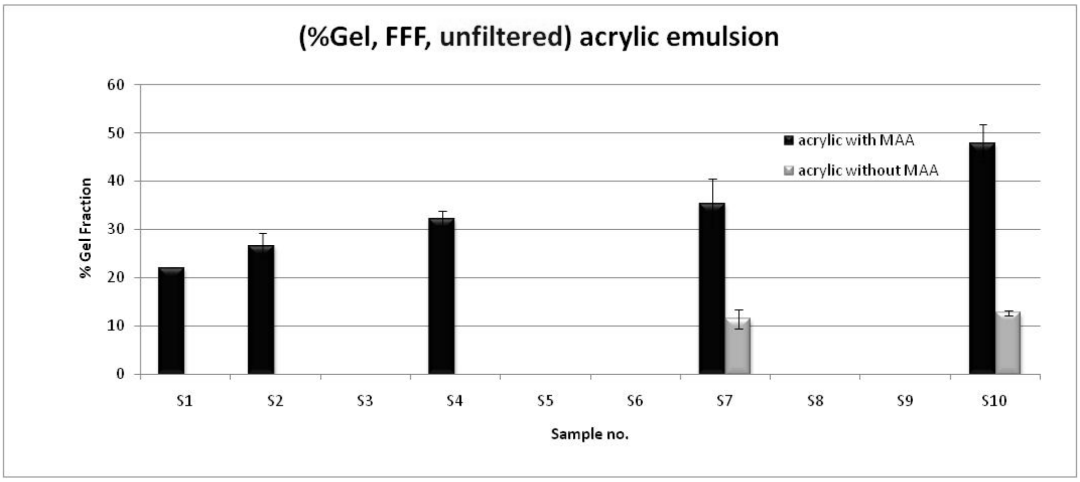

Figure 4.15. Representation of calculated gel content of samples B (with MAA) and samples C (without MAA) as a function of polymerization time.

Table 4.8. Percentage gel content of S1- S10 calculated from the onset of gel species (RI signal) as illustrated in **Figure 4.11** for sample B (with MAA).

Sample	% Gel content – FFF method	% Gel - Kansai method	% Gel – ASTM D2765
S1	22.1 ± 0.1	n.d	n.d
S2	26.7 ± 2.5	n.d	n.d
S4	32.3 ± 1.5	n.d	n.d
S7	35.5 ± 4.9	n.d	n.d
S10	47.9 ± 3.8	51.3 ± 3	57.2 ± 17

The obtained result for S10 using the Kansai Plascon test method was approximately 51 %, while ASTM D2765 was approximately 57.18 %, with a large degree of error. The AF4-RI method indicated a gel content of approximately 48 %. The total time the traditional Kansai Plascon method takes was 5 days compared to the AF4-MALLS-RI method with a 3 day duration for the specific synthesized samples, which is a 40 % reduction in analyses time.

The high recoveries observed in **Figure 4.12 A** for sample C support the absence of gel in the early stages of the polymerization. The consequent decrease in recovery from S7 – S10 is also an indication that the formation of gel species was apparent towards the end of the polymerization.

The analysis of pure acrylic latex samples using AF4-MALLS-RI with and without the incorporation of MAA indicated that the recovery of species after dissolution in THF was higher from S1-S4 for the sample without MAA. The corresponding analysis is, therefore, more accurate and represents a true reflection of the molar mass and size information. The gel content could be determined more accurately by doing comparable analysis with gravimetric methods as stipulated in various works, as well as testing membranes with different chemistries to study the effect of surface chemistry on the elution profile of macromolecules which tend to form gelatinous species in organic media. Alternatively, the absence of a membrane could also be explored to improve recoveries of gel-containing samples.[41]

4.5. Conclusions

In this study it was demonstrated that AF4 can be used for molar mass and molar mass distribution determinations of latices used in water-based coatings. In addition to SEC analysis as a comparative technique, AF4 proved to be much more useful and a far better tool in the ultrahigh molar mass range since higher molar masses were observed using FFF. Branching characteristics were investigated and made correlations between molecular size and molar mass results possible stemming from SEC and AF4 analyses for samples A, B and C. A latex without any gel content (styrene-acrylic) was used as a comparative example to prove that FFF can address higher molar mass ranges compared to SEC.

Latices that contain gel cannot be analyzed by any packed-column chromatographic technique due to the nature of the stationary phase and filtering of samples prior to analysis. AF4 was utilized to determine the molar mass and molar mass distributions of styrene-acrylic latex samples and acrylic latex samples with and without MAA. Additionally, an attempt was made to determine the percentage gel content of the acrylic latices. The evolution of gel content during the latex polymerization was monitored for the acrylic latices with and without methacrylic acid (MAA). AF4 proved that the gel content definitely evolves throughout the latex reaction for a sample containing MAA. The latex sample without MAA indicated that gel species start to form later in the polymerization reaction since high recoveries was obtained in the early stages of the reaction.

To date only SEC measurements for molar mass and gravimetric methods for gel content determinations are in place with a few studies focusing on gel determination with FFF. Accurate interpretations of molar mass and gel content in latices used in coatings is a pivotal aspect and the application of AF4 to determine both these properties can lead to more efficient and better structure and physical property correlations. The challenge that does exist is the interaction of gel species with the membrane that should be minimized as far as possible, with one solution being the testing of different membrane chemistries in AF4 investigations.

4.6. Acknowledgements

The authors would like to acknowledge the synthesis team at Kansai Plascon Research Centre, Stellenbosch, South Africa for providing the materials used in the study.

4.7 References

[1] J. M. Asua, J. Polym. Sci., Part A: Polym. Chem. 2004, 42, 1025.

[2] L. Lewandowski, M. S. Sibbald, E. Johnson, M. P. Mallamaci, Rubber Chem. Technol. 2000, 73, 731.

[3] K. Jores, W. Mehnert, M. Drechsler, H. Bunjes, C. Johann, K. Mäder, J. Controlled Release 2004, 95, 217.

[4] D. Kang, M. Kim, S. Kim, K. Oh, S. Yuk, S. Lee, Anal. Bioanal. Chem. 2008, 390, 2183.

[5] J. V. Koleske, "Paint and Coating Testing Manual", ASTM International, 1995.

[6] E. Hagan, A. Murray, MRS Online Proceedings Library, 2004, 852,.

[7] H. G. Barth, B. E. Boyes, C. Jackson, Anal. Chem. 1998, 70, 251.

[8] S. Mori, M. Ishikawa, Journal of Liquid Chromatography & Related Technologies 1998, 21, 1107.

[9] S. Podzimek, "Light Scattering, Size Exclusion Chromatography and Asymmetric Flow Field Flow Fractionation: Powerful Tools for the Characterization of Polymers, Proteins and Nanoparticles", John Wiley & Sons, New York, 2011.

[10] T. Otte, T. Klein, R. Brüll, T. Macko, H. Pasch, J. Chromatogr. A 2011, 1218, 4240.

[11] F. A. Messaud, R. D. Sanderson, J. R. Runyon, T. Otte, H. Pasch, S. K. R. Williams, Prog. Polym. Sci. 2009, 34, 351.

[12] T. Otte, H. Pasch, T. Macko, R. Brüll, F. J. Stadler, J. Kaschta, F. Becker, M. Buback, J. Chromatogr. A 2011, 1218, 4257.

[13] J. C. Giddings, Anal. Chem. 1995, 67, 592A.

[14] A. Brewer, A. M. Striegel, Anal. Bioanal. Chem. 2009, 393, 295.

[15] A. M. Striegel, Anal. Bioanal. Chem. 2011, 1.

[16] S. Podzimek, P. Lebeda, C. Johann, D. Horak, D. Sponarova, "Asymmetric Flow Field-Flow Fractionation: Characterization of Polymers That Are Difficult to Analyze With SEC-GPC", in American laboratory, June edition, American laboratory, 2009, p. 28/11/2011/1.

[17] S. Podzimek, J. Machotova, J. Snuparek, M. Vecera, L. Prokupek, J. Appl. Polym. Sci. 2014, 131, 40995.

[18] A. C. Makan, M. J. Spallek, M. du Toit, T. Klein, H. Pasch, J. Chromatogr. A 2016, 1442, 94.

[19] S. Podzimek, T. Vlcek, J. Appl. Polym. Sci. 2001, 82, 454.

[20] S. Podzimek, T. Vlcek, C. Johann, J. Appl. Polym. Sci. 2001, 81, 1588.

[21] V. Percec, C. H. Ahn, W. D. Cho, A. M. Jamieson, J. Kim, T. Leman, M. Schmidt, M. Gerle, M. Möller, S. A. Prokhorova, S. S. Sheiko, S. Z. D. Cheng, A. Zhang, G. Ungar, D. J. P. Yeardley, J. Am. Chem. Soc. 1998, 120, 8619.

[22] S. Podzimek, J. Appl. Polym. Sci. 1994, 54, 91.

[23] T. H. Mourey, Int. J. Polym. Anal. Charact. 2004, 9, 97

[24] E. P. C. Mes, H. de Jonge, T. Klein, R. R. Welz, D. T. Gillespie, J. Chromatogr. A 2007, 1154, 319.

[25] C. Johann, P. J. Kilz, J. Appl. Polym. Sci.: Appl. Polym. Symp. 1991, 48, 111.

[26] M. Wintermantel, M. Antonietti, M. Schmidt, J. Appl. Polym. Sci.: Appl. Polym. Symp. 1993, 52, 91.

[27] Y. Liu, W. Radke, H. Pasch, Macromolecules 2006, 39, 2004.

[28] A. C. Makan, T. Otte, H. Pasch, Macromolecules 2012, 45, 5247.

[29] M. Erdogan, Y. Yagci, A. Pekcan, Journal of Macromolecular Science, Part B 2008, 47, 942.

[30] M. F. Cunningham, H. K. Mahabadi, Macromolecules 1996, 29, 835.

[31] S. Lee, A. Molnar, Macromolecules 1995, 28, 6354.

[32] I. González, J. M. Asua, J. R. Leiza, Polymer 2007, 48, 2542.

[33] A. Y. C. Koh, S. Mange, M. Bothe, R. J. Leyrer, R. G. Gilbert, Polymer 2006, 47, 1159.

[34] O. Elizalde, G. Arzamendi, J. R. Leiza, J. M. Asua, Industrial & Engineering Chemistry Research 2004, 43, 7401.

[35] S. C. Thickett, R. G. Gilbert, Polymer 2007, 48, 6965.

[36] S. Dubascoux, C. Thepchalerm, E. Dubreucq, S. Wisunthorn, L. Vaysse, S. Kiatkamjornwong, C. Nakason, F. Bonfils, J. Chromatogr. A 2012, 1224, 27.

[37] M. A. Benincasa, J. C. Giddings, J. Microcolumn Sep. 1997, 9, 479.

[38] R. L. Hartmann, S. K. R. Williams, Journal of Membrane Science 2002, 209, 93.

[39] D. Lee, S. K. R. Williams, J. Chromatogr. A 2010, 1217, 1667.

[40] C. A. Lohmann, W. G. Haseltine, J. R. Engle, S. K. R. Williams, Anal. Chim. Acta 2009, 654, 92.

[41] D. Melucci, A. Zattoni, S. Casolari, M. Reggiani, R. Sanz, P. Reschiglian, Journal of Liquid Chromatography & Related Technologies 2002, 25, 2211

Chapter 5: Particle-Particle interaction study of TiO_2 and polymer latices using multi-detector asymmetric flow field-flow fractionation

5.1 Abstract

The interactions of polymer latices and titanium dioxide (TiO_2) used in water-based decorative coatings were analyzed by field-flow fractionation (FFF) coupled to multiangle laser light scattering (MALLS), ultraviolet (UV) and refractive index (RI) detectors. The elution patterns of the latices mixed with TiO_2 were investigated in order to monitor possible particle-particle interactions between the latices and TiO_2 particles.

Furthermore, AF4 fractions were manually collected after elution of latices, TiO_2 and latex-TiO_2 species and submitted to Inductively Coupled Plasma – Mass Spectrometry (ICP-MS) to determine the quantity of TiO_2 present in each of the fractionated samples.

Results indicated that the ratio of latex particles to TiO_2 particles have an effect on the detected TiO_2 species. The chemical nature of the latex particles also played a role in the amount of TiO_2 being detected. Sonication prior to AF4 analyses indicated that the latices and TiO_2 shifted to earlier elution times in comparison to AF4 analyses without applying ultrasonication.

5.2 Introduction

Decorative coatings play an important role in aesthetics and protection in households, office spaces, and automotive industries to name a few [1]. Designated characterization techniques are important in analyzing the constituents of the complex chemistries present in a typical coating formulation.

Latices are typically used as film forming species, while TiO_2 is used in cosmetics (e.g. sunscreen), medical applications and coatings [1]. TiO_2 is used as opacifier in coatings by reflecting light and in addition increasing the degree of whiteness or hiding power.

The interaction or association between the various particles in typical decorative coatings will affect its gloss properties and coverage over a substrate. The complex matrix formation between rheology modifiers, dispersants, latex and pigment particles all have an important function to achieve desired final physical properties, gloss and hiding power specifically, due to the packing of the particles to reflect light optimally [2,3].

In the event where TiO_2 particles are packed too closely to each other, also known as the crowding effect, light will not be scattered optimally upon applying a TiO_2 containing coating. The resulting coating appearance will have a matt-like finish, mainly due to aggregating or agglomerating particles.

Optimal spacing occurs when TiO_2 particles are evenly spaced amongst all particles present in the coating formulation. Evenly spaced TiO_2 together with the correct pigment volume concentration (PVC) would allow for a better degree of reflection of light, a glossier finish and better hiding power or coverage on the applied substrate [4].

In this study, two acrylic latices: 1) an in-house latex SF0150 and 2) a supplier latex was evaluated by AF4-MALLS-UV. Mixtures of latices and TiO_2 at different ratios of latex-to-TiO_2 were injected into the open channel FFF system and each of the obtained fractograms was monitored closely by analyzing the fractions by coupling offline to ICP-MS. The TiO_2 content was quantitatively determined, investigating the interaction between latices and TiO_2 particles.

5.3 Experimental

5.3.1 Materials

The carrier liquid used for all analyses was a 0.2 % v/v solution of Novachem in doubly distilled deionized water. The Novachem surfactant is a mixture of anionic and non-ionic surfactants Novachem®, C-SUR-100, Postnova Analytics, Landsberg, Germany. Spherical polystyrene latex particle standards with nominal sizes of 60 nm, 125 nm and 350 nm were obtained from Postnova (Landsberg, Germany).

All monodisperse polystyrene nanospheres used in this study were certified by NIST, using an optical microscope (350 nm particles) or transmission electron microscope (TEM, 60 and 125 nm particles). The average particle sizes and uncertainties using the two microscopy techniques were 57 nm ± 4 nm, 125 nm ± 1 nm and 350 nm ± 6nm, respectively.

The two acrylic latices used in the study were as follows: 1) an in-house pure acrylic latex as used in chapter 4, Sample B, synthesized using free radical polymerization and 2) a supplier latex (acrylic ester) with properties claimed to have potential capabilities of reducing TiO_2 in a coating formulation or improving the light scattering efficiency of TiO_2 within the coating (sample C). The material typically contained between 40 – 50 % polymer. Additionally, this material potentially improves the performance of the coating with respect to stain and corrosion resistance.

5.3.2 Instrumentation setup and analysis conditions

AF4 experiments were performed on an ambient temperature AF4-Instrument (AF2000, Postnova Analytics, Landsberg/Germany) which was coupled to MALLS (PN3621), RI (PN3150) and DAD-UV (PN3241) detectors from Postnova Analytics, Landsberg, Germany, defined as AF4-MALLS-UV-RI. The wavelengths monitored for the UV detector was 254 nm and 320 nm, respectively. The channel was connected to three different pumps (tip, focus and cross-flow) while the injection port was equipped with a 100µL sample loop of which 20µL was injected for each measurement. A 350 µm Mylar spacer defining the channel height and a regenerated cellulose membrane were installed for the AF4 (average molar mass cut-off of 5 kDa, Z-AF4-MEM-612-5kD, Postnova, Landsberg, Germany). Elution was realized using two pumps (tip- and focus-flow, PN1122). Two in-line solvent filters (0.1µm pore size, 13mm diameter, PTFE) were positioned between the channel and the pumps to reduce the detector background. The sample bypassed the filters thus entering the channel unaffected.

Titanium was analysed in He-collision mode on an Agilent 7900 quadrupole ICP-MS (Agilent Technologies, Santa Clara CA, USA). Samples were introduced via a 0.4mL/min micromist nebulizer into a Peltier-cooled spray chamber at a temperature of 2°C, with a carrier gas flow of 1.05L/min. The instrument was optimized for robustness (< 1% CeO/Ce ratio) as well as sensitivity, then calibrated and validated using NIST (National Institute of Standards and Technology, Gaithersburg MD, USA) traceable standards from Inorganic Ventures Inc (Christiansburg, Virginia).

5.4 Results and discussion

5.4.1. Analysis of polystyrene particle standards using different cross-flow profiles

Polystyrene latex standards of nominal sizes of 60 nm, 125 nm and 350 nm in diameter were injected using an exponential decay cross-flow and linear decay cross flow profile, **Figure 5.1**.

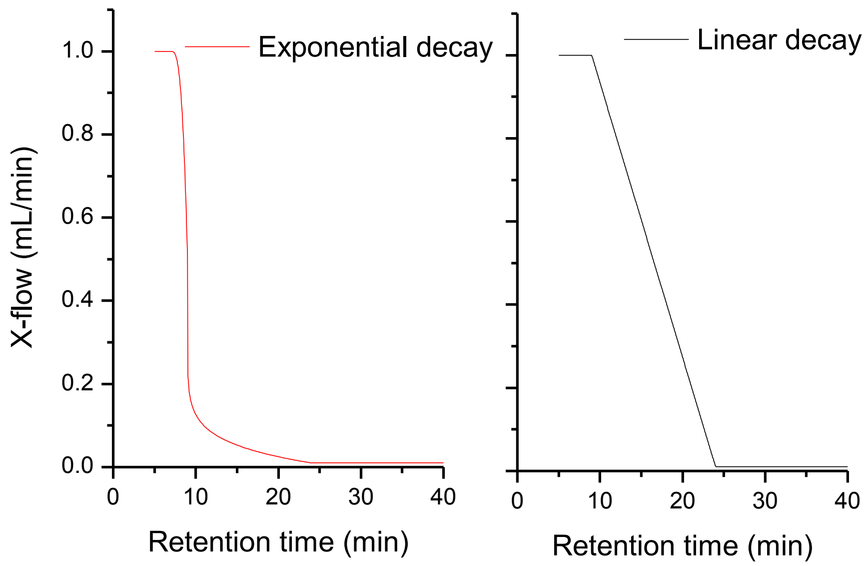

Figure 5.1. Different cross-flow profiles used in the study: Exponential (left) and linear decays (right).

The UV 254 nm, UV 320 nm and MALLS signals for both linear and exponential decay cross-flow profiles are displayed in **Figure 5.2 (A-F).** The UV 320 nm signal appeared very noisy around the baseline shown in **Figure 5.2 C** and **D**. The resolution improved to near baseline separation using the linear decay cross-flow profile compared to the exponential cross-flow profile (**Figure 5.2 B, D** and **F**), with a corresponding retention time trade-off of approximately 7.5 minutes.

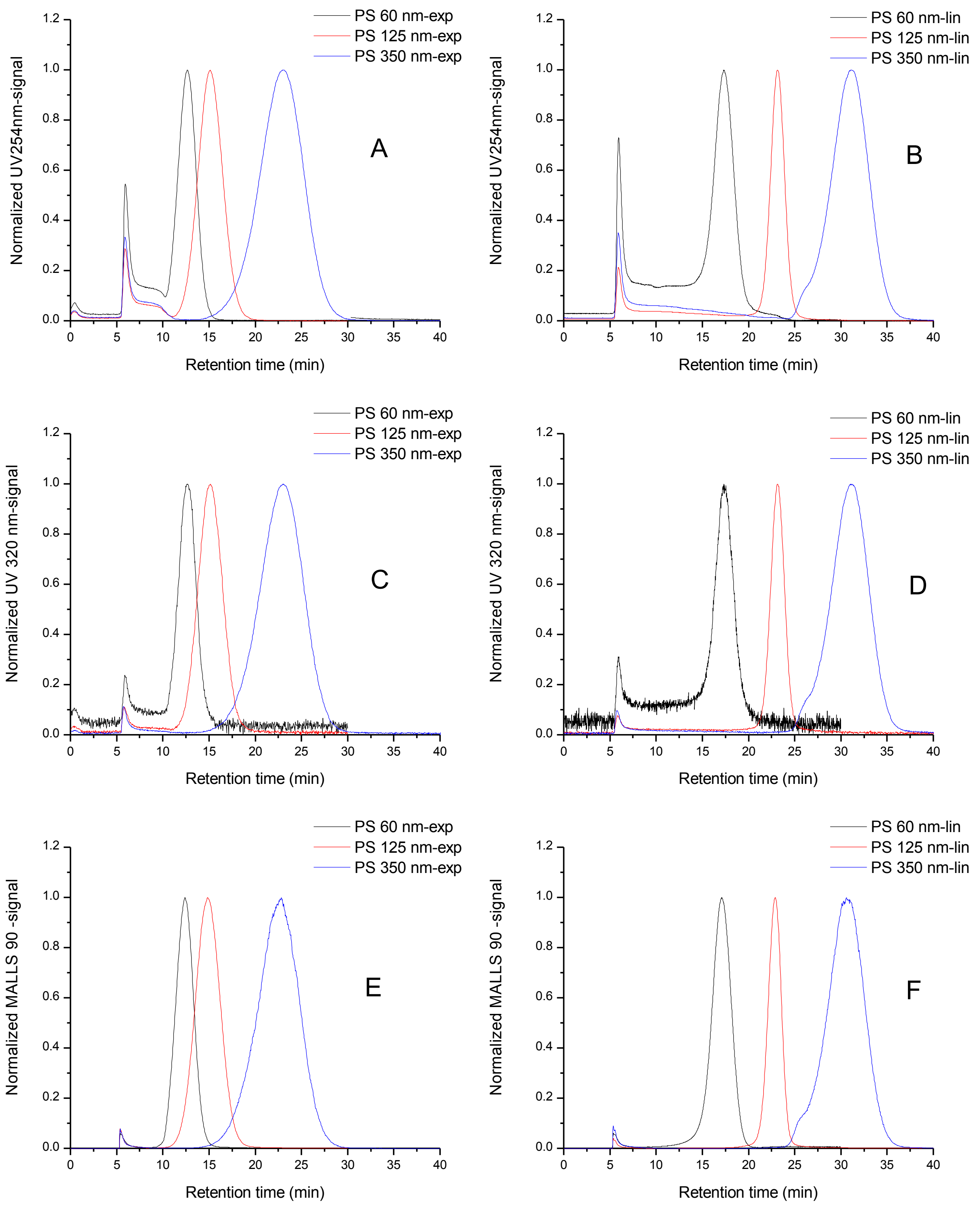

Figure 5.2. UV 254 nm, UV 320 nm and 90˚ - MALLS signals of the exponential (**A, C** and **E**) and linear **(B, D** and **F**) cross-flow profiles

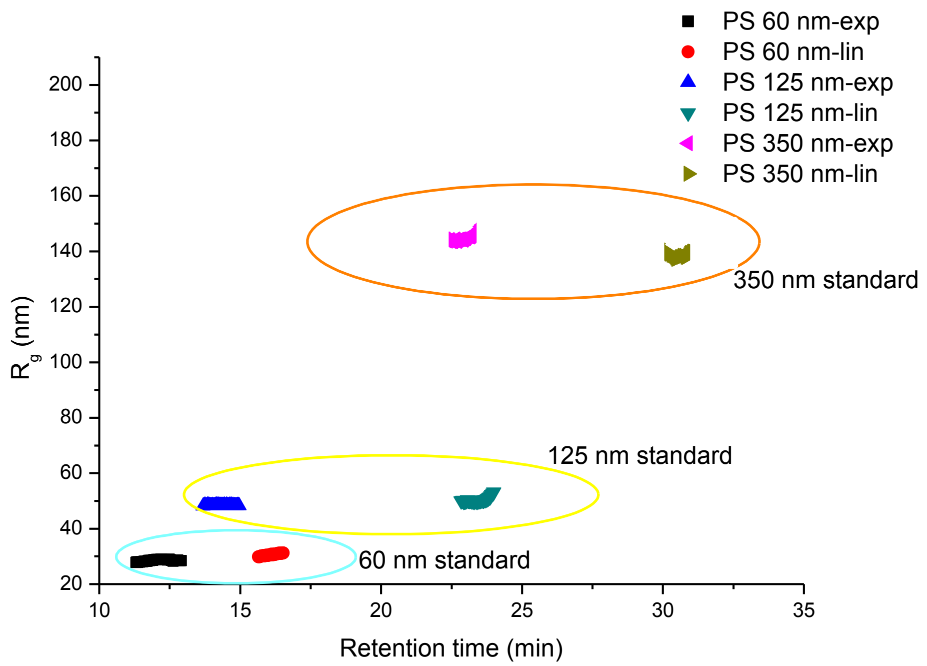

Figure 5.3. R_g vs. retention time plot of the various cross-flow profiles (exponential or linear) for the polystyrene standard latex particles, results calculated from the 90˚ – MALLS signal.

Figure 5.3 and **Table 5.1** display the R_g vs. retention time plot and calculated R_g values, respectively, indicating that the obtained radii are similar to the values given by the supplier. There was a slight difference between the two cross-flow profiles for the PS 350 nm standard, with the linear decay profile being closer to the nominal value. The exponential decay profile result was slightly above the upper end of the standard deviation (135 +/- 6 nm). The corresponding R_g values are displayed in **Table 5.1**.

Table 5.1. R_g values obtained after applying exponential and linear decay cross-flow profiles.

Sample	**Nominal diameter (nm)**	**Corresponding R_g (R_g = 0.775 x D_h/2)**	**R_g – Exponential decay cross-flow**	**R_g – Linear decay cross-flow**
PS 60 nm	60 ± 4 nm	23.3 ± 4 nm	28.7 nm	29.8 nm
PS 125 nm	125 nm ± 1 nm	48.4 ± 1 nm	48.5 nm	49.9 nm
PS 350 nm	350 nm ± 6nm	135.6 ± 6 nm	144.2 nm	137.9 nm

5.4.2. AF4 analysis of sample C (acrylic ester): effect of injection volume, concentration, injection time and cross flow profile on retention time and size (R_g).

Retention time and size (R_g) studies were conducted on sample C by varying the injection volume, concentration, injection time and cross-flow profiles.

Injection times were increased from 1 minute to 10 minutes keeping the focusing time of 1 min and cross-flow flow rate (0.5 mL/min) constant. A shift towards smaller retention times was observed as the injection time increased (**Figure 5.4 A**). Upon zooming in (**Figure 5.4 B**) the shift was evident, even though in small time increments. The constant shift towards smaller retention times is different for sample C as compared to the study done in Chapter 4, where the peak maxima were similar from a retention time of 1 minute through to 10 minutes.

For this example it is possible that some of the particles continuously end up in different flow layers due to a smaller average particle size distribution in comparison to previously studied particles [5,6]. In this case it is possible that after 10 minutes the particle equilibrium has not been fully reached, and a reduction in the cross-flow flow rate could aid due to a weaker force being applied to the particles inside the AF4 channel. Alternatively, due to the longer injection time, the larger particles may start to migrate or interact with the cellulosic membrane, resulting in less particles eluting from the channel [5]. The peak width of all injection time experiments were similar, an indication that no band broadening or narrowing took place upon increasing injection time, eliminating any particle aggregation or sample loss through the cellulosic membrane [6,7].

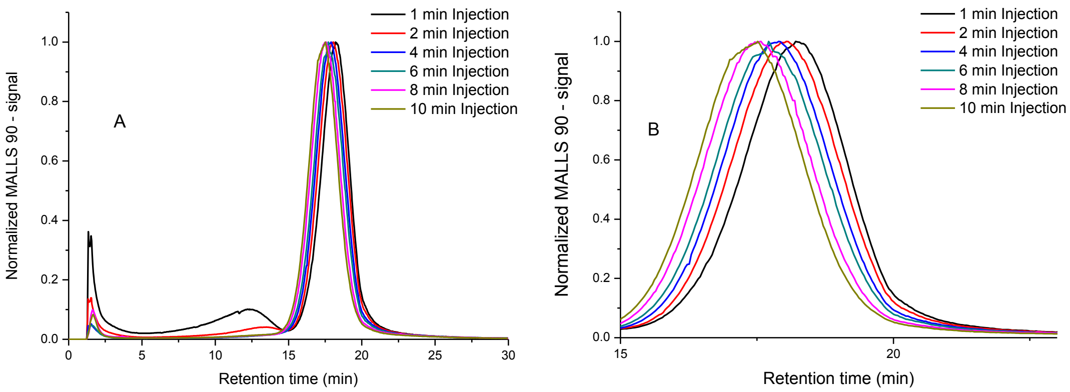

Figure 5.4. A) Normalized 90˚ – MALLS signal at increasing injection times. **B)** Enlarged plot of MALLS 90˚ - signal indicating the shift towards lower retention times upon increase in injection time.

The corresponding R_g vs. retention time plot (**Figure 5.5**) indicates a larger size for the 1 and 2 minute injection time measurements, an indication that the particles have not fully equilibrated in their respective flow velocity layers of the parabolic profile inside the AF4 channel.

If the particles do not have sufficient time to equilibrate while injected, the particle zone concentration or mean layer thickness has mixtures of big and large particles scattered in the different layers [6]. As a result, the unrelaxed particles elute later in comparison to measurements injected for longer times. Another indication of insufficient relaxation is also observed as two pre-peaks between retention times of 7 and 12 minutes appear for the 1 and 2 minute injection time experiments.

The R_g vs. retention time plot (**Figure 5.5**) indicates that the size starts to remain constant and plateaus off without any pre-peaks after injection times of at least 4 minutes, even though the retention times continued to decrease to smaller times. The particle radii of the sample C particles were ranging between 28 nm – 35 nm, corresponding to a nominal diameter (D_h) of 72nm to 90 nm, respectively. An injection time of 4 minutes was used as in Chapter 3 and 4 to conduct the subsequent experiments.

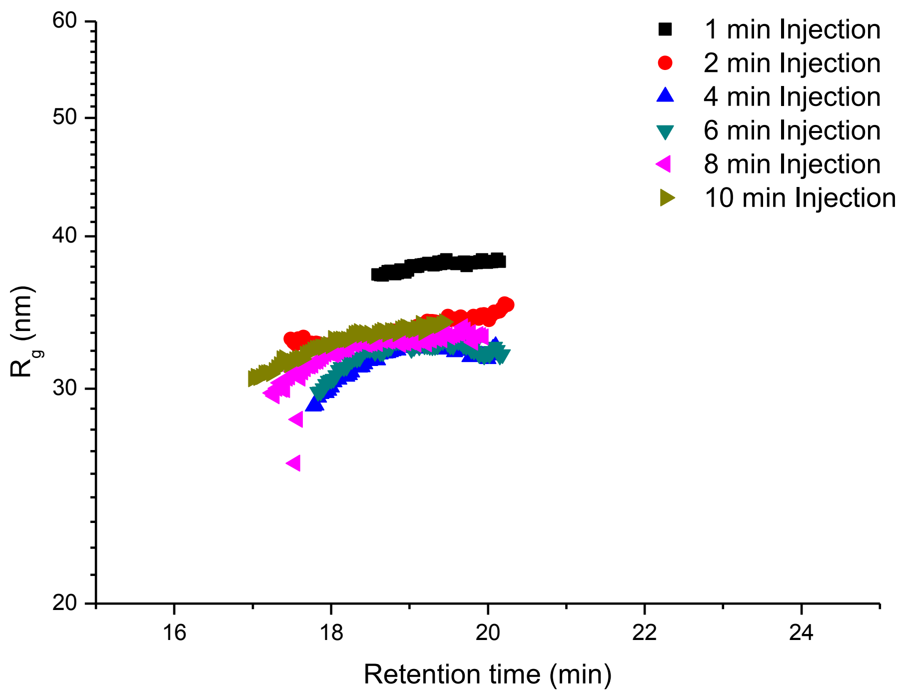

Figure 5.5. R_g vs. retention time plot after varying the injection time from 1 – 10 minutes, results calculated from the 90˚ – MALLS signal.

Upon increasing the cross-flow profile, an increase in the average retention time at peak maximum varied nearly linearly increasing by approximately 2 minutes per 0.5 mL/min increase in cross-flow strength, as observed on the inset graph (**Figure 5.6**). The calculated R_g was slightly lower as compared to the 0.5 and 1.0 mL/min cross-flow strengths, appearing as if a portion of the material was lost through the membrane upon a stronger applied field.

The recovery was calculated using the UV response and the MALLS response for the three applied cross-flow fields. The results indicated that about 10% of species are lost through the membrane when 1.5 mL/min was used.

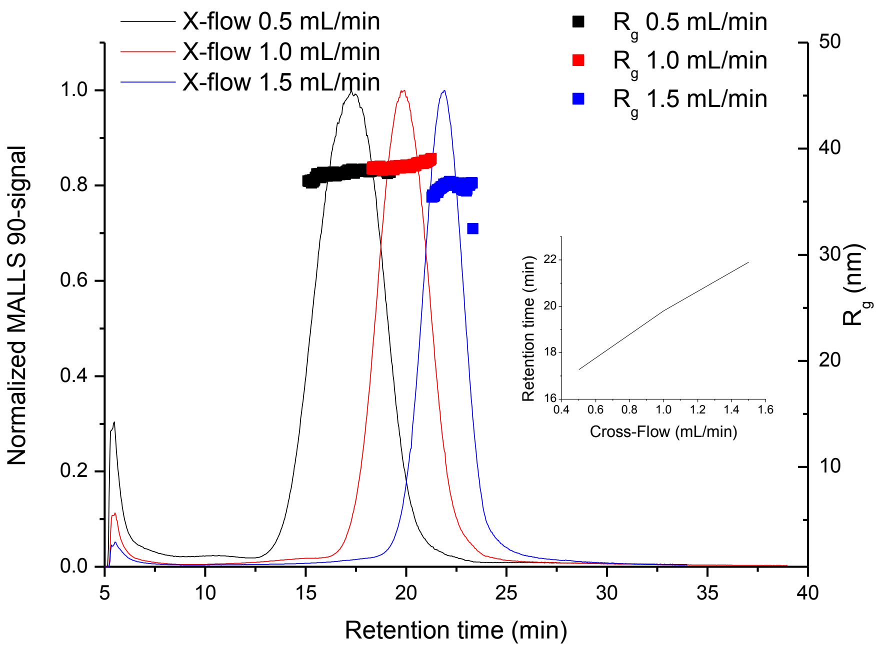

Figure 5.6. R_g vs. retention time plot after varying the cross-flow from 0.5 mL/min to 1.5 mL/min. R_g calculated from the 90˚ – MALLS signal. An inset of retention time vs. cross-flow is displayed as well.

The injection volume was increased from 1 to 50 µL to investigate the effect on the retention time and detector response. The UV 320 nm signal was monitored as a function of injection volume and is displayed in **Figure 5.7**, with the inset displaying the linearity of UV response as a function of injection volume. The linearity and standard error of the slope and intercepts were very low, confirming the linearity of the UV 320 nm response against the concentration increase.

The corresponding R_g values are displayed in **Figure 5.8** where 1 and 5 µL injection volumes show slightly higher radii in comparison to 10 µL and 20 µL injection volumes. The radii calculations of 40 µL and 50 µL injection volumes were not accurate, possibly due to channel overloading and were omitted from the graph. The MALLS signal was saturated for the 40 µL and 50 µL injection volume measurements, therefore no meaningful radius of gyration data is obtainable. Sample C was lastly injected at different concentration levels to monitor the detector responses as well as R_g. **Figure 5.9 A** and **Figure 5.9 B** display the linearity upon injecting the particles from 0.1 mg/mL up to 5 mg/mL. Similar to the injection volume, the standard error on the slope and intercept was low, establishing linearity for both UV and MALLS detector signals.

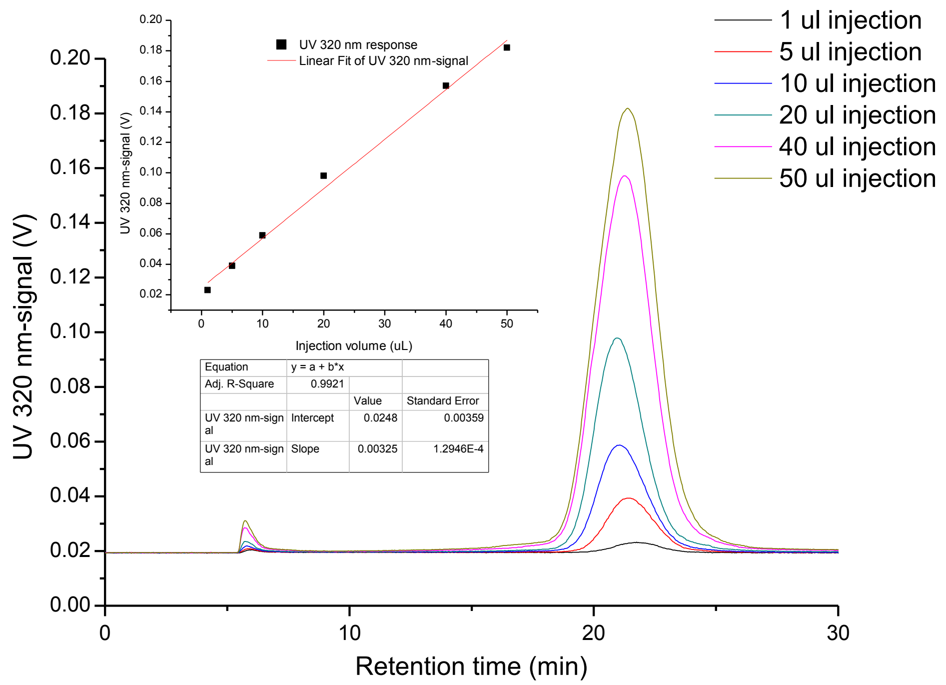

Figure 5.7. UV 320 nm signal vs. retention time as a function of injection volume. An inset graph of UV signal vs. injection volume is displayed additionally to illustrate the linearity.

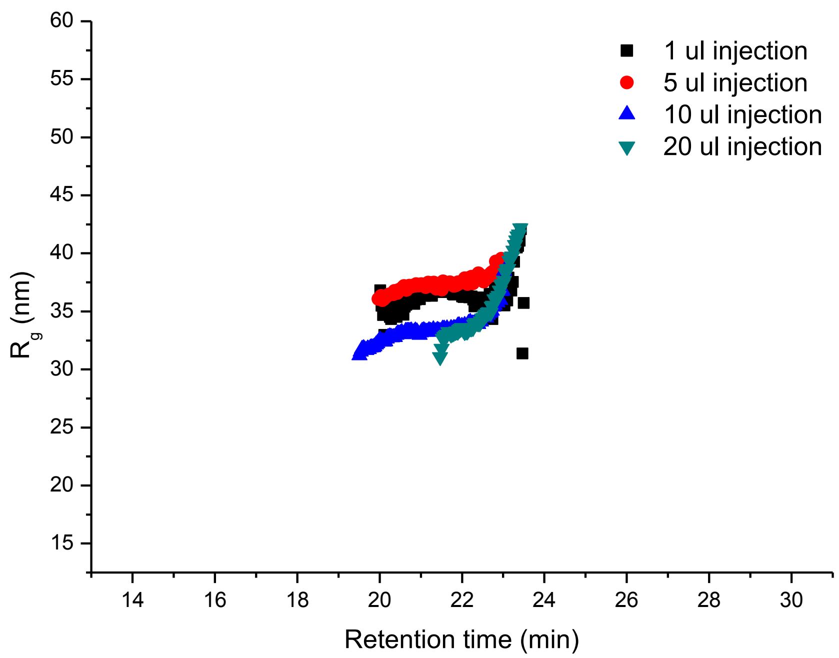

Figure 5.8. R_g vs. retention time plot after varying injection volume R_g calculated from the 90˚ – MALLS signal.

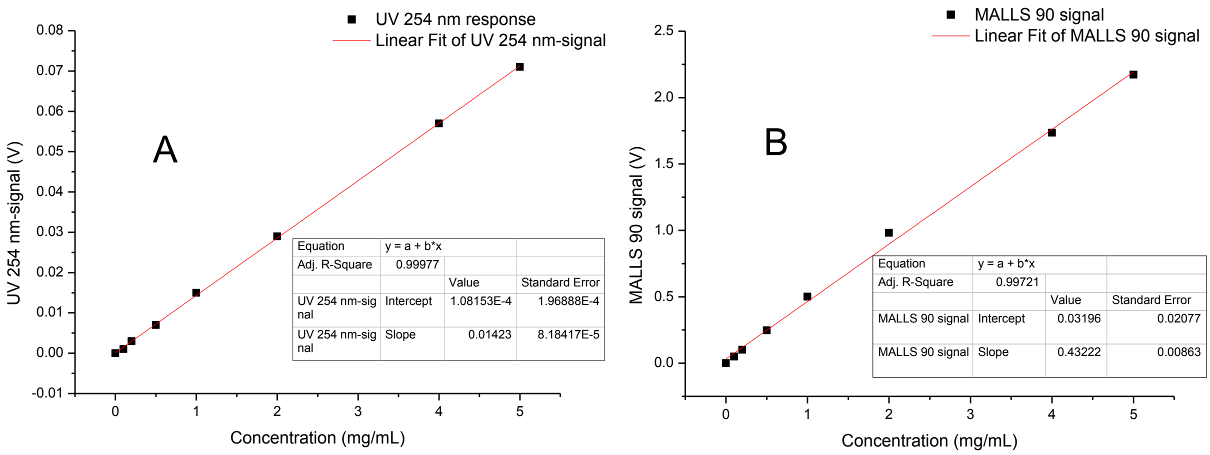

Figure 5.9. A) UV 254 nm and **B)** 90˚ – MALLS signal as a function of injected concentration as illustration of detector linearity upon concentration increase.

The subsequent size calculations are displayed in **Figure 5.10**, indicating that the signal to noise levels for 0.1 and 0.2 mg/mL were not sufficient to obtain a scatter free size reading. A concentration from 0.5 mg/mL and higher gave more scatter-free radii readings ranging from 34 – 38 nm. As observed, the particles appear to plateau off around 38 nm. An indication of monomodality is also apparent since the particle radii spread is not too broad. A narrow particle size distribution in latex particles has added benefit when formulating coatings since it assists in the coalescence of particles during film formation, imparting added stain and scratch resistance [5].

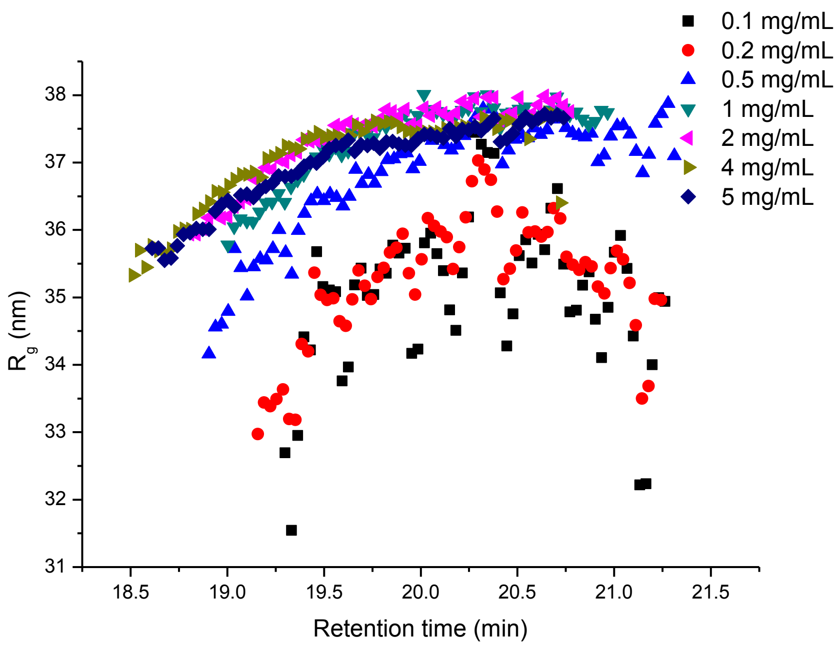

Figure 5.10. R_g vs. retention time plot after varying the concentration. R_g calculated from the 90˚ – MALLS signal.

5.4.3 AF4-MALLS-UV and AF4-ICP-MS analysis of sample B and sample C by varying the mixing ratios of latex to TiO_2.

The samples were prepared using a wt % latex-to-pigment ratio of **1.35 : 1** as per supplier recommendation. Different ratios of latex to pigment were made up prior to FFF analyses to study the effect of the organic-inorganic interaction upon retention time behaviour. The various ratios are displayed in **Table 5.2**.

Table 5.2. Mixing ratios of latex to TiO_2 for latex samples B and C before AF4 analyses.

Sample C	**TiO_2**	**Mobile phase**	**Ratio (Latex:TiO_2)**
1g	0 g	2 g	100:0
1g	0.7 g	2 g	1.35 : 1
1g	0.2 g	2 g	5 : 1
1g	0.1 g	2 g	10 : 1
1g	0.01 g	2 g	100 : 1
1g	0.001 g	2 g	1000 : 1
0g	0.1	2 g	0:100
Sample B	**TiO_2**	**Mobile phase**	**Ratio (Latex:TiO_2)**
1g	0 g	2 g	100:0
1g	0.7	2 g	1.35 : 1
1g	0.1	2 g	10 : 1
1g	0.01	2 g	100 : 1
0g	0.1	2 g	0:100

The latex sample, TiO_2 and the mobile phase (0.2 % Novachem in deionised water) were agitated at a stirring speed of 550 rpm for 20 minutes. After stirring the samples were immersed in a sonication bath for 20 minutes at 100% intensity in order to break up any agglomerates. After sonication the samples were left at room temperature for 20 minutes. Hereafter, 100 µL of the supernatant was pipetted and filled up to 1500 µL. AF4 analyses were also performed on latex – TiO_2 blends without applying the sonication step.

Each of the prepared samples was injected at three different injection volumes (1, 5 and 10 µL) with the intention of monitoring the elution behaviour of the latex-TiO_2 particle blend before fractionation and offline ICP-MS analyses.

Sample C, injected as a function of injection volume between 10 µL and 50 µL (**Figure 5.7**, **Figure 5.11**) indicated that upon an increase in injection volume, the retention time shifted to lower retention times.

The retention time decreased as injection volume increased, which is an indication that the number of particles in the mean layer thickness during equilibrium increased proportionally. The number of particles present in the various layers result in subsequent band broadening as the injection volume is increased. The mean layer thickness represents a particle concentration cloud, where overloading or very high injection volumes result in an overcrowded mean layer. Larger particles will be trapped in faster flow velocity layers and will not be able to diffuse towards the accumulation wall, resulting in earlier retention in comparison to a mean layer thickness without particle overcrowding. An injection volume of 10 µL was chosen to study the effect of the mixing ratio between latex and TiO_2 particles.

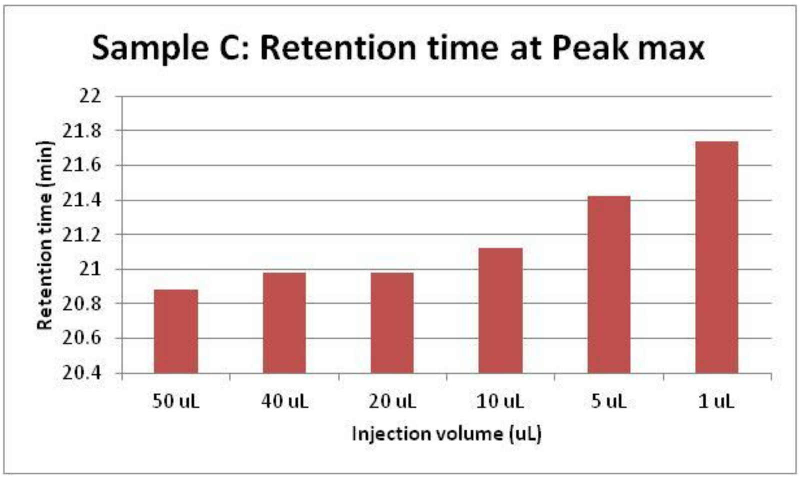

Figure 5.11. Retention time of sample C at peak max as a function of injection volume.

Figure 5.12 and **Figure 5.13 A** indicate how that the latex peak shifts to higher retention times as the ratio of latex:TiO_2 decreased, i.e. more TiO_2 was present in the blend. The subsequent retention time against latex:TiO_2 mixing ratio is displayed in **Figure 5.14**.

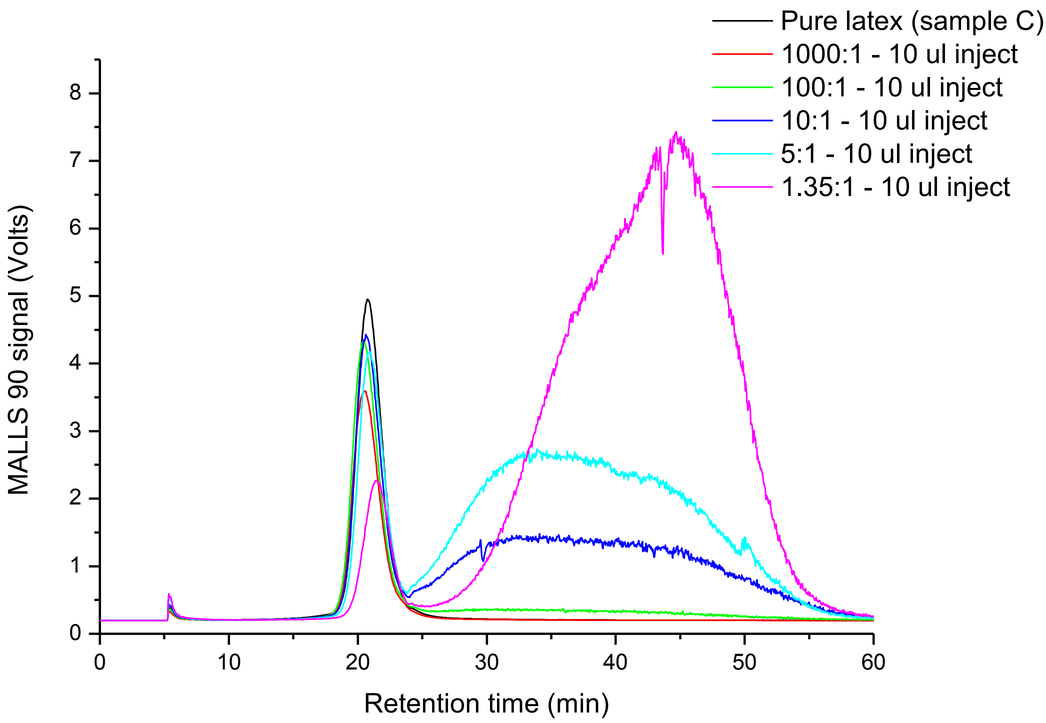

Figure 5.12. Effect of mixing ratios between latex and TiO_2 particles on retention time and MALLS signal for sample C. Mixing ratios varied from latex:TiO_2 ratio of 100:0 (black) to 1.35:1 (pink).

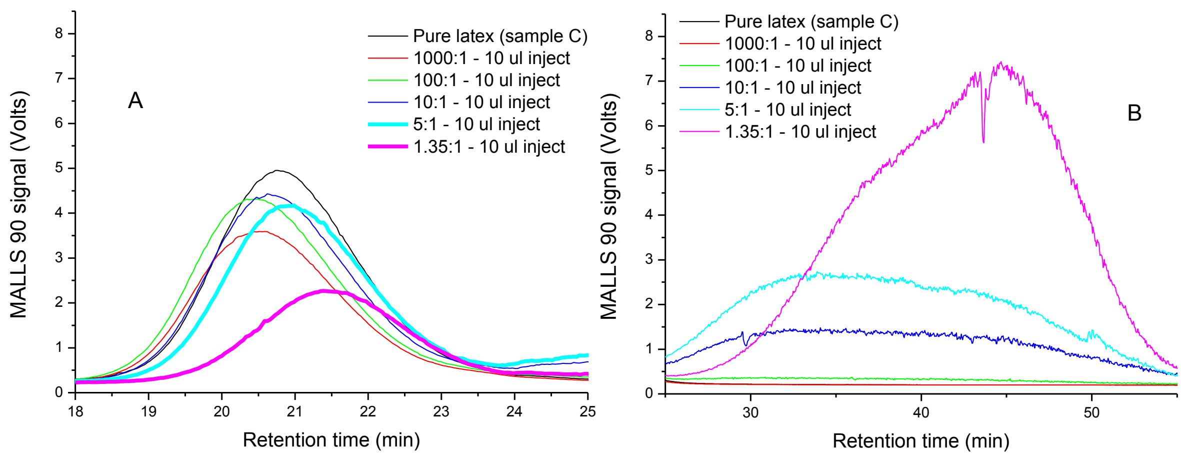

Figure 5.13. Enlarged fractograms A) latex peak of sample C and B) TiO_2 peaks.

Figure 5.14 illustrates how the decrease in latex particles from pure latex to pure TiO_2 results in a shift in retention time. The increase in retention time is probably due to two phenomena or interactions taking place inside the AF4 channel: 1) a decrease in volume fraction being injected, results in an increase in retention time as illustrated in **Figure 5.7** and **Figure 5.13**, or 2) interactions between latex and TiO_2 particles are a result of van der Waals interactions.

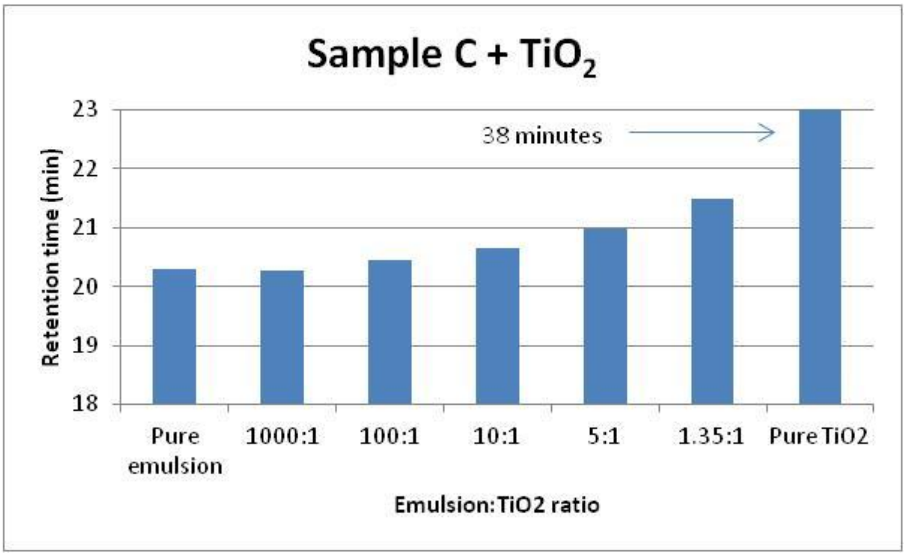

Figure 5.14. Effect of latex:TiO_2 ratio on the retention time taken at peak maximum for sample C.

Dubascoux et al. studied environmental particles by investigating surfactant and salt concentrations upon AF4 analyses. The outcome was explained by particle-particle interactions with the accumulation wall as well as the formation of an electric double layer near the membrane, affecting larger particles eluting in slower flow velocity layers [6].

Particle-particle interactions between latex and TiO_2 particles would warrant that the TiO_2 is detected in the retention time window at which the latex particles are eluting, between 18-24 minutes.

Two mixing ratios of latex-to-TiO_2, 10:1 and 1.35:1, respectively, were used in the ICP-MS study at two injection volumes, 5 µL and 10 µL, respectively. The ratios were applied to sample C (supplier sample) and sample B (pure acrylic in-house latex, chapter 4). The fractograms of each of the mixtures were divided into 6 different time steps for fraction collection labelled F1 to F6 ranging from 15 to 34 minutes.

A blank mobile phase sample and a TiO_2 standard were measured to determine the accuracy of the ICP-MS system before injection. The blank sample gave a result of 1.18 ppb TiO_2 while the 48.7 TiO_2 reference sample had a corresponding value of 48.74 ppb.

The TiO_2 results obtained from ICP-MS are displayed in **Figure 5.15** and **Figure 5.16** for sample C and sample B, respectively. A blank measurement was conducted subtracted from the readings taken of the individual fractions.

For sample C, TiO_2 species were already detected from F1 up until F6, with F6 representing pure TiO_2 in reference to **Figure 5.12** or **Figure 5.13**. As observed, the 10:1 latex-to-TiO_2 ratio had roughly more TiO_2 in comparison to the 1.35:1 blend, mainly due to the injection volume difference between the two mixing ratios of 10 µL vs. 5 µL.

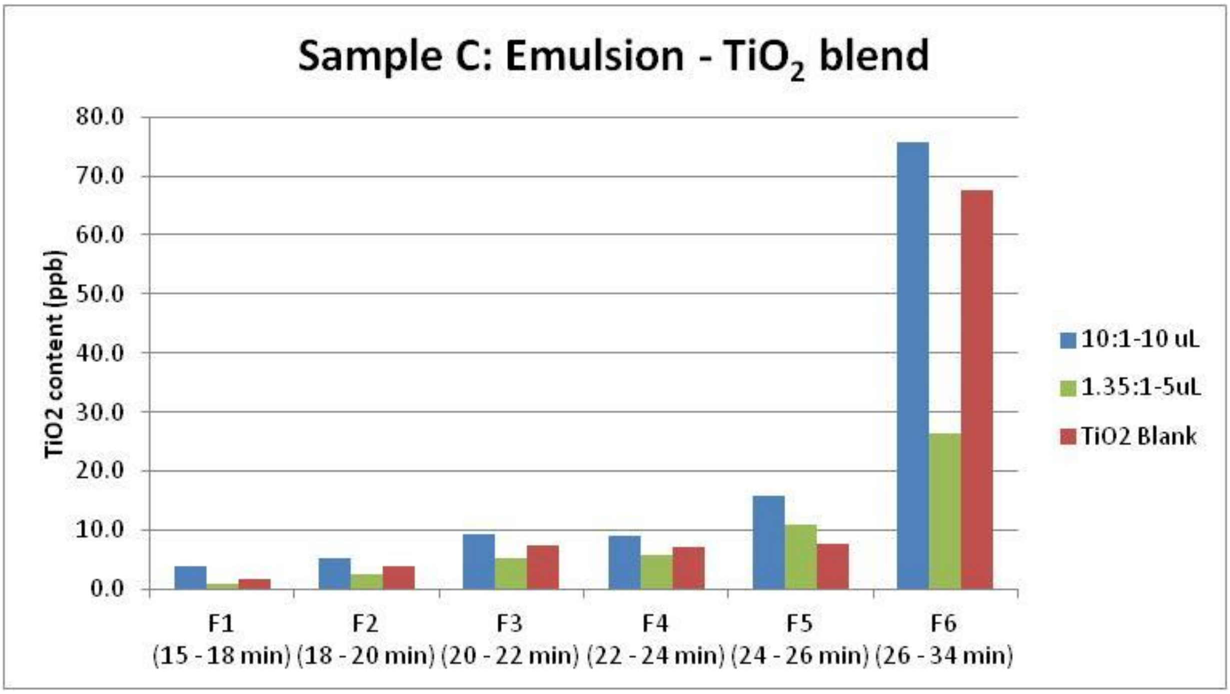

Figure 5.15. ICP-MS determination of TiO_2 for each of the collected fractions across the fractograms for **sample C** (supplier sample) blended with the TiO_2.

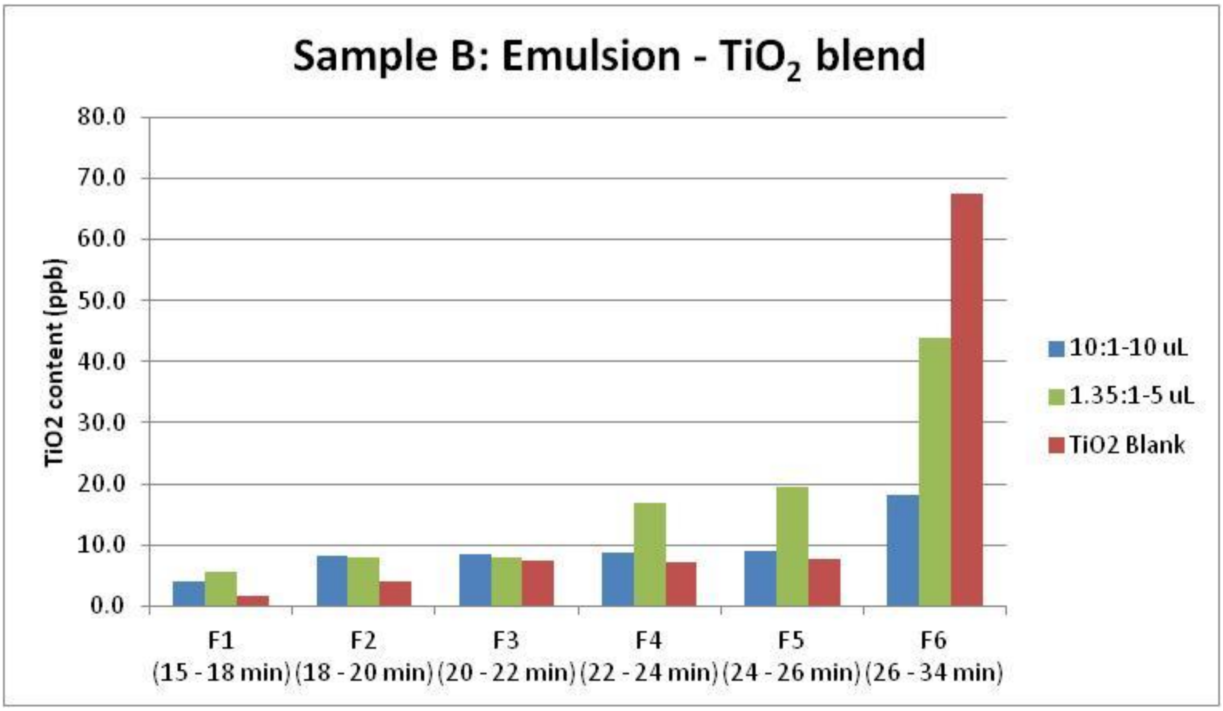

Figure 5.16. ICP-MS determination of TiO_2 for each of the collected fractions across the fractograms for **sample B** (in-house sample) blended with the TiO_2.

When comparing the calculated TiO_2 after ICP-MS analyses for sample B, the observation was the reverse in comparison to sample C, i.e. more detected TiO_2 for the 1.35:1 mixing ratio in comparison to the 10:1 latex-to-TiO_2 mixing ratio (**Figure 5.16**).

In both samples, TiO_2 was detected from a very early retention time (F1), in both the pure TiO_2 injected sample as well as the blends. For sample C, the detected TiO_2 was more that the blank injected TiO_2, an indication that the 10:1 mixing blend shows some form of interaction between latex and TiO_2 particles. In the case of the 1.35:1 ratio, the values were below the pure TiO_2 readings for most of the fractions.

Different to sample C, sample B had more detected TiO_2 content when a higher latex-to-TiO_2 ratio of 1.35:1 was used.

From the observed results, it appears as if the latex particles of sample C (acrylic ester) have more affinity towards the TiO_2 particles at a lower latex-to-TiO_2 mixing ratio. The particle radii observed for sample C were in the 28-35 nm range, therefore the particles may possibly have been small enough to interact with the TiO_2 particles. Sample B (in-house acrylic) indicated that more affinity between particles was experienced at a latex-to-TiO_2 mixing ratio of 10:1 and a particle radius of approximately 46 nm. These observations possibly add to the association of latex particles with TiO_2 particles. A potential schematic for the interaction is proposed and discussed in section 5.4.4.

5.4.4 Effect of ultrasonication on AF4 retention times after mixing latices and TiO_2 particles

The effect of sonication on latex-TiO_2 particle mixtures was evaluated by AF4-MALLS-UV for both sample B (pure acrylic) and sample C (acrylic ester). Upon injecting the latex and TiO_2 samples individually with sonication, two distinct peaks could be observed for both samples B and C. Upon blending the latex sample with TiO_2, the measurement without sonication had peak maxima at retention times larger than the measurement with sonication for both sample C (**Figure 5.17 A and B**) and sample B (**Figure 5.18 A, B and C**).

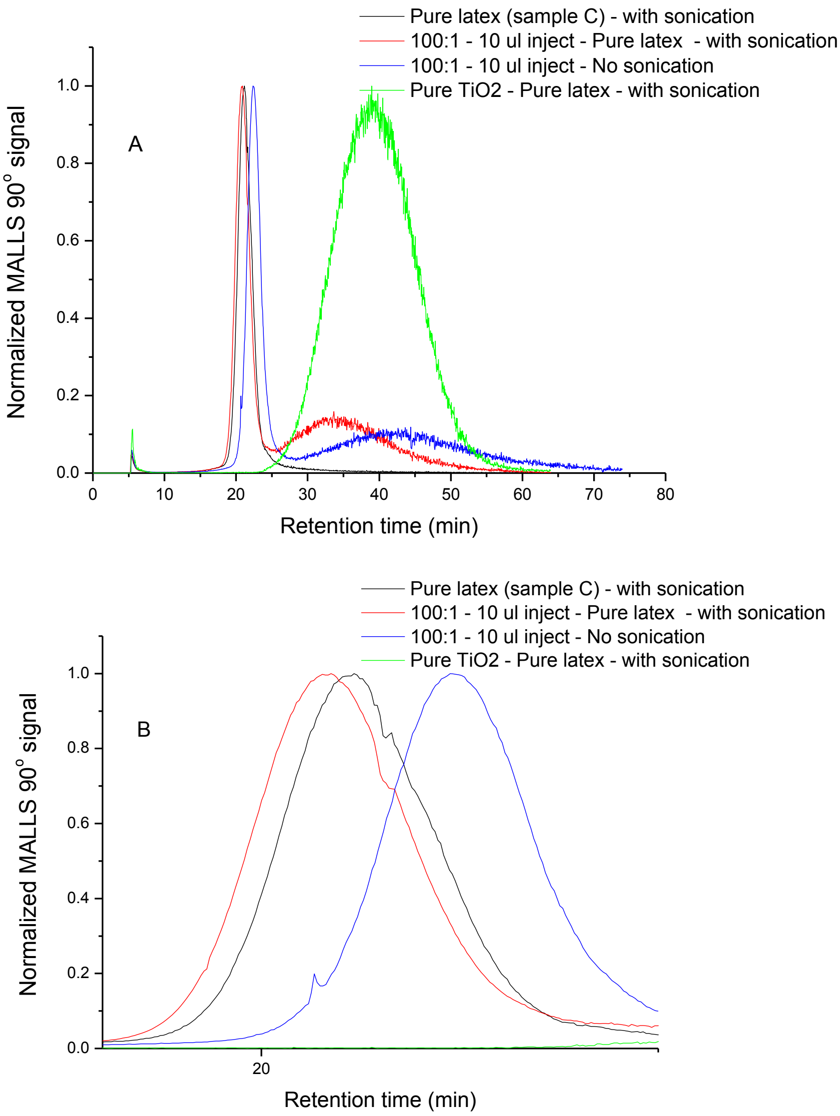

Figure 5.17. A) Pure acrylic latex (sample C) injected individually (black), TiO_2 injected on its own (green), latex-TiO_2 blend without sonication (blue) and with sonication (red). **B)** Zoom-in view on latex peaks.

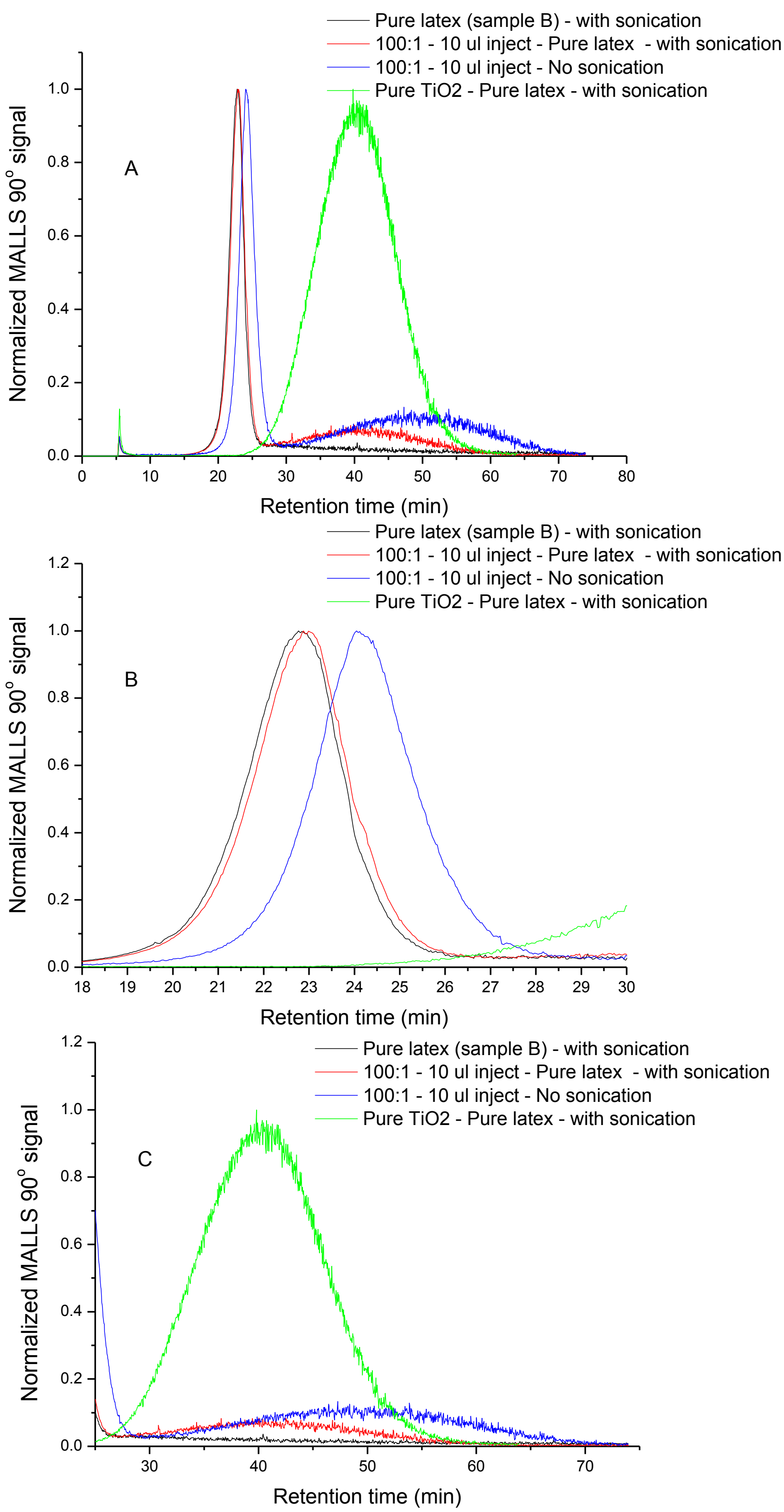

Figure 5.18. A) Pure latex (sample B) injected individually (black), TiO_2 injected on its own (green), latex-TiO_2 blend without sonication (blue) and with sonication (red). **B)** Enlarged latex peaks and **C)** enlarged TiO_2 peaks.

The latex peak maximum had a shift of approximately 2 minutes upon sonication, whereas the TiO_2 peak maximum shifted between 8 and 10 minutes after sonication.

The observation is a clear indication that sonication breaks up agglomerates whether the particles are nanoparticles (latex) or in the nano to micrometer range (TiO_2). In **Figure 5.17** and **Figure 5.18**, the peak widths of the latex peaks do not change much after sonication, probably due to the particle size distribution width remaining the same in comparison with no sonication [8,9]. Upon further investigation of the TiO_2 peaks, it can be observed that the width changed fairly significantly comparing the sonication measurements. The big shift in retention time (8 - 10 minutes) supports the observation.

A proposed schematic of agglomerate breakup during the mixing process, i.e. the various latex – to TiO_2 mixing ratios for sample B and sample C (**Figure 5.19**) and the sonication process (**Figure 5.20**) display how the various latex and TiO_2 particles interact in an aqueous media. In this case 0.2 % v/v of Novachem (anionic and non-ionic surfactants) was added to the mobile phase, which aid in the association of latex and TiO_2 species. Kato et al. studied polystyrene latex systems with TiO_2 and SiO_2 by making use of a zwitterionic emulsifier [10]. Zeta-potential as a function of pH was monitored for the latex and TiO_2 solutions. Dispersions were analysed with Scanning Electron Microscopy (SEM) to observe the interaction between particles.

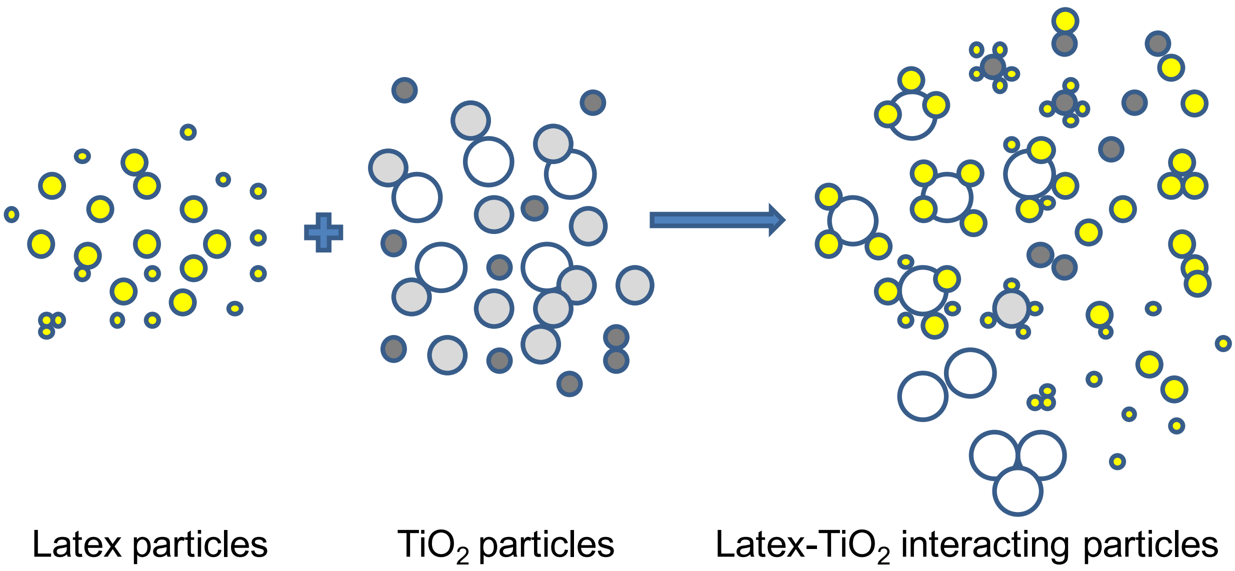

Figure 5.19. Schematic of interaction between latex and TiO_2 particles of various size populations upon various latex – to – TiO_2 mixing ratios.

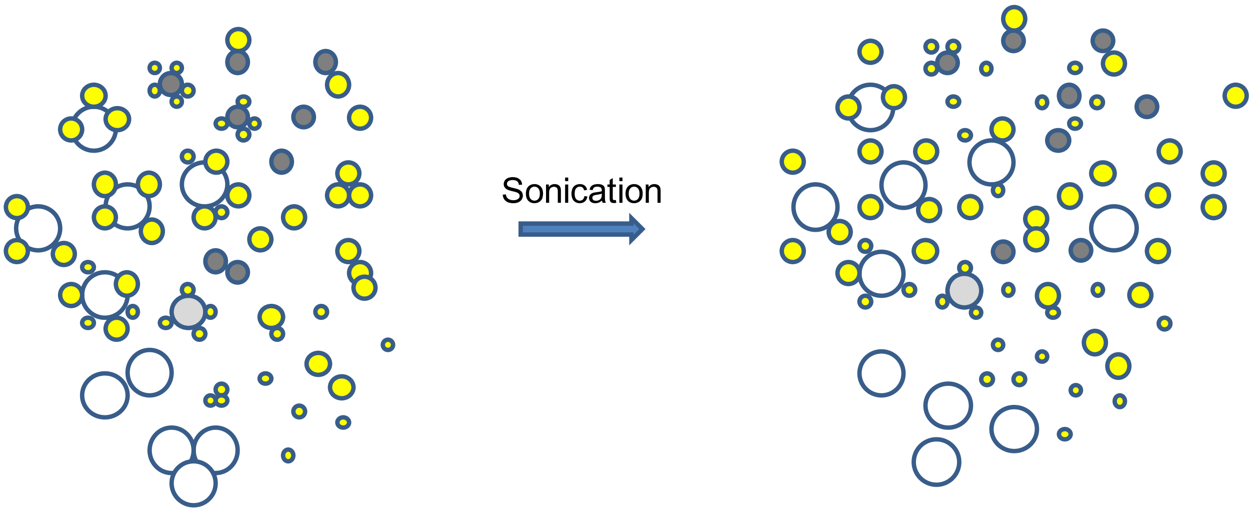

Figure 5.20. Schematic of dissociation of latex and TiO_2 particles upon sonication.

In the current experiments both latex (sample B and sample C) were acrylic in nature and the proposed mechanism where some latex particles adhered to the TiO_2 particles were dependent on the ratio between the two different particle species as per discussion in section 5.4.3. In any given situation, free latex particles are present in the aqueous medium, TiO_2 covered with latex particles as well as free and aggregated TiO_2 particles (**Figure 5.19**). The interacted TiO_2 hybrid particles would not form a distinct third peak due to particle interactions, but rather forms a broad TiO_2 peak. This observation would be as a result of the particle size range of the latex-TiO_2 associating particles being closer to individual and aggregated TiO_2 particles.

5.5 Conclusion

A supplier-recommended latex sample to reduce TiO_2 in a formulation for cost saving, as well as an in-house latex sample were analysed using AF4 coupled to multiple detectors.

Individual AF4 measurements indicated that the supplier latex sample had linear responses across changing the injection time, concentration and injection volume. Mixtures of latex and TiO_2 were measured to monitor the retention time shifts upon changing the mixing ratio.

AF4-MALLS-UV followed by fractionations and ICP-MS analyses indicated potential interactions between the latex and TiO_2 particles for sample C using lower levels of latex to TiO_2, whereas sample B revealed that a larger ratio of latices to TiO_2 enhanced the detectability of TiO_2.

Additionally, the application of sonication to the samples indicated that the latex and TiO_2 peaks shifted to earlier retention times. The TiO_2 peak, especially shifted significantly upon sonication, with a reduction in retention time of approximately 8-10 minutes, for both sample B (pure acrylic) and sample C (acrylic ester). The shift in the peak maxima indicated that sonication assists in breaking up agglomeration of nanoparticles (latices, sample B and C) and nano-micrometer particles (TiO_2). The proposed interactions between latex an TiO_2 particles indicated that the various shifts in retention times could be due to forming interactions during mixing at various particle ratios as well as sonication where particles are broken up into smaller populations.

5.6 References

[1] J.V. Koleske, Paint and Coating Testing Manual, (Gradner-Sward Handbook, 14th Edition), American Society of Testing and Materials, Philadelphia, PA, Color Research & Application 20 (1995) 48-49.

[2] A. Sood, Particle size distribution control in emulsion polymerization, J. Appl. Polym. Sci. 92 (2004) 2884-2902.

[3] M. do Amaral, A. Roos, J.M. Asua, C. Creton, Assessing the effect of latex particle size and distribution on the rheological and adhesive properties of model waterborne acrylic pressure-sensitive adhesives films, J. Colloid Interface Sci. 281 (2005) 325-338.

[4] F. Karakaş, M.S. Çelik, Effect of quantity and size distribution of calcite filler on the quality of water borne paints, Prog. Org. Coat. 74 (2012) 555-563.

[5] A.C. Makan, M.J. Spallek, M. du Toit, T. Klein, H. Pasch, Advanced analysis of polymer emulsions: Particle size and particle size distribution by field-flow fractionation and dynamic light scattering, J. Chromatogr. A 1442 (2016) 94-106.

[6] S. Dubascoux, F. Von Der Kammer, I. Le Hécho, M.P. Gautier, G. Lespes, Optimisation of asymmetrical flow field flow fractionation for environmental nanoparticles separation, J. Chromatogr. A 1206 (2008) 160-165.

[7] K.D. Jensen, S.K.R. Williams, J. Calvin Giddings, High-speed particle separation and steric inversion in thin flow field-flow fractionation channels, J. Chromatogr. A 746 (1996) 137-145.

[8] I. López-Heras, Y. Madrid, C. Cámara, Prospects and difficulties in TiO_2 nanoparticles analysis in cosmetic and food products using asymmetrical flow field-flow fractionation hyphenated to inductively coupled plasma mass spectrometry, Talanta 124 (2014) 71-78.

[9] V. Nischwitz, H. Goenaga-Infante, Improved sample preparation and quality control for the characterisation of titanium dioxide nanoparticles in sunscreens using flow field flow fractionation on-line with inductively coupled plasma mass spectrometry, J. Anal. At. Spectrom. 27 (2012) 1084-1092.

[10] K. Kato, M. Kobayashi, K. Esumi, K. Meguro, Interaction of pigments with polystyrene latex prepared using a zwitterionic emulsifier, Colloids and Surfaces 23 (1989) 159-170.

Chapter 6: Overall conclusions and recommendations

The aim of the dissertation was to investigate different constituents used in water based decorative coatings and its behaviour with respect to dissolved molecules and dispersed particles using classical chromatography and more novel, Field-Flow Fractionation separation techniques. A brief summary of each study of these materials and the various detection methods are discussed below.

6.1 Conclusions – Chapter 3

In this chapter a comparison of particles size using classical Dynamic Light Scattering (DLS), Asymmetric Flow Field-Flow Fractionation (AF4), and Sedimentation FFF (SdFFF) were investigated in styrene-acrylic and acrylic latex particles. The obtained results indicated a difference in size between DLS and AF4, mainly due to hydration layers, being taken into account in the event of DLS analyses, whereas AF4-MALLS do not consider the hydration layer. SdFFF analyses of nana particles indicated the development of an extra peak at early elution times, an indication that a bimodal particle size distribution is present, early in the Free Radical Polymerization reaction.

Furthermore, coupling AF4 with Inductively Coupled Plasma Mass Spectroscopy (ICP-MS) revealed the possibility of elemental speciation in a mixture of organic (latex particles) and inorganic species (TiO_2 particles), highlighting the novelty of using AF4 coupled to an element sensitive detector.

Investigations on the coupling of SdFFF with ICP-MS using different inorganic constituents used in coatings would lead to interesting results, since inorganic species most probably have different densities and sizes. The separation of these species by SdFFF coupled with the ICP-MS speciation may become a very valuable study in future.

6.2 Conclusions – Chapter 4

Chapter 4 dealt with the study of classical Size Exclusion Chromatography (SEC) coupled to MALLS and RI detection in comparison to AF4-MALLS-UV-RI, using polymer latices in a dissolved macromolecular state. THF was used to dissolve the latex polymers (acrylic and styrene-acrylic and results indicated that larger molar masses were obtained using AF4, in comparison to SEC. Abnormal elution behaviour, commonly observed for large molar mass and branched macromolecules were observed in SEC, however not for AF4.

Furthermore AF4 was used to calculate gel content of species eluting from the AF4 channel, specifically for polymer latices polymerized by free-radical polymerization with and without methacrylic acid content. Results were compared to a gravimetric approach, which usually takes two days longer to determine. The AF4 method potentially reduces analyse time by approximately 2 days.

Further studies on the interaction between macromolecules with micro or macro gel species present, should be further investigated using a variety of modified AF4-channel membranes.

6.3 Conclusions – Chapter 5

The interaction of Polymer latex particles, which typically reduces the need of TiO_2 additions in a typical water-based decorative coating formulation, was studied at different latex – to – TiO_2 mixing ratios.

In-house latex was used as comparison in order to monitor the behaviour of the latex peak upon the various mixing ratios. Both latex-TiO_2 systems were studies using AF4-MALLS-UV analyses as well as the collection of Narrow dispersed fractions, submitted for offline – ICP-MS for TiO_2 quantification.

Both latex samples (supplier and in-house) displayed the phenomenon of decreasing retention time upon increasing the mixing ratio of latex – to – TiO_2. ICP-MS analyses after fraction collection, indicated that the supplier sample (Sample C) had more TiO_2 content detected at lower latex – to – TiO_2 mixing ratios, whereas the in-house latex (Sample B) had larger TiO_2 content upon a larger latex – to – TiO_2 ratio. The observed results are an indication of interaction taking place between the latex and TiO_2 particles, most likely in the form of van deer Waals, interactions.

In a separate experiment, the effect of sanitation for the latex-TiO_2 particle mixture, prior to AF4-MALLS-UV injection, were evaluated. Results indicated a shift towards earlier retention times for the TiO_2 peak upon sonication, indicating that agglomerates were minimized upon sonication. For sample C (supplier sample), the latex peak also shifted to a lower retention time, indicating that sonication also assisted in possible reduction in agglomerated particles.

Further work on this topic would include various dispersants used and investigating the sonication time upon retention time behaviour for both latex and TiO_2 particles.

Acknowledgements

First and foremost, a great thanks to the Father Almighty for sparing, guiding and giving me the strength to walk this journey. None of this would have been possible without your guidance.

To my family and friends who believed in me every step of the way, thank you for all your words of encouragement through this epic PhD journey. My late dad Erick and siblings Theodore and Elroy, you are dearly missed in this time. I would have loved to celebrate *'n yskoue* with you on this achievement.

Siblings and extended siblings…. Laetitia, Melvin, Vainola, Howard, Athena, Gaile, Esme, Emile, Vincent, Celeste, thank you for your endless support and understanding where I had to decline many a gathering, birthday parties or celebrations, now I will not have the 'I have to write' excuse anymore and I look forward to catch up on some lost time with each one of you.

My mother Rosy, you have really been an inspiration and true pillar through all of this, every inch counted towards me getting through varsity as a start. The early morning and late night messages and calls gave me that extra gear to push harder, persevere and not give up in tough times. The pakkietjie with biltong and snacks from time to time made a big difference in this campaign. Love you lots.

My new mom, Marechia, thank you for the welcoming atmosphere, warmth and many meals we could share together through my MSc and PhD. Without the stamina, I would not have made it through the long study sessions from time to time.

To the Polymer Science Institute Students and Staff members, thank you for sharing your resources and space since 2006. It has been a remarkable decade of rollercoastership if that is even a word!. Thank you to those who made it possible and almost effortless to make this journey a special one. Kansai Plascon chemists, managers, past and present research executives, thank you for making this part-time study feel almost as if it was a full-time journey. Not easy, but you have played a big part in making it possible and maintaining the momentum to not lose sight of the bigger picture. All your support and giving me the opportunity conduct research and attending conferences abroad has really been valuable and have formed an integral part of the study we embarked on decorative coatings.

Prof. Pasch – Thank you for all your support, even for the coming support after this edition has passed. You have given me the opportunity to be part of your group and I am truly blessed to have spent my entire postgraduate years having you as a mentor. I think the value of you letting my destiny in my own hands shaped me a great deal with many challenges going forward. Being able to work independently and making your own research decisions is not necessary a given in the postgrad world, but you have pretty much instilled a sense of pride in me to have produced a piece of work I am proud of.

Last but not least, My dear wife Nadine. Thank you very much for really being my polymer back bone, your triple bond grit and patience (being tested to infinity) for many years really show a lot of character and has really allowed me to focus my energy and hours to get it done – We have now, finally reached that point and I look forward to payback the lost time. Lief jou baie!